2013

Surface studies of organic thin films using scanning probe microscopy and nanofabrication

Venetia DeNae Lyles
Louisiana State University and Agricultural and Mechanical College

SURFACE STUDIES OF ORGANIC THIN FILMS USING SCANNING PROBE MICROSCOPY AND NANOFABRICATION

A Dissertation

Submitted to the Graduate Faculty of the
Louisiana State University and
Agricultural and Mechanical College
in partial fulfillment of the
requirements for the degree of
Doctor of Philosophy

in

The Department of Chemistry

by
Venetia DeNae Lyles
B.S., South Carolina State University, 2009
December 2013

ACKNOWLEDGEMENTS

This dissertation is the end result of a journey started years ago and would not be possible without the love, support, and courage of many people. I would first and foremost like to give honor to God who has given me strength and courage to progress and keep moving forward in a positive direction. To my loving parents, Willie and Sarah Lyles, who have supported me since I was born, I am thankful for the love and care that you have given me as I have grown into an adult. I am beyond appreciative of the sacrifices you both have made. I would like thank you for instilling the value of an education in me. To my brothers, Sebastian, Chris, Brandon, and Taure, thank you for being just a phone call away whenever I needed anything. Thank you for the answers to my random question and being the best big brothers a little girl can have. To my nieces and nephews, I thank you for being the great children you are and reminding me to make the right decisions. To the rest of my family, thank you for your love and support. I am forever indebted to you.

I would like to thank my friends for all of their encouragement when I was unsure of myself. To Candace and Kenny, thank you for being integral parts of this journey.

To my research advisor, Dr. Jayne Garno, I am grateful for the opportunity you have given me to work, learn, and grow in your group. I am thankful for the guidance, compassion, and patience you have shown me over the years. I hope that I can be as successful as you at enriching the lives of your students.

Finally to the Garno research group both past and present, I would to thank you all for the research discussions, sounding board, and entertainment you have provided me through the years.

TABLE OF CONTENTS

LIST OF TABLES

LIST OF FIGURES

LIST OF ABBREVIATIONS

AFM	atomic force microscopy
Co-Por	cobaltacarborane porphyrin
CP-AFM	conductive probe atomic force microscopy
DNA	deoxyribonucleic acid
DPPC	dipalmitoylphosphatidylcholine
FM-AFM	frequency modulation atomic force microscopy
HEPES	4-(2-hydroxylethyl)-1-pipeazineethane sulfonic acid
HOPG	highly ordered pyrolytic graphite
I-V	current-voltage
MAC mode	magnetic AC mode
MPC	monolayer protected clusters
ODT	octadecanethiol, $CH_3(CH_2)_{17}SH$
OTS	octadecyltrichlorosilane
PBS	phosphate buffered saline
SAM	self-assembled monolayer
SECM	scanning electrochemical microscopy
SPL	scanning probe lithography
SPM	scanning probe microscopy
STM	scanning tunneling microscope
TM-AFM	tapping mode atomic force microscopy
UME	ultramicroelectrode
UPD	underpotential deposition

ABSTRACT

Porphyrins and metalloporphyrins have unique chemical and electronic properties and thus provide useful model structures for nanoscale studies of the role of chemical structure for electronic properties. Porphyrins have been proposed as viable materials for molecular-based information-storage devices, gas sensors, photovoltaic cells, organic light-emitting diodes and molecular wires. The function and efficiency of porphyrins in devices is largely attributable to molecular architecture and how the molecules are self-organized. Modifications of the porphyrin macrocycle, peripheral groups or bound metal ions can generate a range of electrical, photoelectrical or magnetic properties. The conductive properties are greatly influenced at the molecular level by the organization of porphyrins into supramolecular arrays, aggregates, and nanocrystals on surfaces.

Conductive-probe atomic force microscopy (CP-AFM) has been used extensively for studies of alkanes, phenylalkanes and arenethiols; however, the conductive properties of porphyrins have not been studied as rigorously. Characterizations with CP-AFM are becoming prevalent for molecular electronics studies because of the dual capabilities for obtaining physical measurements and structural information with unprecedented sensitivity. For CP-AFM, the tip is placed directly on the sample surface, at a designated force. To acquire current-voltage (I-V) spectra, a conductive tip is grounded, and a bias is applied to the substrate.

For this dissertation, cobaltcarborane porphyrins were synthesized using a ring-opening zwitterionic reaction to produce isomers with different numbers of carborane clusters per macrocycle. Particle lithography was used to prepare regular arrangements of well-defined nanopatterns of porphyrin nanocrystals on conductive substrates. Nanopatterned SAMs of alkanethiols and organosilanes were used successfully to direct the nanocrystals of porphyrins on

the surface and characterized with contact and tapping mode imaging of AFM. Our goals were to elucidate the role of molecular structure, packing and orientation for the conductive properties of porphyrins. Understanding how the self-organization and surface assembly influence electrical properties and reliable measurements of conductive properties when these molecules are coordinated to different metals and surfaces will provide information for developing predictive models.

CHAPTER 1: INTRODUCTION

The research goals of this dissertation were to study surface reactions and material properties at the nanoscale, approaching the level of molecular measurements using scanning probe microscopy (SPM). Experiments were designed for studying organic thin films and nanocrystals of cobaltacarborane porphyrins as potential molecular electronic materials. Nanolithography methods were developed using approaches with particle lithography, as a strategy for preparing well-defined surface test platforms of regularly arranged nanostructures. Molecular self-assembly was achieved with basic steps of solution chemistry, heating, drying and centrifugation to prepare periodic arrangements of exquisitely small, regular nanostructures of well-defined chemical composition. The test structures of porphyrins and self-assembled monolayers furnish an ideal test platform for successive measurements with measurement modes of SPM.

Particle lithography is a generic approach for preparing nanopatterns on surfaces using monodisperse mesospheres of latex or colloidal silica. A film of mesospheres is used to provide either an evaporative mask or a structural template to prepare nanopatterns of selected materials. Different size particles can be used to control spacing, density, surface coverage, and sizes of the nanopatterns. Using particle lithography, planar arrays of porphyrin nanostructures were prepared within an insulating matrix layer of *n*-alkanethiol surrounding the nanopatterns. Conductive-probe atomic force microscopy (CP-AFM) has been used extensively for studies of alkanes, phenylalkanes and arenethiols; however, the conductive properties of porphyrins have not been as rigorously studied. Characterizations with CP-AFM are becoming prevalent for molecular electronics studies because of the dual capabilities for obtaining physical measurements and

structural information with unprecedented sensitivity. The investigations in this dissertation examine different properties of cobaltacarborane porphyrins.

1.1 Liquid Imaging using Atomic Force Microscopy

Atomic force microscopy (AFM) is a versatile analytical technique that can be used to accomplish an array of surface science measurements at the nanoscale. Applications for AFM measurements include fields such as chemistry, electronics, material science, medicine and cellular studies. Optical microscopes are limited by the wavelength of light and cannot reach the atomic resolution that can be routinely achieved with AFM. Electron microscopies often require complex steps for sample preparation and use vacuum environments. Accomplishing AFM studies in liquid offers advantages for the analysis of different samples *in situ* in ambient environments. Atomic resolution images of lattice structures, chemical reaction information, and studies of protein-protein interactions can all be obtained using AFM in liquid. Chapter 2 of this dissertation highlights the advantages of liquid AFM for a wide range of studies and applications.

1.2 Conductive Probe Atomic Force Microscopy

Chapter 3 provides experimental details of specific modes of AFM used for this dissertation. Conductive-probe atomic force microscopy (CP-AFM) has been used extensively for studies of electronic materials. Two types of information are provided with CP-AFM: current maps of the conductivity of samples can be acquired at a fixed sample bias; and I-V spectra can be obtained by sweeping a specified voltage range. For CP-AFM, the tip is placed directly on the sample surface, at a designated force. To acquire current-voltage (I-V) spectra, a conductive tip is grounded, and a bias is applied to the substrate. Current flow is measured between a biased metal-coated cantilever and a conductive substrate. Characterizations with CP-AFM provide capabilities for obtaining physical measurements and structural information with unprecedented sensitivity.

1.3 Charge Transfer Studies of Cobaltacarborane Porphyrins using CP-AFM

The molecular-level organization of porphyrin films on surfaces is known to greatly influence the conductive, photoemissive and photovoltaic properties of devices. A wide range of surface structures can be generated for porphyrins when samples are prepared *ex situ,* depending on slight changes in protocols for sample preparation. Understanding the structural organization and stability of porphyrins and metalloporphyrins on surfaces is essential for development of new technologies for optical, photovoltaic and magnetic device applications. Various systems of porphyrins have been demonstrated to form supramolecular assemblies, arrays, aggregates or crystals. Using conductive probe atomic force microscopy, (CP-AFM) we have investigated changes in charge transport for porphyrins with four to sixteen carborane clusters per macrocycle.

Conductive probe-AFM is accomplished by applying a certain bias voltage to the sample and measuring the current with a metallized probe. Topography and current images are simultaneously acquired by scanning in contact mode with a fixed bias. The topography frames provide height information about the surface morphology while the current images furnish sensitive maps of the conductive domains of the samples. Local current versus voltage (I-V) spectra can be acquired with CP-AFM for porphyrin thin films on conductive or semiconductive substrates. Changes of surface morphologies and conductive properties for cobaltacarborane porphyrins with different molecular designs are reported in Chapter 4.

1.4 Porphyrin Crystals Patterned with Particle Lithography

Porphyrins and metalloporphyrins have unique chemical and electronic properties and thus provide useful model structures for studies of the role of chemical structure for nanoscale electronic properties. The electronic and photophysical properties of porphyrins depend on the organization and spatial orientation of the molecules within surface films at the nanoscale, as well as the nature of the appended substituents and overall architecture of molecular structures.

Combining nanolithography with conductive probe measurements has advantages for rapidly constructing and testing the conductive properties of molecular systems, such as porphyrins. Particle lithography with monodisperse mesospheres of latex or silica provides a generic approach for preparing nanopatterns on surfaces. The spheres are removed from substrates by steps of rinsing and sonication. The spacing, density, surface coverage, and sizes of the porphyrin nanostructures can be controlled by selecting the diameter of the mesoparticles. A strategy was developed for preparing test structures for CP-AFM which incorporates a silane matrix as a reference, for standardizing measurements between different experiments. In Chapter 5, nanolithography was used to create well-defined test platforms of cobaltacarborane porphyrins for surface measurements.

1.5 Future Prospectus

Chapter 6 provides a conclusion and future prospectus for the research presented in this dissertation.

CHAPTER 2: SURFACE CHARACTERIZATION USING ATOMIC FORCE MICROSCOPY (AFM) IN LIQUID ENVIRONMENTS

2.1 Introduction

An intrinsic advantage of atomic force microscopy (AFM) is the flexibility to conduct experiments in different media such as in ambient air, vacuum, or in liquid environments. The capability to introduce liquids to the sample cell and acquire images in fluids broadly expands the repertoire of experimental designs, particularly for studying nanoscale changes to surfaces by capturing AFM images as reactions proceed. For example, liquid AFM has been applied for *in situ* studies of the effects of different liquid media, such as with changes in pH or concentration of ions.[1-4] Liquid media has been used for AFM studies with biological systems in aqueous buffers that simulate physiological conditions,[3,5] for *in situ* studies of electrochemical reactions,[6,7,8] and for time-lapse imaging of progressive surface changes caused by chemical reactions.[9-11] In liquid media, new molecules can be introduced to the sample cell to enable AFM-based nanofabrication.[12] Accomplishing AFM experiments in liquid media also provides advantages for improving resolution, since imaging in liquid reduces or eliminates capillary and van der Waals forces between the tip and sample.[13] Liquid imaging reduces sample perturbation and minimizes or prevents damage caused by shear forces between the tip and surface. This chapter will describe state-of-the-art advances with AFM for designing creative experimental approaches for nanoscale studies in liquid media.

2.2 Theory - Background

2.2.1 History of Atomic Force Microscopy (AFM)

The development of scanning probe instruments during the 1980's has launched entirely new experimental approaches for nanoscale studies and has made pivotal contributions to the interdisciplinary field of nanoscience. Before 1980, there were no instruments with capabilities for

visualizing surfaces at the level of individual molecules or atoms. The operating principle for AFM is based on scanning a small probe across the surface and requires positional control at the nanoscale. The precedent for scanning probe methods was developed by Heinrich Rohrer and Gerd Binnig, who were awarded the 1986 Nobel prize in physics for invention of the scanning tunneling microscope (STM).[14] The first STM was developed at IBM Zurich Research Laboratories in Switzerland and resolved the 7×7 lattice arrangement of silicon atoms for Si(111). Imaging with STM is based primarily on electrical interactions between a conductive tip and the sample, whereas AFM imaging is reconstructed from the mechanical deflection of the probe due to physical forces. Positional control for AFM, STM and other scanning probe methods rely on the piezoelectric effect, which enables precise movement of the probe with angstrom-level control.

The first AFM instrument was introduced in 1986 by Binnig, Quate and Gerber of Stanford University in California, to measure any type of force on an atomic scale.[15] They introduced the first general-purpose AFM instrument for measuring ultra-small forces as low as 10^{-18} N. The resolution that can be obtained with AFM today is comparable or better than that achieved with STM.[16] Unlike STM, imaging with AFM is not restricted to conductive or semiconductor surfaces. The significance of scanning probe instruments is evidenced by diverse applications throughout the science disciplines; nanoscale imaging and measurements with scanning probe instruments provide entirely new approaches for the study of matter at small size scales.

2.2.2 Early Benchmarks for Studies using Liquid AFM

The first AFM experiments were accomplished in air, to probe the surface of a ceramic sample of aluminum oxide (Al_2O_3), achieving lateral resolution of 30 Å and vertical resolution of less than 1 Å.[15] The first AFM experiments in liquid were reported in 1987 by Marti, Drake and Hansma, for surfaces of sodium chloride and highly oriented pyrolytic graphite (HOPG) that were covered in paraffin oil.[16] These experiments resolved the hexagonal packing arrangement of

carbon atoms, achieving lateral resolution of 0.15 nm and vertical resolution of 5 pm.[16] The applicability of AFM in liquid environments for imaging biological molecules was first demonstrated by Drake et al. in 1989.[17] Studies of chemical and biological processes in liquids have continued to progress, setting benchmarks for nanoscale resolution with investigations of corrosion, electrochemical reactions, self-assembled monolayers (SAMs), as well as deoxyribonucleic acid (DNA), proteins, and cells.[18-19]

2.3 Experimental Setup and Method

2.3.1 Basic Operating Principle of AFM

Unlike traditional optical microscopes, scanning probe instruments use a sharp probe that is scanned over the sample to acquire spatial maps of surface characteristics. The interactions between the tip and the sample are mapped to construct images at scales from microns to nanometers. The cantilever is typically made of silicon or silicon nitride with a tip radius of nanometers. The resolution of scanning probe measurements is not limited by the wavelength of light, and can achieve unprecedented nanoscale resolution. For AFM imaging, light from a diode laser is focused on the back of a cantilever and deflected toward a photodiode detector (Figure 2.1). The photodiode detects the cantilever deflection by tracking the position of the reflected beam. An electronic feedback loop controls voltages to the piezoceramic scanner to maintain a constant force between the tip and sample. There are several designs that have been used for positional feedback with AFM. The optical deflection set-up shown in Figure 2.1 is the most common configuration. Other approaches that have been used for monitoring tip position include optical interferometry,[20] capacitive sensing,[21] tuning forks,[22-23] and piezoresistive cantilevers.[24]

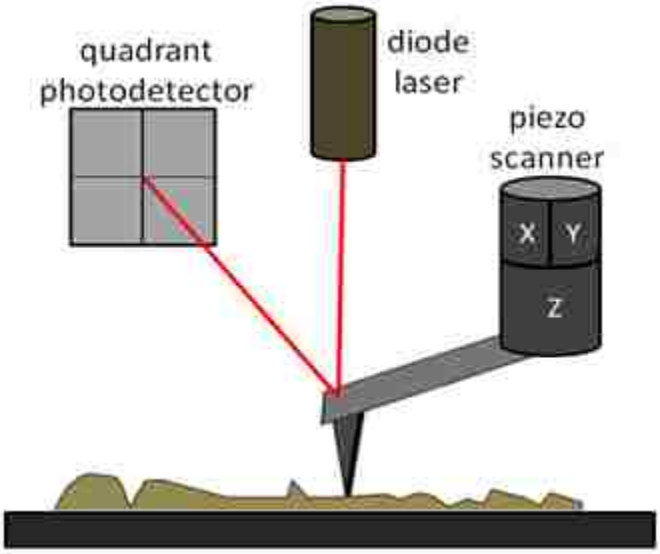

Figure 2.1 Laser-deflection configuration used for AFM imaging

The lattice arrangement of atoms can be visualized with AFM, providing views of molecular and atomic vacancies and adatoms.[25] The atomic lattices of substrates such as Au(111), highly oriented pyrolytic graphite (HOPG) and mica(0001) are commonly used for lateral calibration of X-Y dimensions. The heights of gold steps are used for calibration of Z dimensions. Images generated by AFM are true three-dimensional surface profiles. Samples do not require special treatments or coatings which alter their composition. Both conducting and insulating materials have been imaged with AFM. A vacuum environment is not required for AFM studies, and samples may be imaged in air or in liquid media.

Two basic instrument designs are possible for AFM imaging. The cantilever can be attached to the piezoscanner for scanning the tip across the sample surface; or the sample can be scanned across the probe, while the tip is held in a fixed position. There are also instrument designs which combine approaches for both tip and sample translation. The sample cell can be filled with various solvents to accomplish liquid imaging or for electrochemical AFM studies. As the tip is translated across the sample, forces between the tip and the sample cause changes in the deflection

of the AFM cantilever. Depending on the instrument configuration, the types of forces that can be measured include adhesive or repulsive forces attributable to van der Waals interactions, chemical bonding, mechanical friction, electrostatic charge, or magnetic interactions. The tip can be operated in continuous direct contact with the surface (contact mode) or at a certain fixed distance from the surface (non-contact mode). For intermittent or "tapping" mode AFM (TM-AFM), the tip is driven to oscillate in and out of contact with the surface. The feedback signal for controlling the probe position with TM-AFM is obtained by maintaining a constant amplitude setting for tip deflection, rather than using a force set point. Tapping-mode-experiments can be operated in liquid media, which is particularly useful for imaging fragile systems of biomolecules in buffered media.

2.3.2. Approaches for Liquid Imaging

Initial AFM liquid experiments were accomplished by simply placing a drop of liquid on the AFM tip, and focusing the laser through the liquid interface. Of course, the solvents chosen for liquid experiments should be optically transparent, and must have a relatively slow rate of evaporation, e.g. water, ethanol, butanol or hexadecane. The solvent must be compatible and nondestructive for the sample material; for example, it should not cause dissolution or corrosion of the surface. Sample cells for liquid imaging have been designed with either open or closed containment of liquids. If the liquid cell has a cover, the laser is focused through both the cover and liquid to reflect on the surface of the probe. Closed cells have been constructed using machined transparent materials such as glass,[9, 17] quartz or plastic.[26-27] An example design for an open liquid cell is shown in Figure 2.2, incorporating a metal spacer sealed with an O-ring gasket to encompass a small volume of liquid. A disadvantage of the open cell design is that liquids can evaporate over time, and must be replenished at frequent intervals. Depending on the design, the volume of liquid contained in the cell ranges from 50 μL to several milliliters.

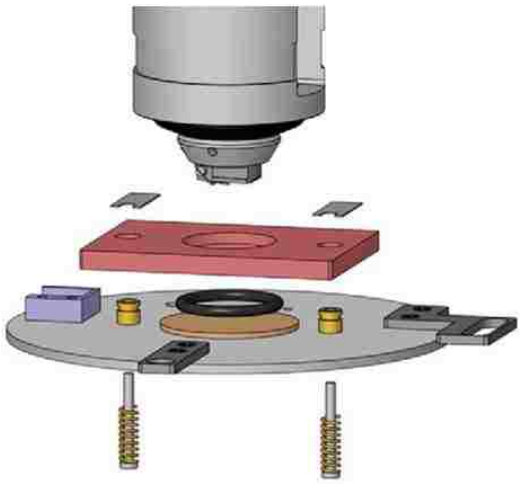

Figure 2.2 Design of a metal sample cell assembly for AFM imaging in liquid media. (*Printed with permission from Agilent Technologies, Inc.*)

2.4 Application of AFM in Liquids

When an AFM probe and sample are submerged in liquid media, predictable changes occur for experimental parameters due to alterations of tip-sample interactions. For example, image resolution can be improved because capillary and van der Waals forces between the tip and sample are reduced or even eliminated.[13] Depending on the viscosity, dielectric constant, conductivity, polarity or pH parameters of the liquid media, experimental conditions can be tuned to control tip-surface interactions. Liquid imaging conditions can reduce sample perturbation and will minimize or prevent damage caused by shear forces between the tip and surface. Also, liquid media can dampen vibrations, leading to reduced acoustic noise from the background. A direct comparison of the changes in vibration were shown by Kiridena et al. and Jourdan et al. who obtained frequency spectra for a free cantilever in air versus liquid media (sec-butanol).[28-29] When a tip was immersed in solvent, frequency spectra reveal that the natural resonance frequency of the cantilever was shifted downfield, and the damping effects of the liquid served to overall reduce the vibration of the tip.

2.4.1 High Resolution AFM Imaging in Liquids

When imaging in liquids, AFM resolution can be improved to disclose subtle details of surface morphology at the molecular-level. A direct comparison of frames acquired in ambient air to views that were captured in liquid media using the same probe are shown in Figure 2.3, for the surface of a mixed monolayer of decanethiol and tetradecanethiol (prepared overnight in1 mM ethanolic solution, 3:1 molar ratio). For this example, the probe was first used to acquire high resolution views in ambient air, and then liquid media (sec-butanol) was injected into the sample cell. The sample is not a pure SAM, rather it is a mixture of *n*-alkanethiols with different chain lengths, differing by ~ 0.4 nm in height. In either air or liquid, the heights of single steps of the Au(111) substrate can be readily differentiated. However, the segregation of the different SAM domains is not resolved for the images acquired in air (Figures 2.3A-2.3C). The images were acquired using contact-mode AFM, and the shapes of the underlying gold terraces and step edges are clearly viewed for all of the topography frames of Figure 2.3. The views of broad areas in Figures 2.3A and 2.3D are quite comparable in resolution; however, as the magnification is increased the images obtained in liquid reveal differences in the nanoscale topology of the surface of the SAM. The images in ambient air (Figures 2.3B and 2.3C) do not reveal the different domains of the decanethiol and tetradecanethiol SAMs. When the images were acquired in sec-butanol (Figures 2.3D-2.3F) subtle changes in height are resolved throughout the flat terrace areas, as well as the details of the lacey contours of the gold step edges. Looking closely at Figure 2.3F with a small scan size of 250 nm × 250 nm, the mottled composition of the binary mixture of SAMs is visible. When imaging in air there are attractive capillary forces operating between the tip and surface leading to overall higher forces used for imaging. Liquid media enables the use of smaller forces as well as reducing the stick-slip adhesion forces, to provide higher resolution imaging.

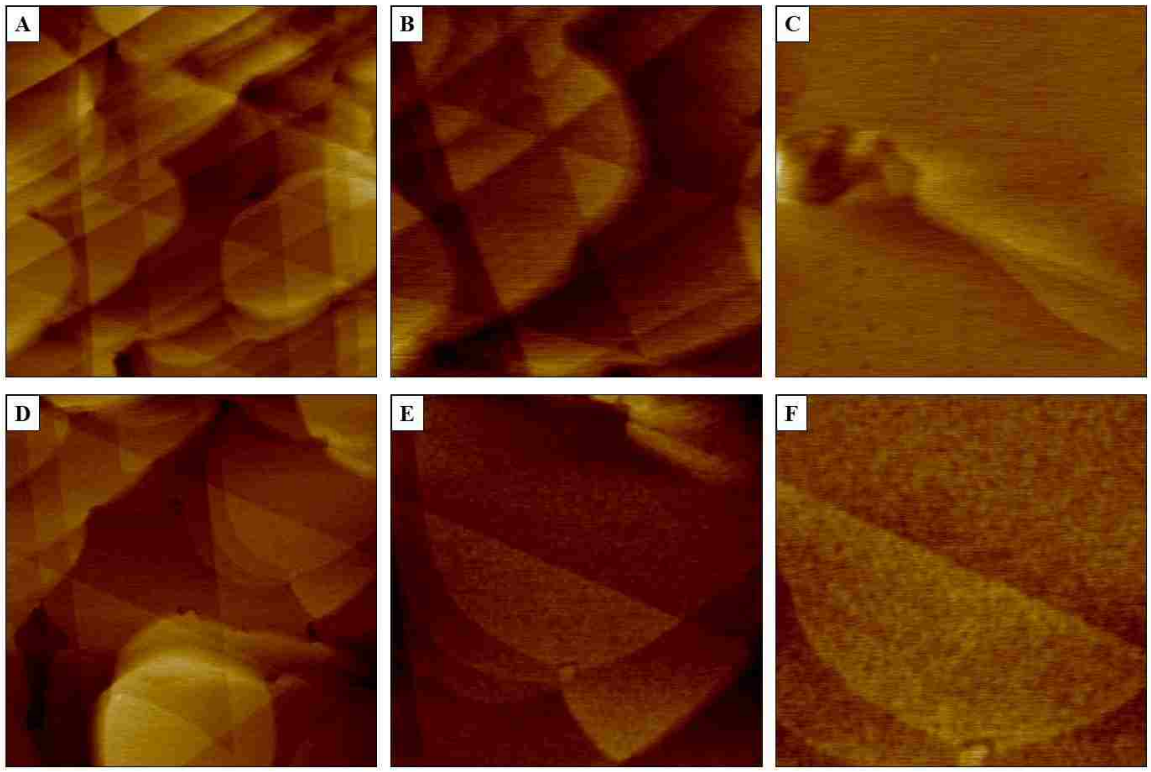

Figure 2.3 Successive zoom-in views of the surface of a two-component monolayer for comparison of AFM resolution in air versus in liquid. Topography frames of a mixed SAM of decanethiol and tetradecanethiol imaged with contact mode in air (A) 1×1 μm2; (B) 500 × 500 nm2; (C) 250 × 250 nm2. Topography frames acquired for the same sample and probe in 2-butanol (D) 1×1 μm2; (E) 500 × 500 nm2; (F) 250 × 250 nm2.

Dynamic changes can cause AFM imaging in liquid media to be difficult, since surface features can change dimensions at the molecular-level when exposed to liquids. This is dramatically illustrated in Figure 2.4, for multilayered ring nanostructures of octadecyltrichlorosilane (OTS). The ring nanostructures were prepared *ex situ* using latex particle lithography and vapor deposition.[30] Similar to the protocol for Figure 2.3, the nanostructures were first imaged in ambient air (Figures 2.4A-2.4B), then liquid media (ethanol) was introduced without changing probes. An increase in the dimensions of the nanostructures is apparent in the AFM views of Figures 2.4C-2.4D, caused by changes in the physical size of the OTS rings. Rather dramatic changes in the lateral dimensions of the nanostructures are revealed for AFM topography frames acquired in liquid media. The width of OTS nanopatterns in dried condition measured 245

± 16 nm. However, after exposure to ethanol, the sizes of the rings were observed to swell by tens of nm, to measure 293 ± 33 nm. The height of the nanostructures appears to have only increased slightly. The methyl-terminated OTS nanostructures consist of an alkane backbone of hydrocarbon chains with bridging links of Si-O-Si bonds, as well as non-bridged free silanol Si-OH groups which change size upon wetting. The sides of the designed ring nanostructures present a 3D interface for studying the interaction of solvents with molecular side groups.

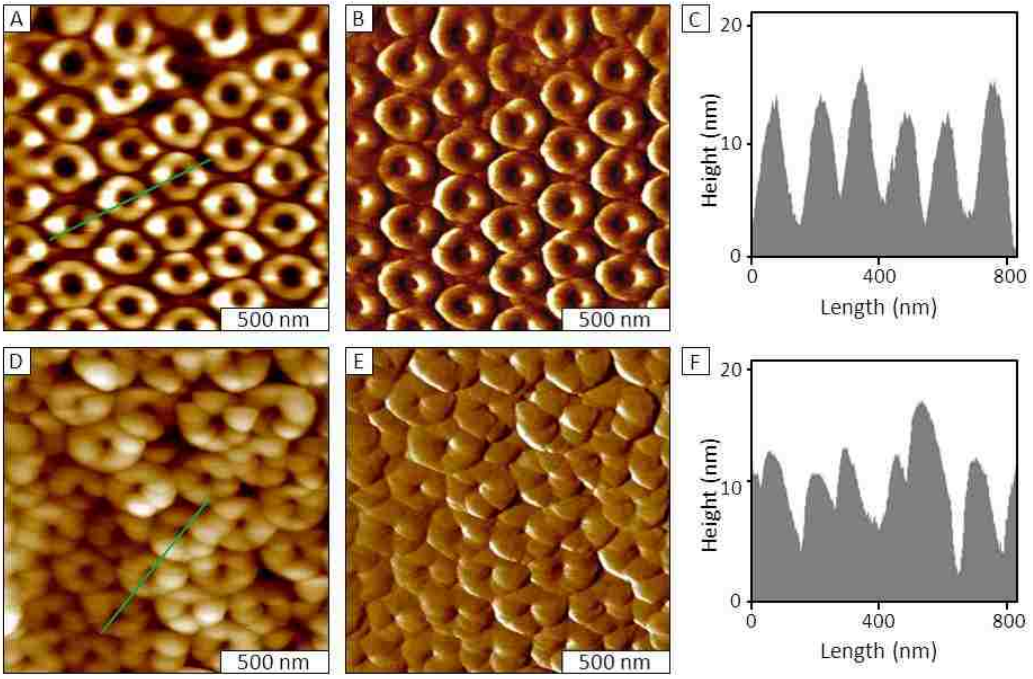

Figure 2.4 Immersion in ethanol changed the surface morphology of OTS ring nanostructures. (A) Topography and (B) lateral force images acquired in air using for contact mode AFM in ambient air. (C) Cursor profile for the line in ***A***. (D) Topography and (E) lateral force images acquired in ethanol using the same probe. (F) Cursor profile for the line in ***D***.

Atomic and molecular lattices have been resolved using contact mode AFM in liquid media. High resolution images acquired using contact mode AFM in liquid media for a cleaved dolomite (104) surface were demonstrated by Pina et al.[31] The images of dolomite obtained in water disclose lattice structures with surface unit cell dimensions in close agreement with that of the bulk structure. Views of HOPG surfaces covered with liquid parafilm oil were resolved at the

atomic scale with contact mode AFM by Marti et al.[16] Molecularly resolved views of *n*-alkanethiol SAMs can be achieved routinely with liquid AFM in solvent media.[25, 32-33]

Other AFM imaging modes can be accomplished in liquid media to combine the benefits of liquid imaging with dynamic protocols such as tapping mode,[34-36] force modulation[28-29, 37] or frequency modulation[38] configurations. Dynamic modes of AFM furnish additional information acquired concurrently with topography frames for mapping chemical groups or mechanical properties measurements, such as elastic response or viscoadhesion.

Atomic resolution of surfaces has been demonstrated with developments with frequency modulation AFM (FM-AFM) in liquid. A reduction of the cantilever oscillation amplitude to the range of 0.2-0.3 nm enhanced the sensitivity of the frequency signal to provide atomically resolved images of poly(*p*-toluenesulfonate) crystals in water.[38] Atomic features of a cleaved muscovite mica(0001) surface exhibiting large-scale corrugations and adsorbates were acquired using FM-AFM in water.[39] The cleavage plane of calcite was characterized in aqueous media using FM-AFM with atomic resolution, to resolve protruding oxygens of the carbonate groups attributed to zigzag patterns along the [421] direction of the calcite(104) surface.[40] High resolution capabilities of FM-AFM have been used to study biological surfaces in buffers, such as phospholipid/cholesterol mixed bilayers[41] and amyloid fibrils.[42]

2.4.2 Measurement of Surface Forces in Liquid Media

For AFM operation with contact mode in air, there are often substantial forces present attributable to tip-surface adhesion, due to capillary forces, friction, and stick-slip adhesion, in the range of 100 nN.43 By immersing both the tip and sample in liquid, the meniscus forces are greatly

reduced.44 Changes of the forces acting on the tip in liquid and in air are demonstrated in Figure 2.5 with representative force-distance curves. Using the same probe, an uncoated silicon nitride tip was brought into contact with the methyl-terminated surface of a dodecanethiol SAM in air (Figure 2.5A) and then immersed in ethanol (Figure 2.5B). Force curves are a plot of cantilever deflection as a function of sample position along the z-axis. Forces are not measured directly, but rather are calculated using the stiffness of the cantilever according Hooke's law relationship to derive values from the measured deflection of the lever. The approach-retreat cycle of typical force-distance curves obtained in air (Figure 2.5A) and in liquid (Figure 2.5B) show changes for the pull-off or retraction portion of the measurement. The capillary forces of attraction are

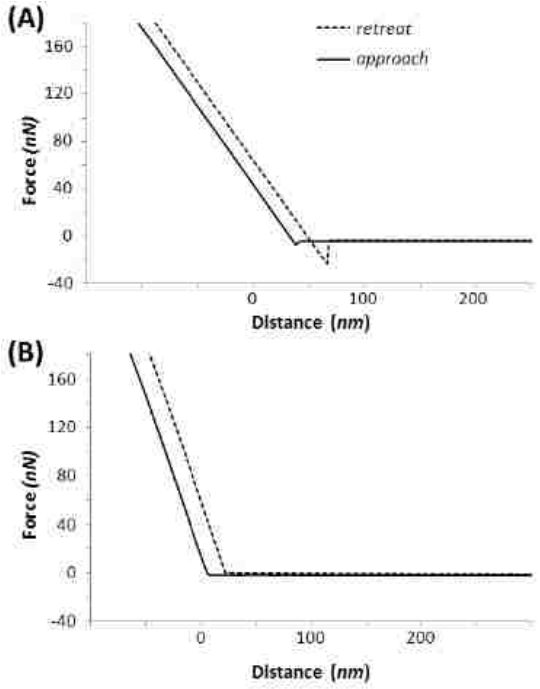

Figure 2.5 Force versus distance curves for contact mode AFM acquired in (A) air and (B) liquid.

substantially decreased when the tip is operated in liquid media (Figure 2.5B).

Force measurements with AFM have emerged as a standard tool for nanoscale physical characterizations for many disciplines.[45] Molecular-level measurements of adhesion forces for biomaterials have become a significant research focus for biological AFM studies.[46] Forces can be

measured with piconewton sensitivity for either specific or nonspecific protein-protein and receptor-ligand interactions, for measuring interactions between cells, and for measuring viscoelastic properties of biomaterials. For these measurements, a force versus distance curve is generated using an AFM probe that is coated with proteins such as antibodies, enzymes or desired functional groups. Imaging in liquid media can be less destructive for soft and sticky biological samples, and provides a means to study effects of pH and electrolyte concentration. The coated probe is brought into contact with the sample and then withdrawn from the surface to generate a plot of the interaction forces as a function of tip displacement. For a typical approach-retreat measurement cycle, the bending of the cantilever is monitored as the probe is brought in and out of contact with the surface. The coated probe will adhere to the sample as it is withdrawn from the surface, often with multiple pull-off points for aggregate samples. The magnitude of this adhesive force can be calculated to provide estimates of molecular bond rupture forces. Changing the pH or ionic strength of the imaging buffer is useful for studying changes for tip-protein interactions as a function of surface charge.

2.4.3 *In situ* Studies of Chemical Reactions with Liquid AFM

Creative experimental designs with *in situ* AFM have employed liquid media to view molecular changes that take place on surfaces over time during the course of chemical reactions. For example, beginning with clean substrates, the adsorption and self-organization of molecules can be viewed with time-lapse AFM images,[9, 47-50] and antigen-antibody binding processes have been monitored with liquid AFM studies.[51-52] Surface or material changes that occur with modification of pH or ionic strength can be studied with liquid AFM, in combination with electrochemistry measurements.[4, 53]

An example time-lapse experiment showing step-by-step views of the unconstrained assembly of *n*-alkanethiol molecules onto Au(111) is shown in Figure 2.6, for octadecanethiol

(ODT).[9,25] Molecular-level studies were accomplished *in situ* by immersing freshly prepared gold substrates in a dilute solution of ODT (0.2 mM) in 2-butanol within a liquid cell. Detailed structural information of the kinetics and surface changes during adsorption is revealed as time elapsed (Figures 2.6A-2.6I). An adventitious adsorbate (the bright spot) and several Au(111) single atomic steps in the lower left region of the images furnish convenient landmarks as a frame of reference for *in situ* imaging (Figure 2.6A). In 2-butanol, molecules of ODT initially adsorb on gold with the molecular axis of their hydrocarbon chains oriented parallel to the surface in a side-on

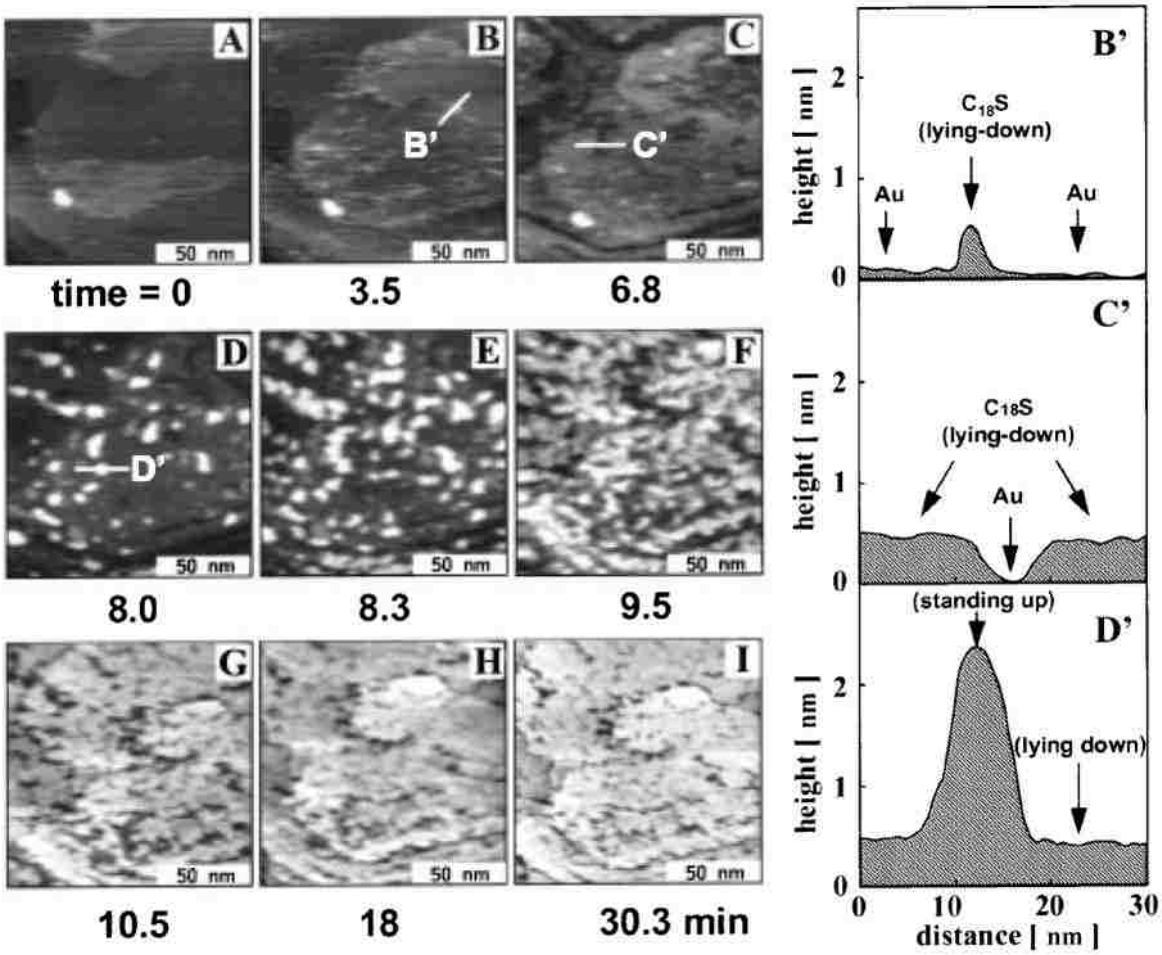

Figure 2.6. Surface chemical reaction viewed *in situ* with time-lapse AFM imaging in liquid. Topography images of the self-assembly of ODT onto freshly prepared Au(111) acquired in 2-butanol. (A-I) Topography images acquired at different time points and (B', C',D') corresponding height measurements of adsorbates. A small bright spot and several gold steps in the lower left region of the image furnish convenient landmarks for *in situ* imaging. (*Reprinted with permission from ref.* [9])

configuration (Figures 2.6B and 2.6C). Over time, the surface coverage increases to near saturation and a phase transition takes place to reveal taller islands composed of upright molecules with the axis of the hydrocarbon backbone oriented ~30° from the surface normal (Figures 2.6D and 2.6D'). Continued exposure over time produces a greater density of these islands and the growth of these nuclei until a SAM is formed with a $\sqrt{3}\times\sqrt{3}R30°$ commensurate structure. *In situ* AFM studies were conducted for different chain lengths, (C10, C22, and C40) to disclose the kinetics and mechanisms of phase transitions for *n*-alkanethiol self-assembly.[9] Measurements revealed that the self-assembly of longer chain length alkanethiols occurred more rapidly and produced a more complete film in comparison to shorter alkyl chains.[9] Studies were also conducted using liquid AFM for the coadsorption of mixtures of *n*-alkanethiols at different molecular ratios and chain lengths, to reveal differences in domain sizes and surface composition.[54]

2.4.4 Electrochemistry Studies with AFM in Liquids

A method known as scanning electrochemical microscopy (SECM) was developed to combine the AFM capabilities of mapping surfaces for electrochemical studies in a liquid cell.[55] Measurements of electron, ion and molecular transfer can be probed with SECM for applications ranging from corrosion to ion transport across cell membranes.[56-57] Representative examples are summarized in Table 2.1. Typically, a system of three electrodes is used for electrochemical AFM studies, with the substrate serving as the working electrode.[6, 11, 58] A microfabricated probe with diameter of 10 μm or less is used as an ultramicroelectrode (UME) for SECM experiments in an electrochemical cell, while operated in non-contact mode, commonly using the shear force mode of positional feedback.[7] The resolution of SECM is on the order of 100 nm, depending on the size of area probed beneath the UME.

Table 2.1 Representative studies with SECM in liquid media.

System/processes studied	Substrate(s)	Ref.
copper electrodeposition by UPD	Pt(100) and Pt(111)	6
polycarbonate membrane, living diatoms	glass slide, constant current mode	7
copper electrodeposition by UPD	Au(111) in different electrolyte solutions	8
track-etched polycarbonate ultrafiltration membranes	glass disk	57
bacterial outer membrane protein F	HOPG, MoS_2, Au, Pt	59
electron-transfer reactions for glucose oxidase	nylon 66 membranes, hydrogel membranes, glass slides	60
anodization of porous alumina	aluminum in a fluid cell	61
galvanic electrodeposition of Pd and Pt particles	flame-annealed gold substrates	62
corrosion of aluminum in chloride solution	aluminum alloys	63
kidney cells in culture medium	petri dish	64
films of DNA in redox solutions	Si(111) wafers	65
electrodeposited patterns of conductive polymer polyaniline	gold, platinum, carbon surfaces	66
redox-active dendrimers mapped by SECM	functionalized glass substrates	67
Lead underpotential deposition studied *in situ*	Au(111)	68
anodic dissolution of a gold microelectrode	indium-tin-oxide	69
surface patterning using click chemistry by SECM	azido-functionalized glass substrates	70

Processes of the underpotential deposition (UPD) of metals have been studied with electrochemical AFM.[6, 8] For these experiments, the structure of the electrodeposited layer of metal cations is mapped while the substrate is maintained at a potential that is under the equilibrium potential of the metal. Scanning probe-based patterning experiments can be accomplished with SECM; microstructures have been fabricated using the local interactions of SECM with UPD or electropolymerization reactions. Voltages are applied between the tip and substrate to enable patterning in liquid media containing reagents for designed local reactions. Atomic resolution was achieved with electrochemical AFM for the investigation of the UPD of copper on Au(111) in a sulfate solution by Manne et al.[8] The atomically resolved structures revealed differences in lattice packing for different electrolyte solutions. Further experiments with electrochemical AFM have been recently reviewed, and applications include studies of electron transfer kinetics, electrocatalysis as well as mass/charge transfer reactions.[56]

2.4.5 Nanofabrication with AFM in Liquid Media

Nanoshaving and nanografting are scanning probe-based lithography approaches which are used to rapidly and reproducibly write nanopatterns of thiol SAMs and other nanomaterials in liquid media. Commercial scanning probe instruments typically provide software to control the speed, direction, length and applied force of the scanning motion of a tip. To accomplish nanoshaving, the tip is used to scratch or scrape away adsorbates under high force for designated areas. For nanoshaving in liquid, the surrounding solvent media can facilitate dissolution of the displaced material. When the liquid cell contains dilute solutions of new molecules, nanografted patterns can be inscribed. Nanografting was first introduced in 1997 by Xu et al. and is accomplished in liquid media by applying mechanical force to an AFM probe to produce nanopatterns within a matrix monolayer.[12] Under low force (less than 1 nN), high resolution AFM characterizations of surfaces can be acquired *in situ* without modification of the surface. The tip becomes a tool for nanofabrication only when the force applied to the probe is increased to a certain displacement threshold. Nanografting is accomplished by force-induced displacement of molecules of a matrix SAM, followed immediately by the surface self-assembly of molecules such as *n*-alkanethiols from the liquid media. The molecules to be patterned are dissolved within the surrounding liquid, whereas the substrates are precoated with a protective layer to prevent nonspecific adsorption of molecules throughout areas of the surface. Various surface chemistries can be designed by choosing SAMs of different lengths and terminal groups.

An example nanografted pattern prepared in ethanol media is shown in Figure 2.7, in which the grafted molecules of 1,8-octanedithiol are taller than the surrounding matrix monolayer of hexanethiol.[71] Under self-assembly conditions of nanografting with nanoscale geometric confinement, nanopatterns of α,ω-alkanedithiols written by nanografting form upright monolayers

directly with heights corresponding to a standing-up conformation to generate a surface presenting free -SH groups.

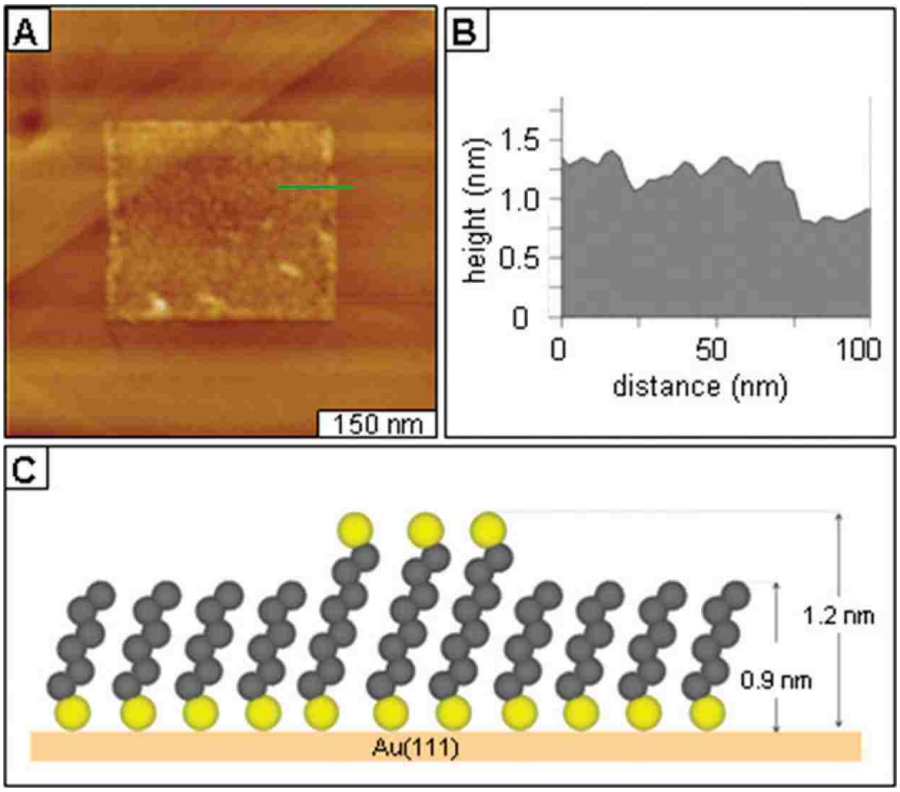

Figure 2.7 Square nanopattern of 1,8-octanedithiol nanografted within hexanethiol SAM in ethanol. (A) Contact-mode topography view of the pattern acquired in ethanol; (B) selected cursor profile for the line drawn in A; (C) model of molecular heights. (*Reprinted with permission from ref.*[72])

A different surface assembly mechanism takes place during nanografting due to spatial confinement to produce patterns directly with an upright conformation.[25] As the molecules of the matrix film are displaced underneath the tip, a transient microenvironment is generated exposing Au(111) for the simultaneous assembly of thiolated molecules. The assembly of nanografted organothiols bypasses the mobile "lying-down" phase due to spatial confinement between the surrounding matrix and the AFM probe; molecules from liquid media assemble immediately onto areas of the exposed substrate into a standing configuration because there is insufficient space on the surface for the molecules to assemble in a lying-down orientation.[25] Kinetic studies have

demonstrated that the spatially constrained self-assembly process occurs 10-fold faster than the unconstrained adsorption of organothiol SAMs.[25] A key requirement of nanografting is that *n*-alkanethiols chemisorb spontaneously to metal surfaces. The speed of the AFM tip influences the composition of the monolayers formed along the writing track. A kinetic Monte Carlo model of solution and nanografted deposition of *n*-alkanethiols on gold surfaces was reported by Ryu and Schatz, which reproduces experimental observations for the variation of the heterogeneity of written SAMs with the writing speed of an AFM tip.[73]

Designed patterns of hexanethiol molecules nanografted within a matrix of dodecanethiol/Au(111) are displayed in Figure 2.8, for an AFM liquid cell experiment conducted in ethanol.[74] Nine patterns of mouse ear designs that were shorter in height than the matrix SAM were prepared by inscribing concentric circles ranging from 40 to 210 nm in diameter (Figure 2.8A). A higher magnification view of a single pattern is shown in the topography frame (Figure 8B) and corresponding frictional force image (Figure 2.8C). Imaging in liquid media enables resolution of fine details such as etch pits, scars and step edges, even after the tip was used to inscribe multiple patterns. The depth of the patterns measured 0.7 ± 0.2 nm shown by a representative cursor plot (Figure 2.8D). The outline for writing the patterns is displayed in Figure 2.8E which indicates the designed tip trajectory when nanografting. For the experiments of Figure 2.8, each concentric ring was executed by tracing the AFM tip twice at an applied force of 4.8 nN.

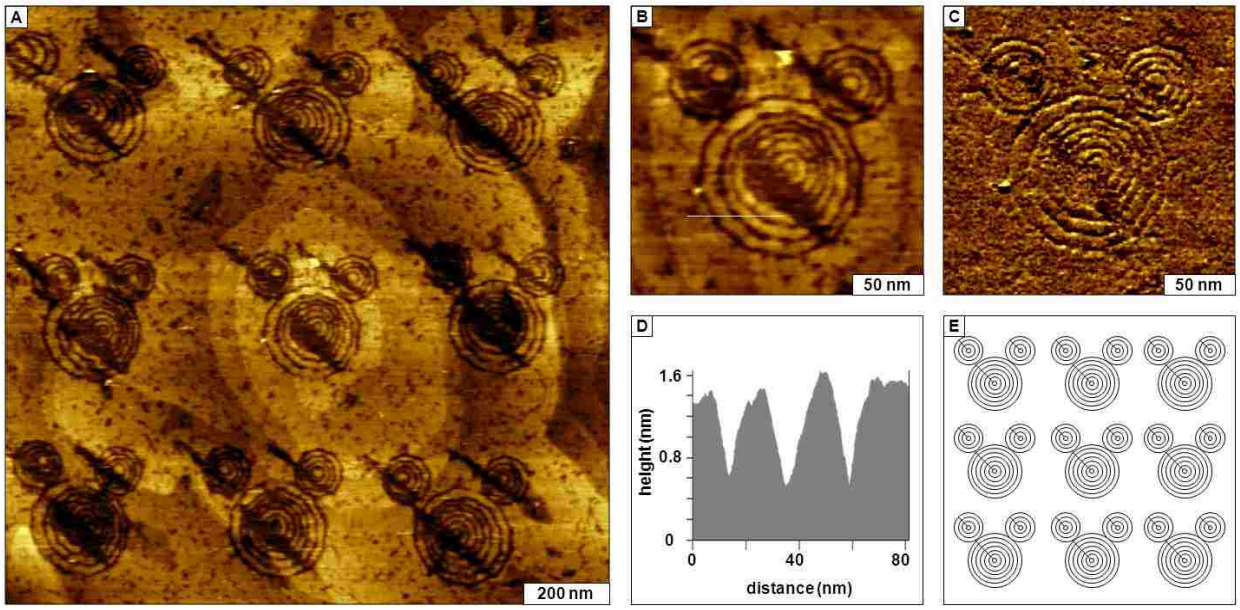

Figure 2.8 Patterns produced by nanografting hexanethiol within a dodecanethiol monolayer in ethanol. (A) Topography frame of 3×3 array of ring designs; (B) zoom-in topography and (C) lateral force frames of a single pattern; (D) cursor profile for line in ***B***. (E) Schematic used for the nanopattern design. (*Reprinted with permission from ref.* [74])

Examples of AFM studies with nanografting are summarized in Table 2.2 to show the diverse types of molecules and liquid media used for experiments. Since nanografting protocols are accomplished in liquid media, further successive chemical steps can be developed to introduce fresh reagents for 3-D fabrication of more complex nanostructures.[75-76] By combining nanografting and the designed spatial selectivity of SAM headgroups, *in situ* studies with nanografting in liquid media provides capabilities for studying surface reactions at the nanoscale. The spatial selectivity of the headgroups can be used in subsequent steps to direct the attachment of proteins,[51, 77] or for molecular assembly.[10]

Table 2.2 Representative experimental conditions and molecules studied with nanografting.

Year	Liquid media	Pattern headgroup	Nanografted molecule	Matrix film	Ref.
1997	2-butanol	CH_3	1-octadecanethiol	1-decanethiol	[12]
1999	2-butanol	CH_3	1-octadecanethiol	1-decanethiol	[32]
2002	decahydro-naphthalene	OH	11-mercapto-1-undecanal	1-octadecanethiol	[78]
2003	water	COOH	3-mercapto-1-propanoic acid	$C_{11}(EG)_6$	[79]
2003	water	OH	6-mercaptohexan-1-ol	$C_{11}(EG)_6$	[79]
2005	ethanol or 2-butanol	CH_3	Mixed *n*-alkanethiols 1-decanethiol and 1-octadecanethiol, 10:1	1-decanethiol and 1-octadecanethiol, 10:1	[80]
2005	2-butanol or = Poly-α-olefin oil	CF_3	$CF_3(CF_2)_9(CH_2)SH$	$HOC_6SH:C_{10}SH=2:1$	[80]
2006	ethanol,	CH_3	1-octadecanethiol	decanethiol	[81]
2006	2-butanol or hexadecane	CH_3	1-octadecanethiol	$C_{10}SH:C_{18}SH= 9:1$	[81]
2007	2-butanol	SH	1-decanedithiol	1-decanethiol	[82]
2007	2-butanol	SH	biphenyl 4,4'-dithiol	1-decanethiol	[82]
2008	ethanol	COOH	11-mercapto-1-undecanoic acid	1-octadecanethiol	[83]
2008	ethanol	CH_3	Dodecanethiol	1,9-nonanedithiol	[84]
2008	ethanol	SH	1,8-octanedithiol	hexanethiol	[84]
2008	ethanol	CH_3	1-hexanethiol	thiolated biotin SAMs	[85]

2.4.6 AFM Studies of Biological Samples in Liquids

Since biological processes take place in aqueous environments, liquid AFM offers *in situ* advantages compared to electron microscopy techniques when investigating biological samples. Using a liquid cell, biomolecules can be imaged in near-physiological, buffered conditions at ambient temperatures. The highest resolution reported for biological imaging with liquid AFM is on the order of 7 Å laterally, and ~1 Å for vertical resolution.[3, 86] In buffer solution, the pH and ionic strength of the imaging media can be adjusted to balance the van der Waals and electrostatic interactions between the tip and the sample.[3] Resolution is affected by the pH and ionic strength of the surrounding environment, which influences adhesive interactions between the tip and sample. To achieve high resolution imaging of biomolecules, Engel et al. describe a process for adjusting the pH and ionic strength of buffers to balance the van der Waals and electrostatic interactions between the tip and sample, at a loading force of 100 pN.[3] Conformational changes of

single biomolecules have been visualized for systems of membrane proteins such as bacteriorhodopsin, porin OmpF and aquaporin-Z using contact mode AFM in buffer.[3,87-89] Structures such as polypeptide loops, α-helices and β-strands of membrane proteins were identified within close-packed arrays of membrane proteins. Example high-resolution images of bacteriorhodopsin are shown in Figure 2.9, for raw AFM topography frames acquired in buffer using different load forces. The circled structures are surfaces of individual extracellular proteins with a trimer center. Sequences of AFM images were acquired and analyzed to provide insight for the nanomechanics and conformational

changes of membrane proteins.[3]

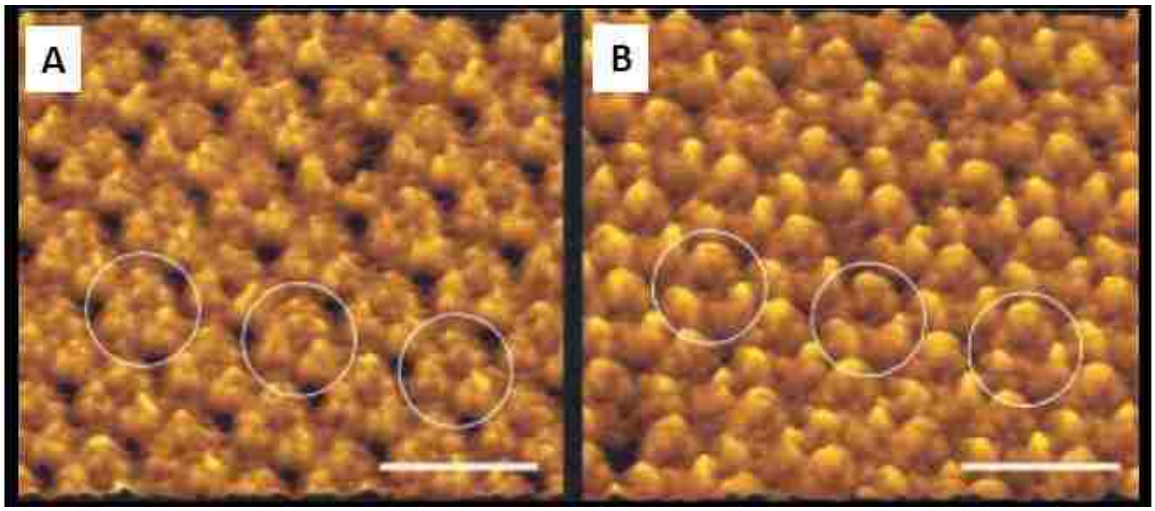

Figure 2.9 High resolution liquid AFM images of the cytoplasmic surface of the bacteriorhodopsin membrane protein acquired using contact mode AFM. (A) Raw AFM topograph acquired at a loading force of ~ 200pN; (B) imaged at loading force of ~ 100 pN. (Scale bars: 10 nm) Circles indicate the trimer structure of individual extracellular proteins. (*Reprinted with permission from ref. [3]*)

Electrochemical AFM studies of biological samples have also been accomplished in buffer solutions for the hexagonally packed intermediate layer of ordered membrane proteins adsorbed to HOPG and other conductive supports.[59, 90] Studies of electron transfer and adsorption of myoglobin on surfaces of a graphite electrode were conducted *in situ* using tapping-mode AFM combined with cyclic voltammetry measurements in Tris-HCl buffer solutions.[91]

Biological surfaces can be problematic for high resolution AFM imaging, because of the soft and sticky nature of the samples. Tapping mode has increasingly become more broadly applied and predominant for biological studies. For TM-AFM, the tip is driven to oscillate in and out of contact with the surface intermittently, which minimizes the destructive stick-slip shear forces that occur with continuous contact mode AFM. The tip does not have sufficient time to form transient interfacial bonds with the sample because it is driven to rapidly oscillate during scans across the surface. For soft, fragile samples of biomolecules such as proteins or cells, tapping mode has become the method of choice for nondestructive AFM imaging.[13] The tip is driven to oscillate by a piezoceramic actuator[92] or by an external AC electromagnetic field, as with magnetic acoustic AFM or MAC-mode.[93-94] Table 2.3 provides examples of the range of sample types and imaging modes that have been used to investigate biological materials using AFM in liquid media.

Liquid AFM studies do not require the use of fluorescent labels to detect binding processes, instead local structural changes can be directly detected. There are advantages for AFM studies of biomolecules such as cells and proteins as compared to methods with fluorescence and electron microscopies, which require chemical treatment and stains. In fluorescent microscopy, biomolecules are tagged with fluorophores that can potentially influence the overall binding affinity.[95] Liquid AFM offers capabilities for investigations in non-denaturative environments without the requirement for fluorescent labels, providing insight into biomolecular mechanisms and binding interactions. High-resolution views of the extracellular and cytoplasmic surfaces of bacterial membrane channels involved in osmoregulation (aquaporin Z, *Escherichia coli*) were captured in buffer using contact-mode AFM by Scheuring et al.[88] Structural changes of the protein surface were analyzed after samples were treated with trypsin for cleavage of the N-terminal fragment.

Table 2.3 Examples of biological samples studied in different liquid media using AFM.

Biological System Studied	**Substrate**	**Media**	**AFM Mode(s)**	**Ref.**
outer membrane proteins: porin OmpF, aquaporin-Z, bacteriorhodopsin	mica	buffer	contact	*3*
bovine serum albumin tobacco etch virus capsid protein, tobacco mosaic protein, specific antibodies (IgG)	-COOH monolayers	water	contact	*26*
amylin fibrils	mica	buffer	contact time-lapse AFM	*47*
collagen fibrils	mica	buffer	tapping	*48*
DNA-protein binding	mica	buffer	tapping	*49*
F-actin filaments, human amylin fibrils, nuclear pore complexes	mica	buffer	contact time-lapse AFM	*50*
Esherichia coli bacteria	glass slide	2-butanol	contact	*86*
Escherichia coli water channel, aquaporin Z	mica	buffer	contact	*88*
myoglobin	graphite	buffer	tapping	*91*
fibronectin	TiO_2	water	MAC-mode	*93*
purple membrane protein (Halobacterium salinarum)	mica	buffer	MAC-mode	*94*
Dipalmitoylphosphatidylcholine and cholesterols	mica	PBS	frequency modulation	*41*
bone marrow-derived mast cells	glass coverslips	PBS	tapping/contact	*96-97*
double-stranded plasmid DNA	mica	*n*-propanol	contact	*98*
DNA	mica	butanol	tapping	*99*
Escherichia coli RNA polymerase	mica	buffer	tapping	*100*
G protein-coupled receptors rhodopsin and opsin	mica	buffer	contact	*101*
ATP synthase rotor proteins	mica	buffer	contact	*102*
RNA polymerase binding to DNA	mica	buffer	contact time-lapse AFM	*103*
canine kidney cells	glass coverslips	PBS	contact time-lapse AFM	*104*
DNA	mica	aqueous solutions	contact time-lapse AFM	*105*

The ability to directly monitor dynamic changes of the conformation or association of biomolecules using time-lapse images is an inherent advantage of liquid AFM. By successively acquiring *in situ* images in liquid media, progressive changes of surfaces or materials that occur over time can be recorded. The self-assembly of collagen fibrils onto mica was tracked using time-lapse AFM by Cisneros et al., with tapping-mode AFM experiments conducted in liquid.[48] A time-lapse sequence of AFM images for the process of the assembly of RNA polymerase and DNA into complexes was reported by Guthold et al. for experiments conducted in Hepes/$MgCl_2$ buffer,

revealing high-resolution views of protein binding to DNA.[103] Madine-Darby Canine Kidney (MDCK) cells were studied using time-lapse AFM in physiological conditions, revealing movement of fibers through the cells during imaging.[104] Studies of the structure and dynamics of DNA were conducted in aqueous solutions by Lyubchenko and Shlyakhetenko using time-lapse AFM.[105] Time-lapse images disclosed steps of the unfolding and branch migration of a Holliday junction over time. The succession of interaction events for the tumor suppressor protein p53 with a DNA fragment were investigated with time-lapse AFM using tapping mode in liquid.[49] Interactions such as association, re-association, sliding and direct binding of the protein to DNA were detected for samples attached to mica surfaces. The growth of amyloid fibrils was observed in liquid media by Goldsbury et al., evidencing bidirectional growth of amylin over time.[47] Changes were monitored over intervals of hours as the mica surface was continuously scanned.

The capabilities of *in situ* imaging and AFM-based nanofabrication have been combined for molecular-level studies of DNA and proteins.[75, 77, 106] Nanostructures of proteins were produced on gold substrates using nanografting with gold-binding residues such as cysteine,[107] or with thiol modification of the protein molecules.[108] In a multi-step approach, nanografted patterns of SAMs can be used for site-selective adsorption of proteins. The terminal moieties of SAM nanopatterns can be designed with chemistries that avoid nonspecific protein adsorption, yet make specific interactions with targeted proteins. Examples of nanografted patterns have been reported with protein binding mediated by covalent,[51, 109] electrostatic.[109] and specific[110] molecular interactions. By incorporating a short thiol linker at the end of the strands, nanografted structures of single-stranded oligonucleotides of DNA as narrow as 10 nm were produced using nanografting.[111-115] Typically, for the natural adsorption of thiolated DNA on gold surfaces, the DNA molecules tend to lie down with the molecular backbone aligned parallel to the substrate. However, for patterns

of DNA oligomers that are nanografted, a relatively close-packed structure with a standing conformation is produced with the molecules oriented in an upright configuration.[113-114] Investigations of enzyme-digestion and label-free hybridization of single stranded DNA nanostructures were conducted *in situ* for nanografted patterns of DNA in liquid media.[112-115]

2.5 Future Developments of Liquid AFM

An emerging challenge for nanoscale measurements is to capture and quantify the magnitude of structural changes for different materials in response to environmental parameters. Environmental factors such as pH, solvent polarity, ionic strength and temperature are dynamic variables which influence scanning probe experiments. With liquid imaging, *in situ* studies of electrochemistry, surface assembly reactions, and chemical/physical mapping of samples can be accomplished with time-lapse capture of surface changes. Combining liquid AFM with other imaging modes has made it possible to acquire information while simultaneously imaging samples, for nanoscale mapping of surface properties. Improvements to SPM instruments for probe designs and increased imaging speed will better facilitate investigations for studies of chemical/biochemical kinetics.

Future developments of liquid AFM techniques will couple other analytical approaches such as Raman or infrared spectroscopies for multifunctional instrumentation. The practical hurdles for developing such approaches are the low intensity optical signals and lack of sensitivity for such small size scales. Imaging in liquids provides a way to detect surface changes as influenced by solvents or pH effects at the nanoscale, for dynamic studies of the influence of environmental stimulus. The capabilities of liquid AFM will be important for emerging research efforts in developing stimuli-responsive materials and polymers.

CHAPTER 3: ELECTRONIC MEASUREMENTS WITH MOLECULAR SYSTEMS

3.1 Introduction to Molecular Electronics

The vision of molecular electronics will require that methods be developed to assemble nanoscale objects (molecules, nanoparticles, carbon nanotubes and nanowires) to form devices and circuit architectures.[116] The design of practical molecular devices for photonic, electronic, or optoelectronic applications holds potential to solve the scalability problems for miniaturization and storage density for computerized information, and there are also opportunities to significantly reduce the fabrication and energy costs as compared to conventional manufacture of semiconductor-based technologies. Fabrication of complete circuits at the molecular level poses a challenge because of the difficulty of connecting molecules together in devices.[117-118] Characterizations with scanning probe microscopy (SPM) have revolutionized our ability to understand the underlying mechanisms of chemical reactions on surfaces, as well as to correlate nanoscale properties (conductance, magnetism) with structural architectures of diverse molecular systems – ranging from biomolecules to self-assembled monolayers to polymers and nanoparticles.[119-121]

According to James Tour, a leading researcher in the field of molecular electronics, "it has become clear that even though the syntheses of multitudes of molecules have been laborious, the testing of the molecules in electrical devices has fallen far behind the pace of synthetic efforts."[122] There is a need for new approaches and more reliable measurements of charge transport for molecularly thin films, pressing the limits to experimental measurements of single molecule conductance.[123] The majority of research regarding electrical measurements in molecular electronics has been accomplished using methods such as break-junctions,[124-127] single electron transistors,[128] gold nanoparticles on SAMs,[129-131] crossed wire tunnel junctions,[132-134] nanoimprint

lithography,[135] and nanopores.[136-138] Charge transport in organic molecules has also been investigated by approaches such as electrochemical measurements,[139-141] mercury drop electrodes,[142-143] atomic force microscopy (AFM),[144-147] and scanning tunneling microscopy (STM)[148-150] conductive probe measurements as well as theoretical calculations.[151-152] Each method has associated advantages and difficulties. A disadvantage of most of the measurement techniques (except for AFM and STM approaches) is that information about the local structure; surface organization and molecular orientation are not provided. Because of the dual capabilities for obtaining physical measurements and structural information with unprecedented sensitivity, scanning probe characterizations are becoming prevalent for molecular electronics investigations.

For comparing molecular conductance, a particular problem is presented for reproducibility with nanoscale measurements. The discrepancies when comparing the various measurement approaches is most likely attributable to variations in the orientation of molecules on surfaces. The surface orientation of molecules is known to affect the conductive properties of pi-conjugated systems, and has been corroborated by molecular mechanics calculations. Geometric considerations such as molecular coupling to the substrate, the angle of molecular orbitals relative to the surface, distance/proximity effects due to the tilt of the molecular backbone, as well as lateral intermolecular interactions have been implicated to have a role for conductance measurements at the molecular level.[153-160]

3.2 Conductive Probe Measurements using Atomic Force Microscopy (AFM)

The atomic force microscope was invented in 1986, and uses a force feedback mechanism to scan a probe across the surface of either insulating or conductive samples.[15] In contact mode, the probe remains in contact with the sample while raster scanned across the surface. Using a conductive tip, electronic measurements can be made similar to the properties investigated by STM. Conductive probe atomic force microscopy (CP-AFM), also called current sensing (CS-

AFM) and conducting atomic force microscopy (C-AFM), is a scanning probe technique that uses a conductive tip to map the conductive areas of a sample.[161-164] Conducting AFM was first described in 1989 by Japanese researchers investigating surface conductance of various metals. In the research, Morita et al. compared images acquired using an AFM with a conducting tip to images of the same metal surfaces imaged with STM. The authors illustrated the potential use of the AFM to investigate conductive properties of sample surfaces similar to the approach for STM.[161] The use of CP-AFM was expanded by research groups lead by Professors Stuart Lindsay and C. Daniel Frisbie, both of whom were the first to use the CP-AFM approach with organic molecules. While both groups researched the conductivity of organic molecules using CP-AFM, the overall goal was achieved with different molecular systems. Dr. Lindsay's research focused on achieving conductivity measurements of single molecules while Dr. Frisbie's studies targeted measurements of the conductivity of self-assembled monolayers (SAMs) of alkanethiols.[144, 163, 165-170] Studies of the conductivity of organic molecules demonstrated the effectiveness of CP-AFM in the field of molecular electronics.[171]

3.2.1 Operating Principle of Conductive Probe Atomic Force Microscopy (CP-AFM)

With CP-AFM, the tip is placed in direct contact with the material to be probed under a controlled force setting, as shown in Figure 3.1. For current-voltage (I-V) measurements, a conductive SPM tip is grounded, and a bias is applied to the substrate. Current-voltage characteristics can be measured by applying a voltage and measuring the resultant current. A sensitive pre-amp is placed near the conductive probe to enable low-noise measurements of current in the range of femto- through pico- amperes. Current flow is measured between a biased metal-coated cantilever and the conductive substrate.[172] Two types of measurements can be accomplished with CP-AFM. A point-contact measurement can be made with the tip at a fixed position of the sample. For I-V measurements, resistance is measured between the probe and a contact point of

the sample. The second type of measurement, current mapping provides topographic imaging with measurements of resistance (or measured current) as a function of probe position. With a certain bias applied to the sample, the current can be measured point-by-point to reconstruct a map of the conductivity of the sample.

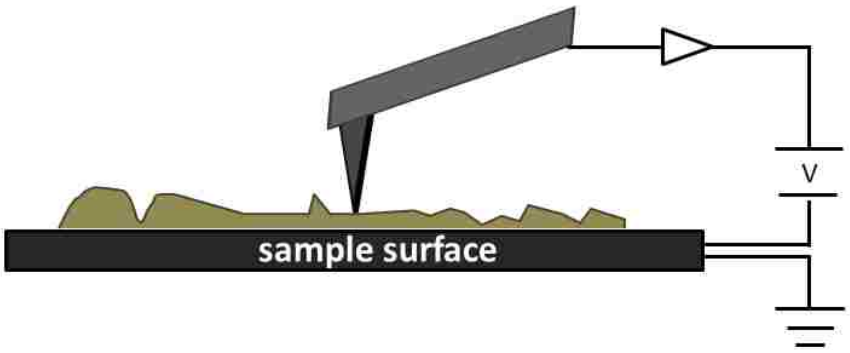

Figure 3.1 Instrument set-up for CP-AFM.

Two types of data can be obtained with CP-AFM. The first measurement is a current-voltage curve made with point to tip contact as shown in Figure 3.2. The nature of the sample being investigated determines the shape of the graph. With a non-conductive sample, the I-V curve will be a horizontal line on the current axis because there is no current to be measured (Figure 3.2A). If the sample is conductive, the I-V curve will show a line with a steady slope (Figure 3.2B). A certain current will be measured with conductive material when a bias is applied. An I-V curve obtained from a semiconductive sample will look like a combination of the conductive and non-conductive curve. There will be areas of non-conductivity along with areas of conductivity (Figure 3.2C). Examining the shape of the graph can help determine the type of material being investigated.

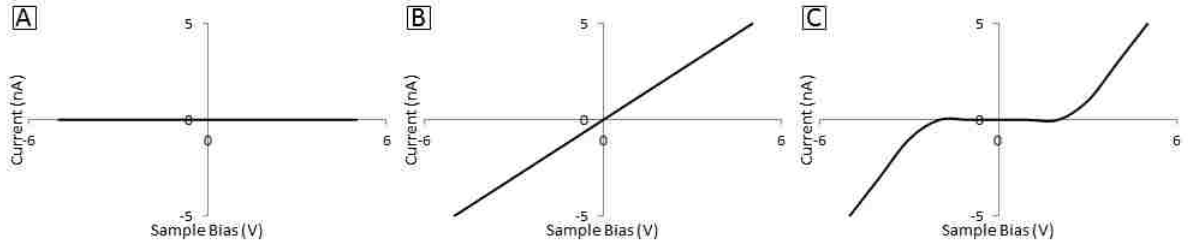

Figure 3.2 Theoretical current-voltage curves from CP-AFM. Example I-V profiles are shown for (A) A nonconductive sample; (B) a conductor; (C) a semiconductor.

An example of the current map is shown in Figure 3.3. The current map is acquired simultaneously with the topography image of the sample. In Figure 3.3 the sample is a bare gold substrate. In the topography image (Figure 3.3A) the irregular shapes of the terraces of gold steps are shown, often used to calibrate the z dimensions of an AFM instrument. The corresponding current map acquired simultaneously with the topography frame is shown in Figure 3.3B. Gold is a conductive substrate, but the heterogeneity of the conductive regions is shown in the current map. The areas around the step edges are seen to be more conductive that the middle of the gold step. The sample was scanned at a positive bias of 0.7 V. At the nanoscale, subtle differences in conductivity of the gold substrate at different regions can be visualized.

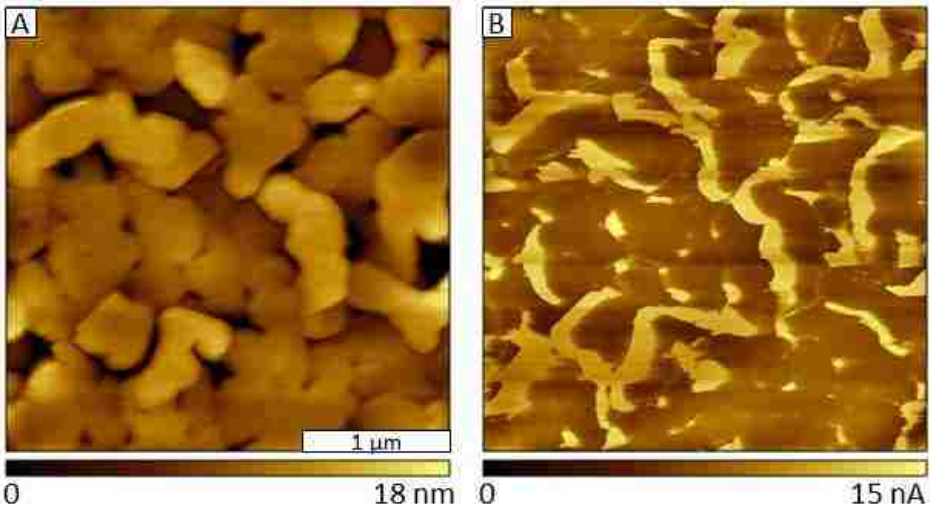

Figure 3.3 Simultaneously acquired topography and current images of bare Au(111) substrate obtained with CP-AFM

3.2.2 Probes Used for CP-AFM

The probes used for CP-AFM are usually silicon or silicon nitride tips that have been coated with a conductive metal film. Different metals have been used to coat AFM probes, including tungsten, platinum, iridium, and titanium.[163, 173-174] In addition to the conductive metal coated tips, there are also pure tungsten tips, and doped diamond tips. Current-voltage relationships are influenced by the electronic properties of the tip-sample contact.[163-164] Studies have been reported of how the material of the tip influences the measurements of current with CP-AFM.[173, 175] Typically, low force is used when imaging and taking measurements with CP-AFM to prevent damaging the coating of the tip. The conductivity of the tips is checked by taking measurements with known conductive surfaces such as gold, platinum, or doped silicon surfaces.[171, 173-174]

Figure 3.4 Optical micrograph of conductive AFM tip. (60x)

3.2.3 Molecular Systems Studies Using CP-AFM

Since its introduction, CP-AFM has been used to examine the electronic properties of metal surfaces, organic thin films, and biological molecules; representative examples are summarized in Table 3.1. Although CP-AFM has been used extensively for measurements with alkanes,[176-179] phenyl-alkanes[180] and arenethiols,[181] systems such as porphyrins and phthalocyanines have not been as rigorously investigated for conductive properties.

Table 3.1 Examples of Systems Studied using Conductive Probe AFM

System studied (surface & environment)	**Year**	**Ref.**
Au, Ag, Ti, Cu surfaces (Au, Ag, Ti, Cu foil)	1989	[161]
Metal-oxide-silicon capacitors Very large scale integration (VLSI) oxide layers (silicon substrate)	1993	[182]
Freshly cleaved highly ordered pyrolytic graphite (HOPG)	1995	[173]
SiO_2 thin films (crystalline silicon or poly silicon substrates)	1995	[183]
Tungsten film (silicon wafer)	1996	[175]
p-type silicon surface, silicon on insulation (SOI)	1996	[184]
Carotenoid (Au(111) on mica)	1998	[168]
Sexithiophene (SiO_2 or Au)	1998	[163, 170]
$CH_3(CH_2)_nSH$ $5 \leq n \leq 9$ (polycrystalline Au)	2000	[144]
1,8 octanedithiol (Au(111))	2001	[166]
Polyaniline (PANI) and poly(methyl methacrylate) thin film (Au on silicon)	2001	[185]
$CH_3(CH_2)_{n-1}SH$ $4<n<10$ Benzylthiol (Au on Si substrates)	2001	[186]
Phenylene oligomer SAMs (Au (111))	2003	[187]
Pseudomonas aeruginosa azurin (Au or HOPG)	2003	[188]
Undoped poly(decylthiophene) (Au)	2003	[189]
Polypyrrole thin film (Au on silicon substrate)	2004, 2005	[190-191]
Organic light emitting diodes [Indium tin oxide substrate with monolayer of (4,4'-bis[(*p*-trichlorosilylpropylphenyl)phenylamino]-biphenyl)[2], thin film of [*N, N'*-di(α-naphthyl)-*N,N'*-diphenyl-1,1'-biphenyl-4,4'diamine] and [tris(8-hydroxyquinalato)aluminum(III)]	2004	[192]
SiO_2 (n-type silicon substrate)	2007	[193]
Azobenzene (Au(111))	2008	[194]
(Boc)-Cys-(S-Acm)-$(Ala\text{-}Leu)_n$-NH-$(CH_2)_2$-SH peptide n = 4-7 (Au substrate)	2012	[195]

3.2.4 Current-Voltage Measurements using Scanning Tunneling Microscopy (STM)

Scanning tunneling microscopy (STM) was invented in 1981 by researchers at IBM and was a monumental achievement in the field of scanning probe microscopy and nanoscience.[196] The first

STM instrument used a wire to probe the surface of samples to obtain high resolution images. The STM has capabilities of obtaining electronic measurements with topographical, conductive images and tunneling spectroscopy.[197] However, the feedback mechanism of the STM is based on the tunneling of current between the tip and the sample.[186, 198]

Conductive probe measurements with STM are quite different than AFM measurements.[176] For current-voltage (I-V) spectroscopy with STM, the tunneling of electrons between the tip and sample are part of the feedback loop for tip positioning. As an advantage, measurements with STM can be accomplished in UHV environments, to eliminate the water meniscus layer which forms under ambient conditions. However, STM measurements cannot be accomplished if the molecules are highly insulating. The STM tip does not make direct contact with the sample, so the resulting computational models of experimental results must take into account the gap distance between the probe and sample. For conductive probe AFM (CP-AFM) measurements, the electrical information is not part of the feedback process. The AFM tip is placed directly on the sample surface, at a designated force. An intrinsic advantage of AFM instruments is unparalleled control of applied forces - ranging from pico to nanonewtons. The current through a molecule is known to depend on the force used to contact the molecules and also depends on the tip geometry.[199] A further convenience of CP-AFM measurements is the versatility of imaging environments, enabling studies in liquid media or ambient environments.

Conventional I-V measurements are taken when the STM tip is brought to within a few angstroms of the sample surface using a positional feedback mechanism which controls the magnitude of the tunneling current. Scanning tunneling spectroscopy (STS) is an STM technique for measurements of current-voltage. Once the tip is in position, the tunneling current feedback and scanning is turned off. In STS, a bias is scanned over a defined range and the current is

recorded.[200] Unlike the I-V measurements obtained with AFM, the tip of the STM does not touch the sample. The STS technique has been used to study the charge transport of different molecular systems including single crystal magnetite and inorganic acids such as 12-molybdphosphates on a graphite surface.[201] The I-V characteristics of organic monolayers such as hemiquinone on a gold surface have also been examined using STM.[202]

Both CP-AFM and STM I-V measurements have been applied to measure the electrical properties of molecularly thin films and nanostructures. Both techniques are able to provide topography information and a conductive map of the sample surface.[161, 163-164, 171] Because CP-AFM can also be used to image insulating surfaces, it has an advantage in providing images and conductive measurements of mixed samples.[185, 190, 192] A difference between the two SPM-based methods is that for STM the tip is not placed in direct contact with the sample surface, and thus the measurements include a tunneling gap of certain dimensions. In CP-AFM, the tip is placed in direct contact with the sample under a certain force for acquiring measurements. Depending on the type of sample material, the measured current may increase as a function of the force applied to the tip with CP-AFM.[173-174]

Beyond electrical measurements, characterizations with AFM and STM also furnish high-resolution views of the local morphology of molecular films and nanostructures, to enable assessment of sample quality. At high voltage the samples can be damaged or altered. Thus, to ensure reliable and reproducible conductive probe measurements it is important to acquire molecular-level views of surfaces after applying voltage to detect possible structural changes resulting from processes of local heating, desorption or oxidation.

3.3 Measurements of Charge Transport using other techniques

Along with scanning probe methods, there are other techniques used to measure the charge transport of different molecular systems. These techniques follow the donor-bridge-acceptor

classification described by Ratner in which electron transfer is measured from the donor to acceptor via a bridging molecule or wire.[203] The donor/acceptor can be either an electrode or a molecule.[203-204]

3.3.1 Metal Nanoparticles on Self-Assembled Monolayers

Metal and semiconducting nanoparticles on self-assembled monolayers (SAMs) have been used to investigate the electron transfer of different molecular systems. Gold nanoparticles in conjunction with dithiol SAMs have been used to examine the conductivity of the nanoparticles.[166, 205] A scanning probe microscope is used to acquire the current-voltage measurement. This method requires that there be some type of bond formed between the nanoparticle and SAM. The STM tip and SAM on a conductive substrate serve as the donor and acceptor while the nanoparticle serves as the bridging molecule. Quantum dots have also been used as the bridging molecule.[206] Monolayer protected clusters (MPCs) are nanoparticles with an outer molecular layer and have also been studied using this method.[207] This method is applicable to molecules that can be bonded to the nanoparticle and the SAM underneath which limits the molecules that could be studied.

3.3.2 Molecular Break Junctions

Break junctions can be used to measure the conductance of a single molecule or molecular cluster. The electrodes are manufactured to have a distance of nanometers.[208] Mechanical break junctions have been used to probe the charge transfer properties of different molecules. In a mechanically controlled break junction, a bending beam is mounted on a piezo material. A metal wire is secured on top of the bending beam and broken by the bending of the flexible substrate. After breaking the wire, a tunneling gap can be adjusted and measurements acquired for different molecular systems.[127] Break junctions offer the advantage of being able to measure the conductance of a single molecule. The break junctions are useful for investigating self-assembling single molecule junctions because they eliminate artifacts associated with surface defects.[209] The

difficulty for the break junction method is to place a single molecule between the contacts, which can be difficult.

A break junction can be defined as a single molecule trapped between metal electrodes.[204] Scanning probe tips have also been used as electrodes in break junctions. The STM and AFM tips have been used as an electrode in break junction measurements while a substrate serves as the other electrode.[144, 186, 209-210] The molecules are usually on the surface of a conductive substrate or embedded in a self-assembled monolayer on the surface.

3.3.3 Measurements with Mercury Drop Electrodes

The electrical properties of different SAMs of alkanethiols have been investigated using the mercury drop method. [196, 207-209] Mercury has a high affinity for thiols, with the thiol chain oriented perpendicular to the surface. A drop of mercury drop is used to form metal-insulating-metal (MIM) junctions.[198] The MIM junctions were used to study the conductivity and dielectric constant of alkanethiol SAMs.[198, 211-213]

The mercury drop method uses liquid mercury as an electrode. The measurements are made with different approaches. The organic molecules can be directly assembled onto the top of a drop of mercury, sandwiched between two mercury drops, or a drop of mercury can be placed onto a SAM that was formed on a substrate.[198, 211-213] The use of liquid mercury as one electrode and a thin solid evaporated metal film as a second electrode is the easiest configuration to assemble and manipulate compared to using mercury drops for both electrodes.[198] Because of the high affinity of mercury for alkanethiols, this method is good for investigating the conductive properties of SAM molecules. Using liquid mercury as the surface helps create a SAM that has minimal defects compared to those assembled on a gold surface.[198, 212] However, molecules that do not form SAMs on a surface of mercury are not suitable for study by this method.

3.4 Summary

Fundamental questions to be investigated with conductive probe studies are the roles of molecular architecture, surface orientation, geometries of nanostructures and intermolecular interactions for measurements of charge transport. The importance of coupling between adjacent molecules in molecular electronics has not been investigated, due to the difficulties of controlling molecular assembly at the level of single molecules. In this dissertation, conductive probe measurements will be accomplished with different molecular systems and orientations by generating coplanar assemblies in thin films of naturally formed surface assemblies versus designed nanopatterns. It is likely that as the dimensions of nanopatterns become successively smaller, quantum effects may be detectable in I-V spectra. Fundamentally, the goals are to elucidate the role of molecular structure, packing and orientation for electron pathways, which is largely unknown.

It is critical to know the organization and arrangement of molecules on surfaces when measuring and modeling charge transport. For this reason, the capabilities of AFM for high resolution imaging are critical for studies with molecular systems. Conceptually, by arranging and orienting molecules such as porphyrins and phthalocyanines in well-defined arrangements, local surface measurements of charge transport can be enabled for different pathways through the molecules. A key objective for the studies in this dissertation is to develop approaches with nanolithography to construct arrays of designed test structures of known orientation. By using a combined approach with scanning probe imaging, nanolithography and current measurements with designed molecular platforms, the methods developed will be suitable for addressing questions about the role of intramolecular organization in electron transfer. It has been predicted that quantum effects in electronic conduction will be observed as the size of electronic devices approach molecular scales. Our strategy will be to arrange designed molecular architectures on

surfaces with defined orientation to enable local measurements of charge transport for different pathways through the molecules. Reference molecules of insulating *n*-alkanethiol matrix layers will furnish an internal calibration standard for normalizing measurements of current-voltage (I-V) spectra. Also, by generating nanopatterns of successively smaller dimensions, the size scaling effects can be systematically probed.

CHAPTER 4. CHARACTERIZATION OF DESIGNED COBALTACARBORANE PORPHYRINS USING CONDUCTIVE PROBE ATOMIC FORCE MICROSCOPY

4.1 Introduction

The choice of studying model systems of porphyrins is highly practical, because of the associated electrical, optical and chemical properties of this functional class of molecules. Porphyrin and metalloporphyrin systems are excellent materials for molecular electronics, due to their diverse structural motifs and associated electrical, optical and chemical properties, and thermal stability.[214-219] At a basic level, electronic properties are controlled by the degree of π delocalization.[220] Porphyrins can be organized into supramolecular arrays, aggregates and crystals with diverse functions. The rigid planar structures and π- conjugated backbone of porphyrins convey robust electrical characteristics. The porphyrin macrocycle consists of four pyrrole rings joined by four methine carbons. The architecture of porphyrins has been proposed as viable for electronic components for molecular-based information-storage devices,[221-224] gas sensors,[225-226] photovoltaic cells,[227-228] organic light-emitting diodes,[229-232] and molecular wires.[233-235]

Synthesis of cobaltacarborane porphyrin conjugates was first reported by Hao et al.[236-238] The cobaltacarborane ligand consists of an alkoxy chain terminated with two carborane cages with a single cobalt atom situated between the carboranes.[236-240] The abundance of boron in the cobaltacarborane ligands was studied for potential applications in boron neutron capture therapy and the fluorescence properties were studied for potential use for photodynamic therapy.[236-237] The cobaltabisdicarbollide anion in the cobaltacarborane ligand was studied for attributes of chemical, thermal, and photostability.[237, 241] In this report, the conductive properties of selected cobaltacarboranes was investigated for potential applications in molecular electronics.

Research in the molecular electronics field has been advanced by the invention of the scanning tunneling and atomic force microscopes. Scanning probe microscopes have advantages for investigating nanoscale phenomena, with capabilities to acquire images with nanometer resolution as well as make spectroscopy measurements of single molecules or clusters.[197] Several scanning probe techniques can be used to obtain electronic information of molecular systems.[197, 242-246] Scanning probe measurements have been used to examine electronic properties such as conductance, dielectric constants and capacitance while providing surface views and topographic information of the samples.[242-245, 247-249] For conductive probe atomic force microscopy (CP-AFM) a conductive tip is scanned across the sample, while a bias is applied to the substrate. Most commonly, the current is measured by a sensitive preamp, located near the probe. With CP-AFM, two types of data acquisition are possible: a conductive map of the sample surface and a current voltage profile of selected local areas of the surface. The feedback mechanism of CP-AFM is based on applying a chosen force set-point; therefore, the conductive AFM probe remains in direct contact with the sample during spectroscopy measurements.

For these investigations, selected cobaltacarborane porphyrins were investigated using contact mode and CP-AFM to evaluate the role of molecular structure for surface assembly, self-aggregation and conductive properties. Specifically, changes with surface measurements were evaluated and compared according to the numbers and arrangement of cobaltacarborane substituents.

4.2 Experimental Section

4.2.1 Sample Preparation

Gold substrates, Au(111)/mica, were purchased from Agilent Technologies, Inc. (Chandler, AZ). Cobaltacarborane porphyrins were synthesized as previously reported.[237] The

gold substrates were rinsed with deionized water, then a 15 µl drop of porphyrin solution (10^{-6} M) was deposited on the gold substrate and dried in ambient conditions overnight.

4.2.2 Atomic Force Microscopy (AFM)

Conductive probe atomic force microscopy (CP-AFM) experiments were accomplished in air with a model 5500 AFM/SPM from Agilent equipped with Picoscan v5.3 software. Triangular cantilevers with a tip radius of less than 35 nm, tip height of 20-25 µm and a force constant of 6.0 N m^{-1} were used for contact mode imaging and CP-AFM, the tips were acquired from MikroMasch (San Jose, CA). A copper wire was placed in physical contact with the gold substrate so that a bias could be applied to the sample (± 2.0 V). Digital images were processed using Gwyddion software.[250]

4.3 Results and Discussion

Tetraphenyl porphyrin macrocycles were functionalized with 2, 4, or 8 cobaltacarborane substituents arranged as shown in Figure 4.1. The cobaltacarborane porphyrins were synthesized via a ring-opening zwitterionic reaction in high yields (90-97%), as previously reported.[203, 236] Each of the substituents contains a cobalt atom which is coordinated between two carborane cages. The numbers and arrangement of the cobaltacarboranes should systematically influence the measured I-V characteristics, thus providing a model surface material for CP-AFM.

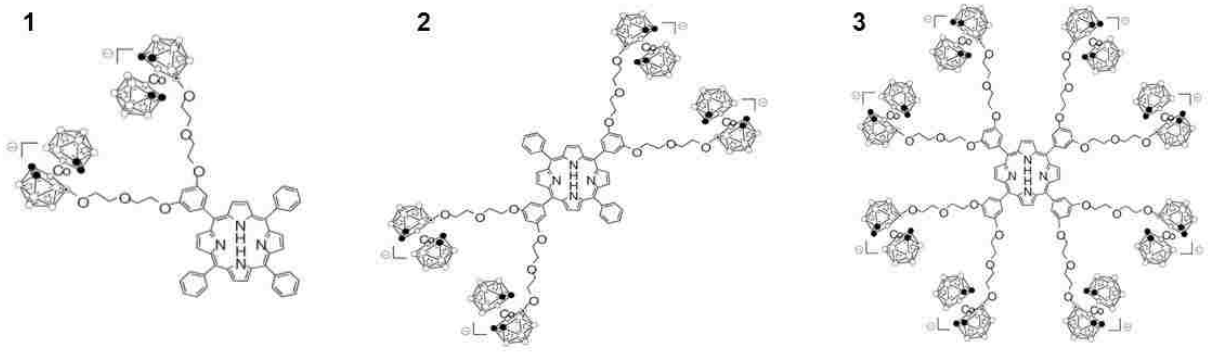

Figure 4.1 Cobaltacarborane porphyrins selected for AFM studies.

The symmetry of the molecules and arrangement of cobaltacarborane moieties was found to influence the surface assembly and molecular aggregation of samples prepared on Au(111). Representative images (topography and corresponding lateral force frames) of the three cobaltacarborane porphyrin (Co-Por) samples of Figure 1 are presented in Figure 4.2. Typically, porphyrin macrocycles orient on the surface in a coplanar configuration, and stack together to form columnar assemblies. However, the nature and size of substituents influences the surface arrangement and self-aggregation of the nanocrystals. With two cobaltacarborane ligand for Co-Por1, the surface assemblies exhibit polydisperse sizes arranged randomly across the surface of gold (Figures 4.2A-4.2A´). The nanocrystals tend to attach near the edges of the gold steps, however there is sufficient surface density for stacks to locate at terrace sites. The thickness and lateral dimensions of the nanostructures is disperse, however the geometry retains a nearly spherical shape. However, with four cobaltacarborane ligands oriented symmetrically as shown for Co-Por2, the surface structures changed to exhibit a rod-like or needle shape (Figures 4.2B-4.2B´). There does not seem to be any preferential attachment to the edges of gold steps, the nanocrystals of Co-Por2 are regularly shaped and randomly distributed throughout areas of the surface. With eight cobaltacarborane ligands, Co-Por3 forms exquisitely regular spherical stacks that locate at the step edges of the gold surface (Figures 4.2C-4.2C´). The vertical and lateral dimensions of the nanocrystals are monodisperse, and tended to form linear assemblies that decorate step edges.

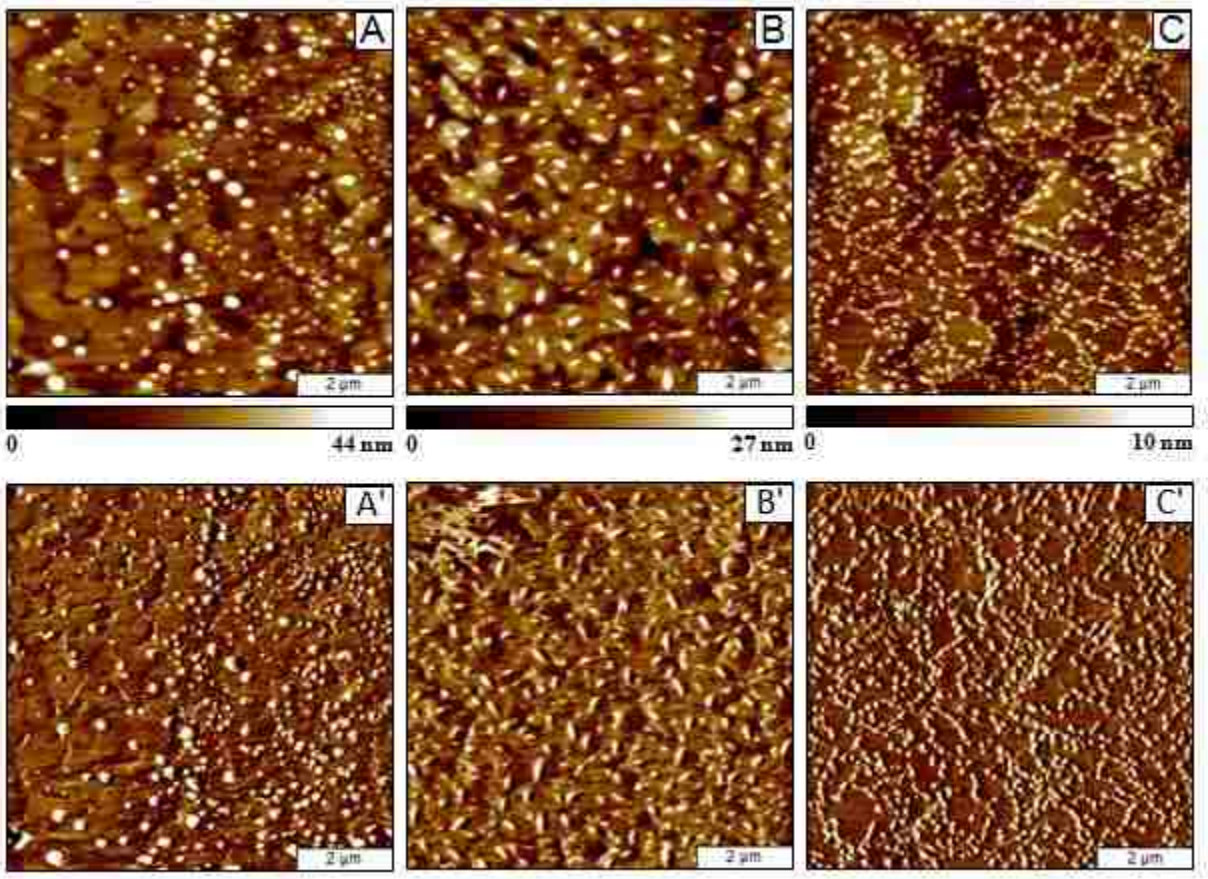

Figure 4.2 Cobaltacarborane porphyrin samples prepared on gold, imaged with contact mode AFM. The top row shows the topography frames, and the simultaneously acquired lateral force images are shown below. (A) Co-Por 1 (B) Co-Por 2 and (C) Co-Por 3.

The systematic changes in surface shapes and dispersity highlights the role of molecular structure for surface assembly for the cobaltacarborane porphyrins. Previous studies with porphyrins have shown that pi-pi intermolecular interactions are a dominant force for directing macrocycles to assemble into stack structures, with the plane of the macrocycle aligning with the substrate. Differences in the number and placement of cobaltacarborane ligands leads to changes in the shapes of surface assemblies, as well as in the arrangement to form linear chains or dispersed islands. The asymmetric arrangement of two cobaltacarborane ligands for Co-Por 1 produced a wider range of sizes and dispersity. The symmetric para arrangement of four ligands for Co-Por 2 produced elliptical rod shapes of symmetric crystals. A highly uniform spherical shape and size

was observed for Co-Por 3, with eight ligands arranged symmetrically around the macrocycle. The selected cobaltacarborane molecules nicely demonstrate that molecular symmetry directs the 3-D assembly of macromolecules to form nanocrystal shapes.

A zoom-in view of the cobaltacarborane porphyrin nanocrystals is shown side-by-side in Figure 4.3. The shapes and surface arrangement of each molecular structure is compared with topography frames in the top row, and the edges of the crystals are more clearly resolved in the corresponding lateral force images in the middle row. The heights of a few nanocrystals are shown with example cursor line profiles in the bottom panels. For the nonsymmetric structure of Co-Por 1 (Figures 4.3A and 4.3B) the nanocrystals have a mostly spherical shape, exhibiting a range of sizes. Many of the crystals are located at step edges, however a few are located within terrace sites. The step edges can be resolved in the lateral force frame, Figure 4.3B. A cursor profile indicates the heights of three nanocrystals of Co-Por 1 measure 11, 23 and 18 nm, from left to right. In contrast, the rod-like shape of the para substituents of Co-Por2 are viewed in Figures 4.3D and 4.3E. The segregated islands of Co-Por 2 do not appear to attach preferentially at sites of step edges and are randomly distributed across the surface. The heights of three nanocrystals outlined in Figure 3D measure 11, 13, and 12 nm (Figure 4.3F). A close-up view (3×3 μm^2) of densely packed nanostructures of Co-Por 3 is shown in Figures 4.3G-4.3H. At this magnification the linear arrangement of chains of near-spherical nanocrystals can be resolved, and some of the crystals have begun to pile together into taller aggregations. A cursor profile across nine nanocrystals (Figure 4.3I) indicates heights ranging from 2 to 8 nm.

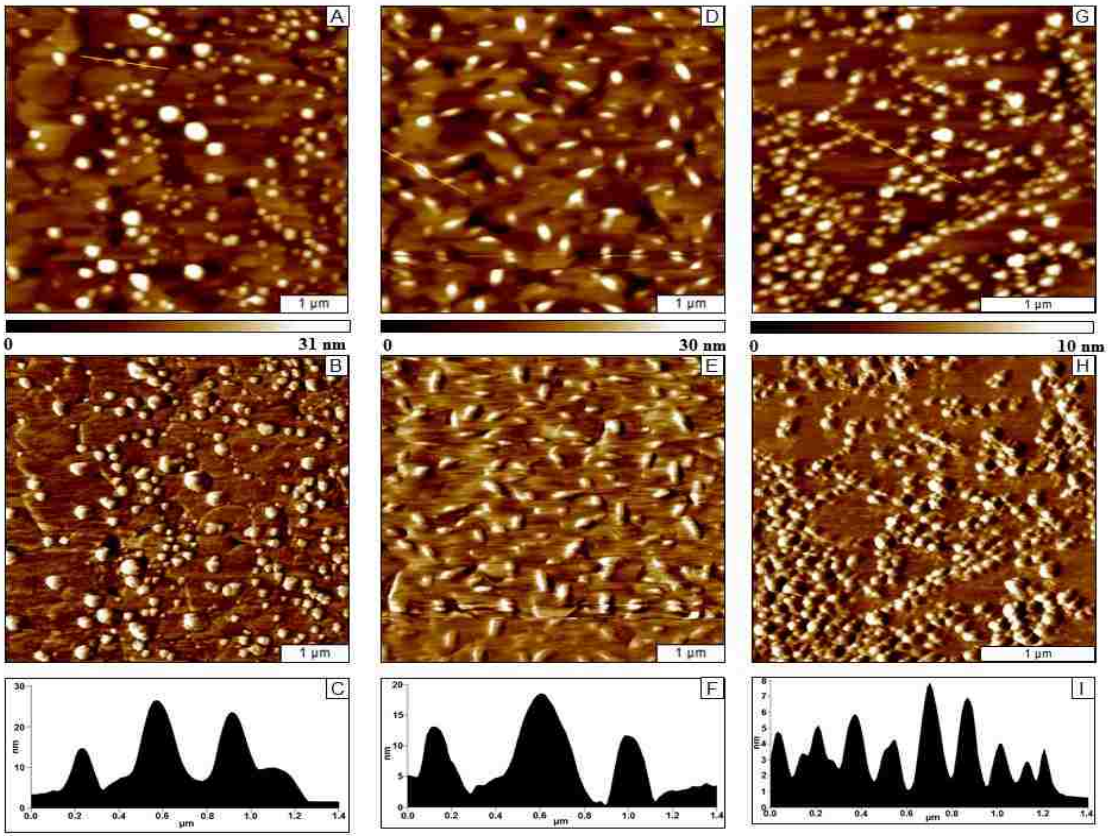

Figure 4.3 Magnified view of cobaltacarborane porphyrin nanocrystals on gold, imaged with contact mode AFM. (A) Topography; (B) lateral force and (C) example cursor profile for Co-Por 1. (D) Topography; (E) lateral force and (F) corresponding cursor profile for Co-Por 2. (G) Topography; (H) lateral force and (I) cursor profile for Co-Por 3.

The distribution of heights for the cobaltacarborane porphyrins is presented with size histograms in Figure 4.4. The widest range of sizes is observed for Co-Por 1, ranging up to 40 nm in height with an average measuring 15 ± 7.2 nm. A smaller range of sizes (up to 25 nm in height) was observed for tetra-substituted Co-Por 2, with an average height measuring 14 ± 3 nm. The narrowest size range and smallest nanostructures were observed for the octa-substituted Co-Por 3, with an average height measuring 4 ± 1 nm. Porphyrin nanocrystals consist of multiple molecular layers assembled in a stacked arrangement. The cobaltacarborane ligands appear to interfere with the molecular self-assembly. The structure with the fewest ligands (Co-Por 1) formed taller stacks, whereas increasing the numbers of substituents produced smaller structures. With a fully

substituted arrangement with eight cobaltacarborane ligands, smaller crystals formed due to steric effects.

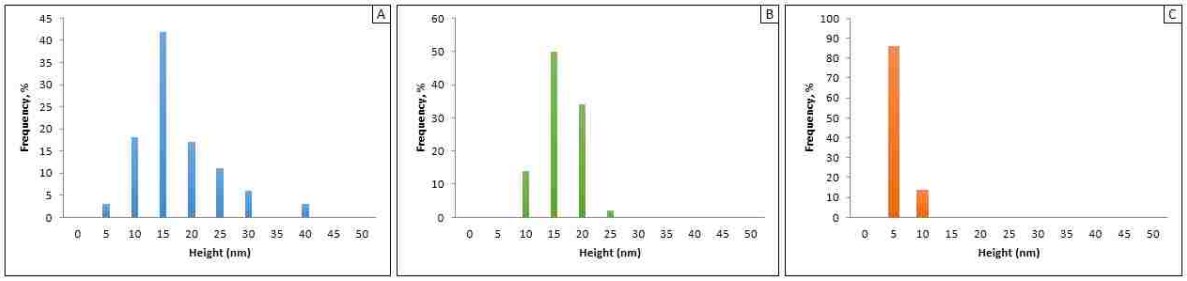

Figure 4.4 Height distribution measured with cursor profiles for cobaltacarborane porphyrins (*n* = 100): (A) Co-Por 1; (B) Co-Por 2; and (C) Co-Por 3.

Representative current-voltage profiles of the cobaltacarborane porphyrins are compared in Figure 4.5. The electrical transport properties of the three samples are distinct as regards the magnitude of the measured current and onset of conduction. A staircase profile was reproducibly detected for Co-Por 1, indicative of Coulombic charging (Figure 4.5A). Discrete increments of 2 nA current were measured at approximately 1 V intervals for the molecule designed with two cobaltacarborane substituents. Coulombic behavior was not detected for the other samples. An I-V curve that is typical of a semiconductive sample was detected for Co-Por 2, with an asymmetric profile (Figure 4.5B). The onset of current was detected at -8 V and + 5 V, within a measuring range below 0.1 nA. The I-V profile for Co-Por 3 was also asymmetric, (Figure 4.5C) however the magnitude of current ranged ±2 nA. The current onset was detected at ~ 0.05 V for this sample.

The size of the nanostructures did not show apparent differences in I-V profiles. Regarding the Coulombic profiles of Co-Por 1, there have been previous reports of current profiles with Coulombic staircase characteristics obtained at room temperature.[251-252] Wakayama et al. reported that organic molecules could be used as Coulomb islands of single-electron tunneling devices; a porphyrin derivative (tetrakis-3,5 di-*t*-butylphenyl-porphyrin (H_2-TBPP)) was found to be suitable

as a Coulomb island. The H_2-TBPP was layered between SiO_2 on Si(100) and was investigated with STM at 5 K under ultra-high vacuum.[253]

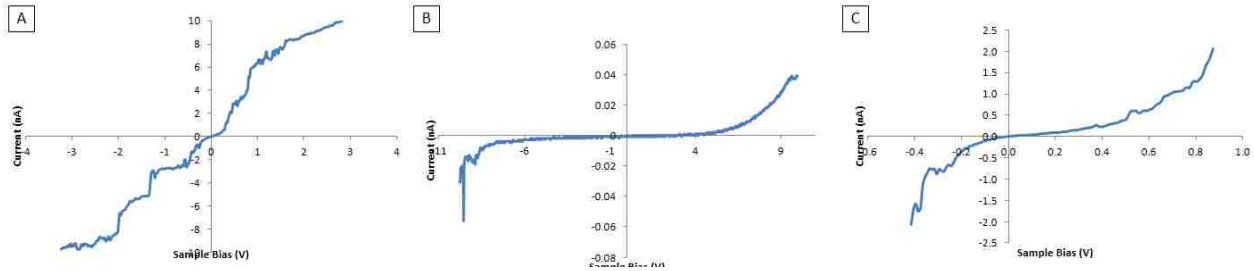

Figure 4.5 Representative current-voltage profiles for cobaltacarborane porphyrins: (A) Co-Por 1; (B) Co-Por 2; and (C) Co-Por 3.

4.4 Conclusions

In the future, the conductive properties of selected molecular architectures will be accurately computed using theoretical approaches. However, currently there is a need for accurate and reproducible experimental measurements of conductive properties of molecular architectures for reliable comparison to theoretical models of charge transport in molecular systems. Systematic changes in surface shapes and dispersity shown with AFM images of porphyrin nanostructures illustrates the critical role of molecular structure for the self-assembly of cobaltacarborane porphyrins on surfaces. The conductive properties of cobaltacarborane porphyrins change according to the numbers and arrangement of substituents. It is critical to know the organization and arrangement of molecules on surfaces when modeling charge transport. We anticipate that well-defined defined arrangements of molecules and aggregates on surfaces will lead to accurate and reproducible local measurements of charge transport for different pathways through the molecules and provide insight on structure/property relationships.

CHAPTER 5: DIRECTED SURFACE ASSEMBLY OF DESIGNED PORPHYRINS USING PARTICLE LITHOGRAPHY WITH ORGANOTHIOL AND ORGANOSILANE SELF-ASSEMBLED MONOLAYERS

5.1 Introduction

There are few methods of positioning molecules on a nanometer scale that will facilitate functional electronic devices. Preparing nanosized test structures of porphyrins is not a trivial effort, since there are few lithographic tools available for controlling the size of molecular junctions with high precision. Combining particle lithography with steps of surface self-assembly is a practical approach for development of nanoscale test structures, to enable an accurate approach for measuring charge transport properties. Particularly for molecular systems such as porphyrins and phthalocyanines, self-aggregation causes spontaneous assembly of aggregates and clusters to form, rather than well-organized films or surface arrangements with uniform dimension. Porphyrins and metalloporphyrins are highly conjugated molecular systems that have interesting photophysical and electronic properties. The electronic and optical properties of porphyrins largely depend on the surface arrangement and orientation of the molecules. Advancement of molecular electronics will require the ability to achieve reliable and precise measurements of conductance and charge transport for nano-sized test structures. It is predicted that quantum effects in electronic conduction will be observed as the size of electronic devices approach molecular scales. A considerable challenge is posed for developing reliable and reproducible methods for measurements in nanosized systems, for scaling nanostructures to nanometer length scales, and for evaluating the effects of molecular structure on electrical properties. The goal for this chapter is to pioneer methods to controlling the sizes, shapes or nanostructures of porphyrins, and to assess the orientation of porphyrins on surfaces. Conceptually, by arranging and orienting porphyrins in well-

defined arrangements, local measurements of charge transport can be enabled for different pathways through the molecules. Also, the resulting size-dependent properties can be evaluated with reliability and sensitivity. Accurate and precise electronic property measurements will shed insight on the fundamental mechanisms that give rise to properties such as resistance and rectification with changes in chemical structure. This chapter presents results applying particle lithography to create well-organized arrangements of porphyrins with uniform dimensions within a surface template of an *n*-alkanethiol or organosilane nanopatterns.

5.1.1 Porphyrins and Metalloporphyrins as Materials for Molecular Electronics

Porphyrins and related tetrapyrrolic compounds have useful properties for applications, due to unique physical,[254-256] chemical,[257-261] and spectroscopic properties.[219, 262] Porphyrin rings are generally stable under strong acidic and basic conditions. The macrocycle of the porphyrin can undergo substitutions and reactions to alter the porphyrin properties. For example, the inner protons of the porphyrin macrocycle can be replaced by metal atoms and peripheral substitutions can be made to add ligands to the porphyrin macrocycle.[263-264] Applications for porphyrins and related tetrapyrrolic compounds are reported in cancer therapies,[237, 259] data storage,[261, 265] and molecular sensors.[255, 260, 265] Porphyrins and metalloporphyrins have also been applied for studies of energy and electron transfer[238, 261] and catalysis.[264]

The choice of focusing research efforts on model systems of porphyrins is based on the associated electrical, optical and chemical properties of this functional class of molecules. Porphyrin and metalloporphyrins are excellent materials for molecular electronics, due to the diverse structural motifs and associated electrical, optical and chemical properties, and thermal stability.[214-219] At a basic level, electronic properties are controlled by the degree of π delocalization.[220] Porphyrins can be organized into supramolecular arrays, aggregates and crystals with diverse functions. The rigid planar structures and π- conjugated backbone of porphyrins

convey robust electrical characteristics. The architecture of porphyrins has been proposed as viable for electronic components for molecular-based information-storage devices,[221-224] gas sensors,[225-226] photovoltaic cells,[227-228] organic light-emitting diodes,[229-232] and molecular wires.[233-235]

5.1.2 Particle Lithography

Particle lithography, also called colloidal[266] or nanosphere lithography[267] is a method of creating ordered patterns of nanostructures on surfaces using the close-packed arrangement of mesoparticles as a surface mask or template.[268-271] Particle lithography has been used to prepare nanopatterns of proteins,[272-275] metals,[276-277] polymers,[278-279] nanoparticles,[267, 280-281] and self-assembled monolayers (SAMs).[268-269, 282] Organosilanes and alkanethiols SAMs have been patterned with particle lithography to direct the subsequent deposition of proteins,[283] nanoparticles,[280, 284] and polymers.[278] Compared to other lithography methods such as electron beam lithography and photolithography, particle lithography offers a relatively inexpensive, high throughput approach to generate organosilane and organosulfur nanostructures on surfaces.

Alkanethiol SAMs have been studied for applications ranging from molecular junctions to DNA detection.[127, 166, 285] Particle lithography with *n*-alkanethiol SAMs has been accomplished on surfaces of noble and coinage metals.[286] The high affinity of thiols to metal surfaces produces well-defined monolayer films on surfaces through a mechanism of molecular self-assembly.[286-287] Gold has been the standard substrate when studying thiol SAMs because it is an inert metal and is commonly used for electrochemistry, quartz crystal microbalance and ellipsometry measurements.[288]

5.1.3 Patterning Porphyrins using Particle Lithography

A cobaltacarborane porphyrin (Scheme 1) was used for nanolithography, by backfilling SAM nanopatterns. The cobaltacarborane porphyrin conjugates have previously been studied for potential use in photodynamic therapy (PDT) and boron neutron capture therapy (BNCT).[236-237,

[240, 259] The cobaltacarborane porphyrin conjugates were found to aggregate in HEPES buffer and undergo secondary aggregation. The formation and disruption of aggregates via sonication were accompanied by a color change.[259] The electronic and magnetic properties of the cobaltacarborane porphyrin conjugates are currently being investigated.

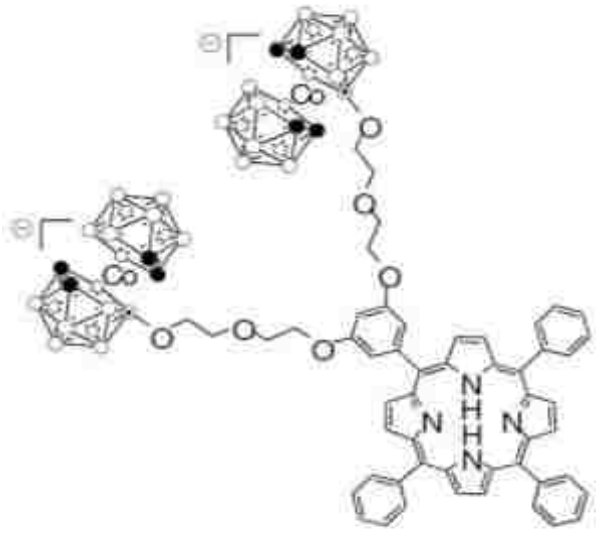

Scheme 5.1 Molecular structure of the disubstituted cobaltacarborane porphyrin conjugate.

Particle lithography has been used to pattern organosilane SAMs on silicon substrates[283, 289] and also for patterning *n*-alkanethiol SAMs on gold surfaces.[286] For this research, nanostructures of both types of SAMs were evaluated as surfaces templates for patterning porphyrins. Alkanethiol SAMs have been used in studies of charge transport and molecular conductance, which provides precedence for future studies with conductive probe AFM.[127, 286, 290] Dodecanethiol and octadecyltrichlorosilane (OTS) were chosen for patterning because the hydrophobic characteristics of a methyl-terminated SAM will provide a suitable resist.[291-294]

5.2 Experimental Methods

5.2.1 Materials

Gold substrates, Au(111)/mica, were purchased from Agilent Technologies, Inc. (Chandler, AZ). Glass substrates were purchased from VWR International (Radnor, PA). Polished boron doped silicon substrates were purchased from Virginia Semiconductor (Fredericksburg, VA). Cobaltacarborane porphyrins were synthesized as previously reported.[237] Epoxy for preparing template-stripped gold films was purchased from Epoxy Technology, Inc. (Billerica, MA). Silica mesospheres were acquired from Fiber Optic Center, Inc. (New Bedford, MA). Latex mesospheres were purchased from Thermo Scientific (Waltham, MA). Dodecanethiol was purchased from Sigma-Aldrich Co. (St. Louis, MO). Octadecyltrichlorosilane was purchased from Gelest Inc. (Morrisville, PA).

5.2.2 Sample Preparation

Template-stripped gold surfaces were prepared as reported in Hegner et al.[295] Glass substrates were cleaned in piranha solution (3:1 v/v sulfuric acid to hydrogen peroxide) for approximately 30 min. The glass substrates were rinsed with deionized water and dried. Gold substrates were rinsed with deionized water and dried under a stream of argon. A drop of epoxy was placed on a glass cover slip and subsequently placed on the gold surface to create a mica/gold/glass "sandwich." After annealing for 1 h at 150°C the gold was stripped off of the mica. Silicon substrates were cleaned using a Uv-ozone treatment for 30 min.

5.2.3 Nanolithography Procedure

Particle lithography combined with vapor deposition was accomplished using silica mesospheres. A drop of silica mesospheres was deposited on gold and dried in ambient conditions for 20 min. The sample was then placed in an oven at 150°C for 2 h. After annealing the silica mesospheres to the substrate, the sample was placed in a glass chamber with 400 µL of 0.1 M

dodecanethiol solution. The chamber was placed in an oven at 70°C for 6 h to enable vapor deposition of dodecanethiol. After the vapor deposition step, the sample was rinsed with deionized water and sonicated in deionized water for 18 min and rinsed again to create nanopatterns of dodecanethiol. Porphyrin solution (10^{-6} M in 4-(2-hydroxyethyl)-1-piperazineethanesulfonic acid or HEPES buffer at 20 mM, pH 7.4) was subsequently deposited on the dodecanethiol nanopattern and dried in ambient conditions. For silicon substrates, latex mesospheres were used. A drop of latex mesospheres was deposited on the silicon and dried in ambient conditions for 20 min. The sample was then placed in an oven at 70°C overnight. After annealing the latex mesospheres to the substrate, the sample was placed in a plastic chamber with 300 μL of neat OTS. After vapor deposition, the sample was rinsed with ethanol and sonicated in ethanol for 45 min. The sample was then rinsed with deionized water followed by ethanol and sonicated again in ethanol for 45 min.

5.2.4 Atomic Force Microscopy (AFM)

Since its development in the 1980s, scanning probe microscopy (SPM) has been vital for investigating surface phenomena and interactions.[15, 197] The atomic force microscope (AFM) has been used to investigate nanoscale properties such as magnetism and conductance, as well as for measuring forces at the molecular level.[4, 43, 296-299] The AFM can achieve resolution of up to 1 nm in the horizontal direction and 0.1 nm in the vertical direction. For studies with porphyrin nanostructures, the AFM was operated in contact and tapping mode to examine the placement of cobaltacarborane porphyrins within SAM nanostructures.

Contact mode AFM experiments were accomplished in air with a model 5500 AFM/SPM from Agilent equipped with Picoview v1.10 software. Triangular cantilevers with a normal tip radius of 10 nm, tip height of 140-145 μm and a force constant of 0.05 N m^{-1} were used for contact

mode AFM, the tips were acquired from Bruker Corporation (Camarillo, CA). Tapping mode AFM experiments were done in air with aluminum reflex coated rectangular cantilevers with a pyramidal tip radius <10 nm, tip height of 12-16 μm, and a force constant of 48 N m^{-1} from VISTAprobes (Phoenix, AZ). Image processing was done with Gwyddion v2.20 software.[250]

5.3 Results and Discussion

The function and efficiency of porphyrins in devices is largely attributable to how the molecules are organized on surfaces. Understanding the self-organization and assembly of porphyrins is critical for optimizing the function of these molecules in device applications. Equally important are accurate and sensitive measurements of I-V spectroscopy for systems of individual or small ensembles of candidate molecules. In this chapter, protocols were developed to prepare robust surface test platforms of cobaltacarborane porphyrins. Evaporative particle lithography was applied for high-throughput nanopatterning of porphyrins. Results will be presented for AFM characterizations of samples prepared after steps of evaporative particle lithography.

5.3.1 Particle Lithography with Organosilane and Organothiol SAMs

The general protocol used for particle lithography combined with vapor deposition that was developed for patterning porphyrins is outlined in Figure 5.1. A solution of silica or latex mesospheres (250 nm or 150 nm, respectively) was deposited on a prepared substrate (gold or silicon) and dried in ambient conditions (Figure 5.1A). As the solution of mesospheres dried, capillary forces pull the mesospheres together to self-assemble into a close-packed arrangement. After drying, the sample was exposed to a vapor of dodecanethiol or OTS. The vapor-phase molecules bind to the surface in uncovered areas between the silica mesospheres (Figure 5.1B). In the next step, the mask of mesospheres was rinsed away to leave a self-assembled monolayer with nanopores arranged in a hexagonal pattern (Figure 5.1C). An aliquot of cobaltacarborane porphyrin solution (10^{-6} M) was then deposited onto the nanopatterned surface. As the surrounding

buffer solution evaporated, the porphyrin crystals aggregated within the nanoholes in the SAM (Figure 5.1D). The methyl-terminated SAM serves as a resist to direct the deposition of porphyrins into nanopores.

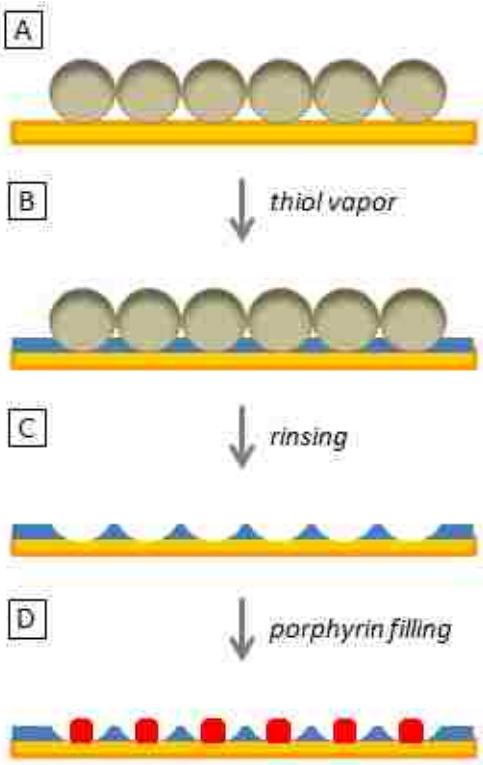

Figure 5.1 Process for patterning porphyrins using particle lithography combined with vapor deposition. (A) A surface film of silica or latex mesospheres was prepared as a template; (B) the organic molecules were deposited via vapor phase; (C) the mesosphere template was removed by rinsing steps; (D) porphyrin nanocrystals were deposited into nanopores.

5.3.2 Nanopores of Dodecanethiol Produced by Vapor Deposition

Most typically, organothiol SAMs are prepared using "beaker" chemistry, in which gold substrates are simply immersed into dilute thiol solutions. To evaluate the quality of a dodecanethiol SAM prepared by vapor deposition, a control sample was prepared without using a mask of mesospheres (Figure 5.2A). A comparison of the control sample and a sample prepared with a mask of mesospheres is presented side-by-side in Figure 5.2. The top row shows the results for a sample prepared without silica mesospheres; and the bottom row shows nanopores within the

SAM for a sample prepared after the mesosphere mask was removed. The topography (Figure 5.2A) and corresponding lateral force image (Figure 5.2B) show 1×1 μm^2 area of the dodecanethiol SAM. Angular step edges and terraces of the underlying Au(111) substrate are apparent, with a number of prominent pinhole defects.

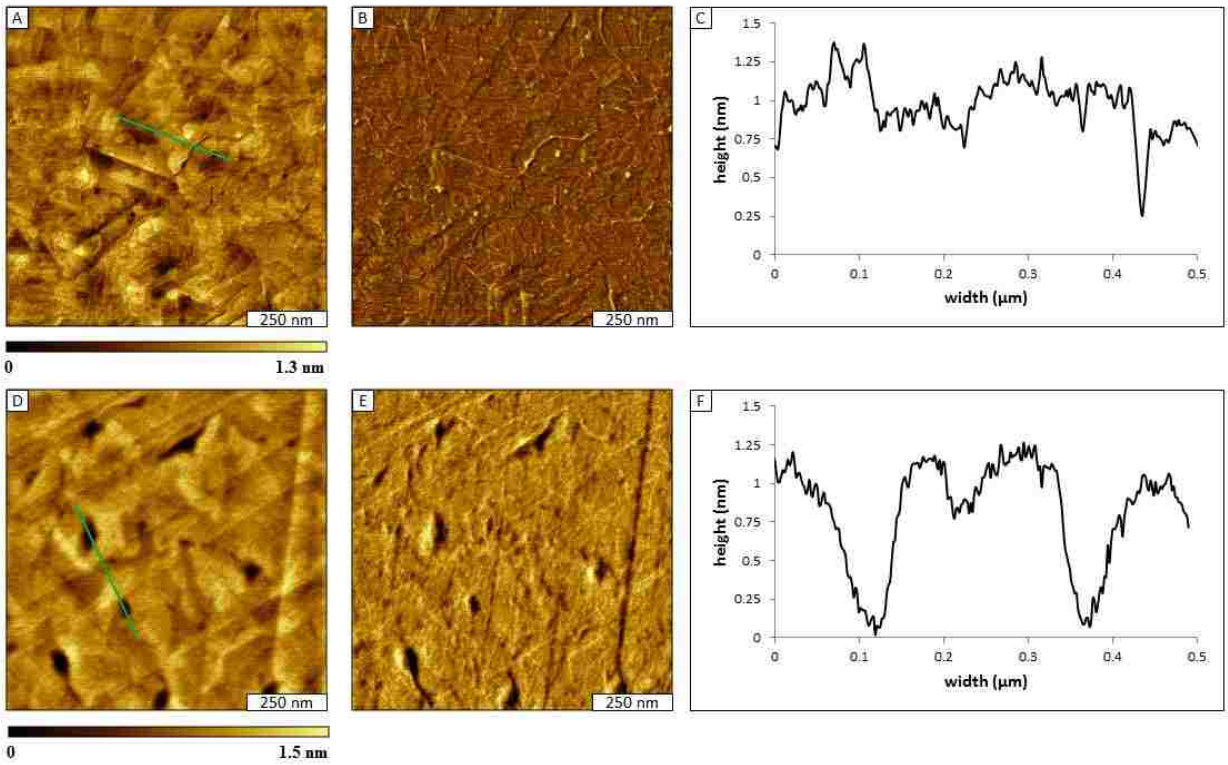

Figure 5.2 Vapor deposition of dodecanethiol onto gold. Dodecanethiol self-assembled monolayer formed on Au(111) prepared without a mask of mesospheres: (A) topography view; (B) corresponding lateral force image; (C) cursor profile of the green line in *A*. Nanopores within a dodecanethiol self-assembled monolayer on Au(111) produced with a mesosphere mask: (D) topography image; (E) simultaneously-acquired lateral force image; (F) cursor profile for the line in ***D***.

A representative line profile (Figure 5.2C) indicates the roughness of the substrate is less than 2 nm, at this magnification. The images in the bottom row show how the surface changes when a mask of mesospheres was used during vapor deposition. Nanopores are evident in the topography and corresponding lateral force images (Figures 5.2D and 5.2E). The height of the nanopores measures 1.7±1.1nm, which closely matches the expected theoretical height of a

dodecanethiol SAM. The spacing between the centers of the pores matches the 250 nm diameter of the mesospheres used for particle lithography. Interestingly, the shapes of the nanopores where the mesospheres were displaced are not perfectly round and symmetric. This can be attributed to imperfections of the surface, which is not perfectly flat. However, the sizes of the nanopores are exquisitely tiny and regularly spaced for depositing new molecules or nanocrystals.

Further magnified views of the nanopores of dodecanethiol are shown in Figure 5.3. Unlike a typical SAM, the topography and lateral images reveal an arrangement of dark triangular nanopores scattered across the surface (Figures 5.3A, 5.3B). Prominent landmarks of step edges and terraces can be clearly resolved, with a few dark scars in the right corners. A zoom-in view reveals ~12 nanopores within a 1×1 μm^2 area (Figure 5.3D). The height of the SAM measured ~1.6 nm, shown in the cursor profiles, which closely matches the theoretical height of a

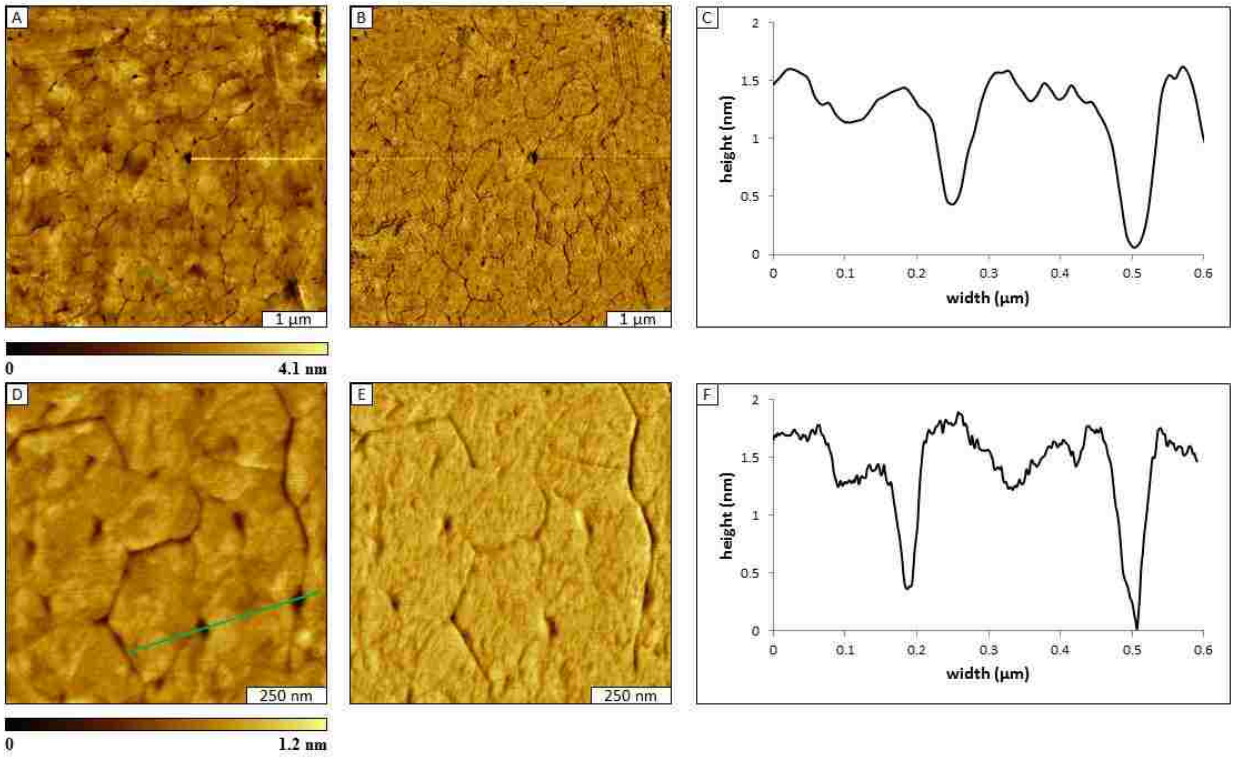

Figure 5.3 Further AFM views of nanopores within a dodecanethiol SAM. (A) Wide area topography view of nanopores; (B) corresponding lateral force image; (C) cursor profile of the

line in *A*. Zoom-in views of nanopores: (D) topograph; (E) lateral force image; (F) cursor profile for the line in *D*.

dodecanethiol SAM. The distance between the centers of the nanoholes corresponds to the diameter of the silica mesospheres used to create the pattern (250 nm). The periodicity of the patterns can be changed by choosing different sized mesospheres.[268-269, 282] Analysis of the topography images indicates the surface coverage of uncovered gold within the areas of the nanopores measures 2.8 ± 0.7%.

5.3.3 Nanostructures of Cobaltacarborane Porphryins within Nanopores of Dodecanethiol

Nanopatterns of cobaltacarborane porphyrins were successfully prepared within a matrix of dodecanethiol SAM nanopores using evaporative particle lithography (Figure 5.4). Unfilled nanopores of dodecanethiol are shown in the top row of Figure 5.4, and the bottom row shows the same sample after porphyrins were deposited in the nanopores. The periodicity of the nanopores measures 250 nm shown by the cursor profile of Figure 5.4C. Nanocrystals of cobaltacarborane porphyrins deposited into the thiol nanopatterns can be resolved in Figure 5.4D. The sizes and shapes of individual porphyrin aggregates deposited in the nanopores can be clearly resolved in Figure 5.4D and in the corresponding lateral force image (Figure 5.4E). The porphyrin aggregates have an average height of 7.7 ± 5.1 nm, including the depth of the nanopores.

The hydrophobic nature of the methyl-terminated groups of the dodecanethiol SAM was used to direct the porphyrins to deposit within the nanopores. It is likely that nanocrystals of the porphyrin were already formed in the buffer solution, which leads to a polydisperse range of crystal sizes within the nanopores (Figures 5.4D-5.4E). However, there are also areas of very small deposits within the nanopores which can be used for size-dependent measurements of molecular conductance. There were still a few unfilled nanopores with porphyrin aggregates. The aggregates range in size, with an average height measuring 15 nm. However, the lateral force image (Figure

5.4E), can be used to aid in distinguishing the regions of the cobaltacarborane porphyrin and dodecanethiol.

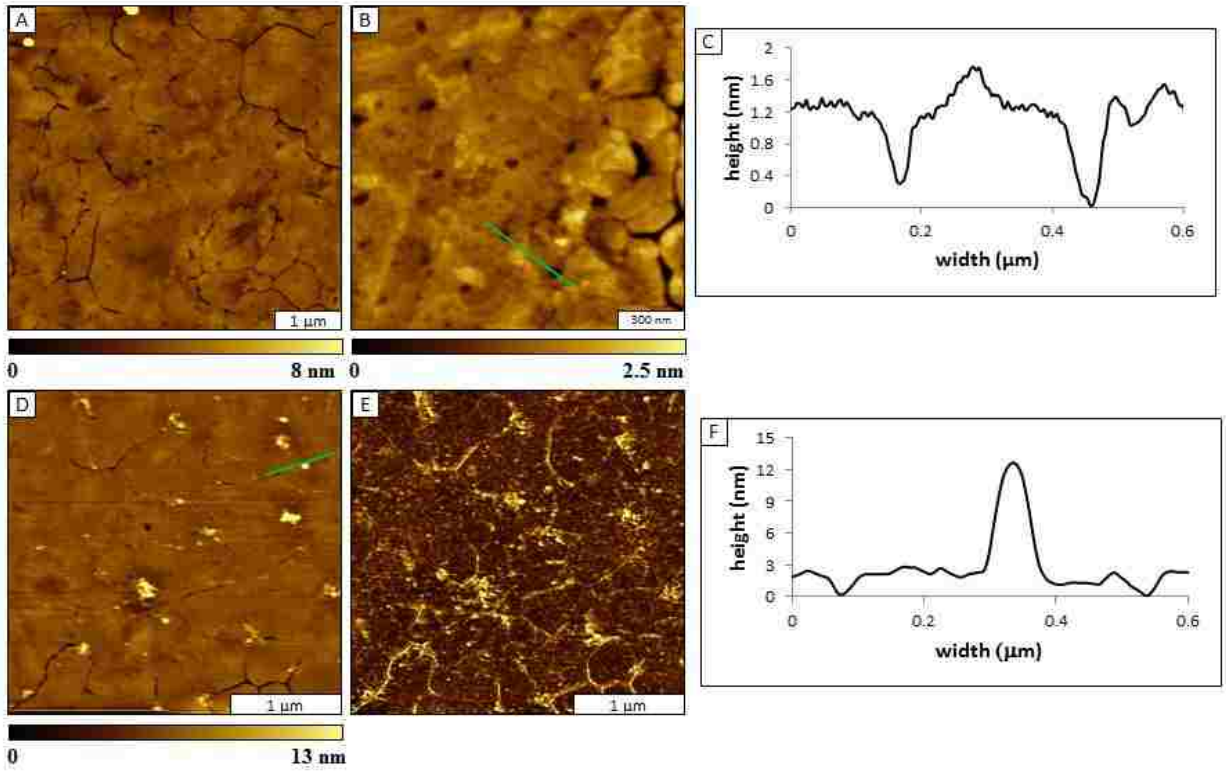

Figure 5.4 Nanopores within a dodecanethiol SAM before and after backfilling with cobaltacarborane porphyrin. Unfilled nanopores: (A) wide view topograph; (B) zoom-in topography view; (C) cursor profile for the line across two nanopores in ***B***. After backfilling the sample with cobaltacarborane porphyrin: (D) topograph; (E) lateral force frame; (F) cursor profile for the line in ***D***.

5.3.4 Nanostructures of Cobaltacarborane Porphryins within Nanopores of OTS/Si(111)

Organosilane nanostructures were produced on Si(111) by combining particle lithography with steps of vapor deposition with octadecyltrichlorosilane (OTS). Ring nanostructures of OTS viewed with tapping mode AFM images are shown in Figure 5.5A for an area spanning 8×8 μm^2. The dense packing and periodic arrangement of nanostructures is apparent for broad areas of the surface, with regularly shaped ring geometries. Nanoscopic residues of water at the meniscus sites

surrounding the mesosphere masks influence the shapes of nanostructures produced by vapor deposition of organosilanes.[269] Trace amounts of water are required to initiate the hydrolysis step of silanation, however if there is too much water present the molecules self-polymerize to form chains. At the base of the mesospheres there is sufficient water present to form multilayer nanostructures. The shapes of the sites of the OTS multilayers exhibit the ring shape of the water meniscus sites. The example line profile (Figure 5.5C) reveals the uniformity of the spacing and heights of the nanorings. Approximately 296 nanorings are shown with a magnified view (3×3 μm^2) in the topography (Figure 5.5D) and corresponding phase image (Figure 5.5E). The center-to-center spacing of the rings matches the size of the mesospheres (150 nm) used for patterning, as shown with a representative cursor profile (Figure 5.5F). The nanorings measure 7.4 ± 1.3 nm in height (average value) which corresponds to 3-4 layers of OTS.

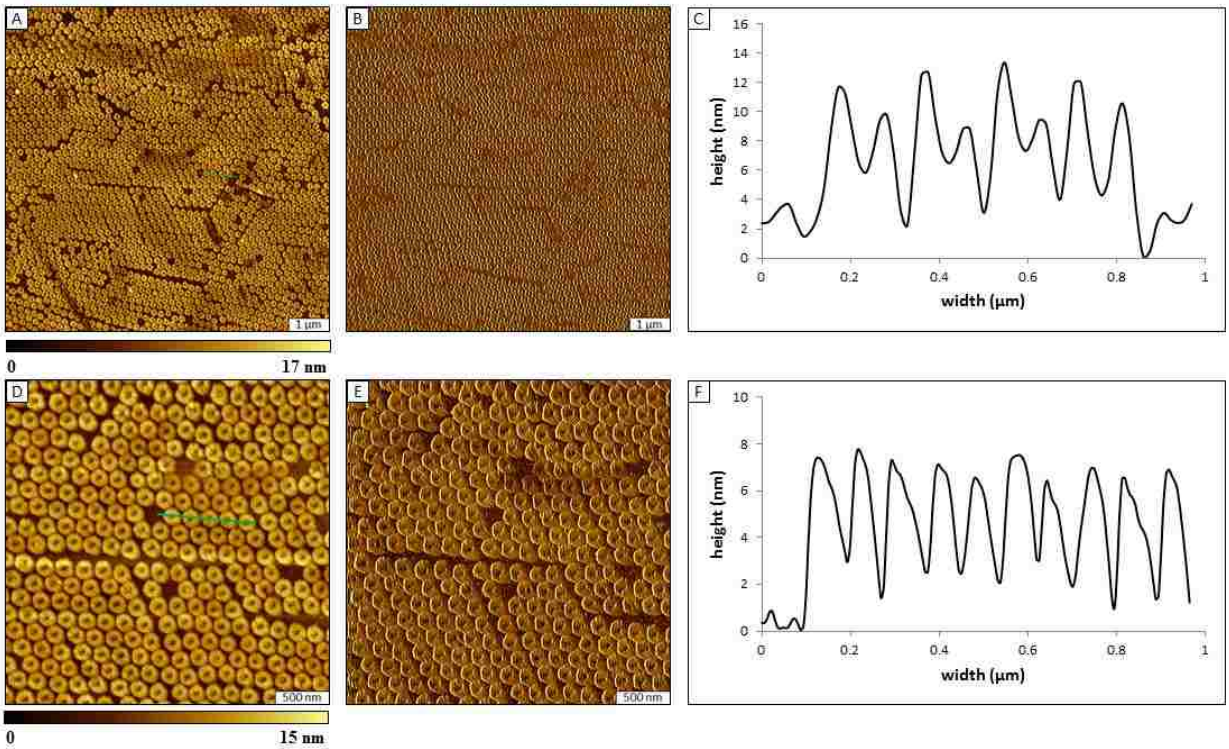

Figure 5.5 Nanostructures of octadecyltrichlorosilane on Si(111) produced by vapor deposition. (A) Wide view topograph of nanorings; (B) simultaneously-acquired phase image; (C) cursor profile of the line in ***A***. (D) Zoom-in views of OTS nanorings; (E) phase image; (F) cursor profile for the line in ***D.***

The OTS nanorings were used as a surface resist to direct the deposition of cobaltacarborane porphyrin (Figure 5.6). The locations of the porphyrin nanocrystals within the OTS nanorings can be detected in the topography (Figure 5.6A) and corresponding phase image (Figure 5.6B). The 2×2 μm^2 zoom-in topography (Figure 5.6D) and corresponding phase images (Figure 5.6E). Although a few crystals are located on the edges of the OTS nanorings, mostly the crystals appeared to deposit within the centers of the rings. Clusters of the porphyrin nanocrystals are well resolved in the phase images (Figures 5.6B and 5.6E), the shapes and arrangement of the porphyrins are not as clearly evident in the topography frames. The shapes and arrangements of nanocrystals within the OTS rings are well resolved with close-up views of the nanostructures shown in Figures 5.6D and 5.6E. Approximates 3-6 nanocrystals pack tightly within the OTS nanorings.

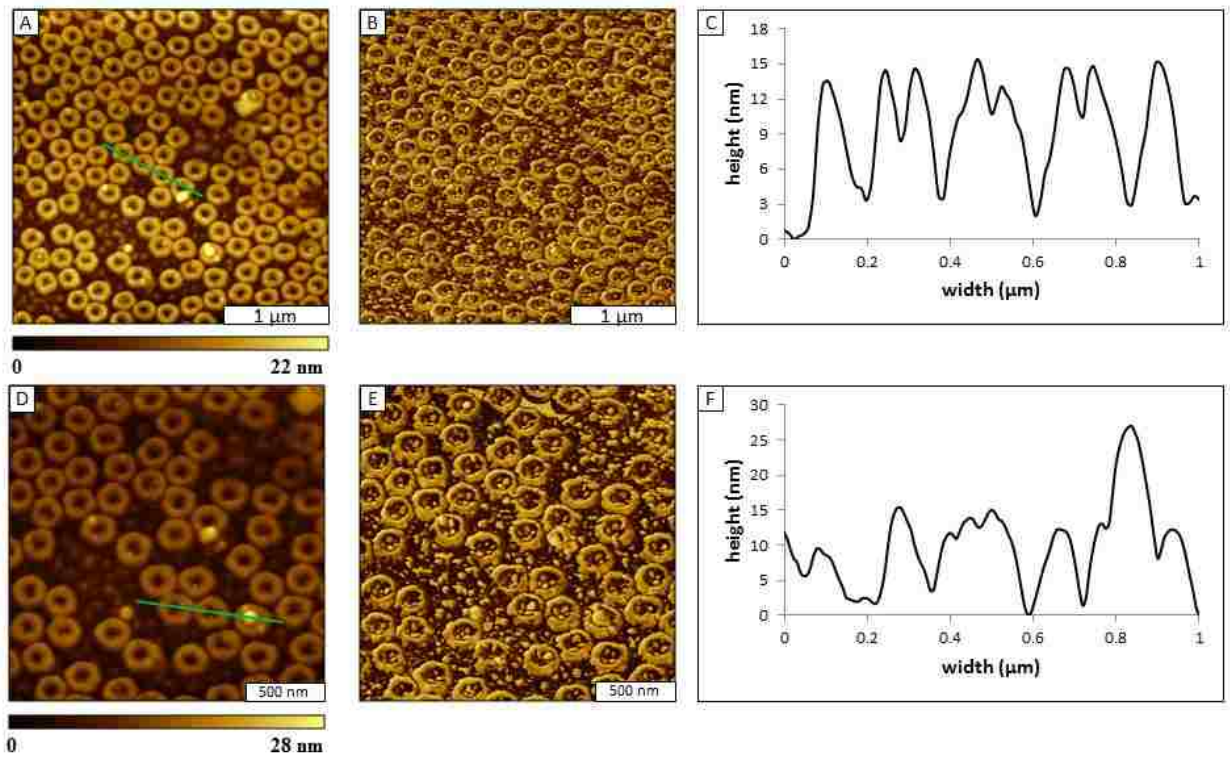

Figure 5.6 Cobaltacarborane porphyrin nanocrystals patterned within OTS nanorings. (A) Topography and (B) corresponding phase image; (C) cursor profile for the line in ***A***. (D) Zoom-in topography view of nanocrystals; (E) phase image; (F) cursor profile for the line in ***D***.

5.4 Conclusions and Future Prospectus

Particle lithography combined with vapor deposition was used to create an array of nanopores within SAMs of dodecanethiol and octadecyltrichlorosilane. Using the hydrophobic characteristics of the SAM, aggregates of a cobaltacarborane porphyrins were directed to selectively fill the nanopores. The porphyrin nanocrystals deposited within the nanopores were visualized using contact mode AFM. Future directions for these experiments will be to characterize the nanostructures with conductive probe AFM, and evaluate the changes in charge transport for different size nanocrystals. These experiments will work best when using a conductive substrate such as gold. To incorporate designed supramolecular structures into devices requires deposition onto surfaces with retention of both structure and function. This remains a challenge and can present a significant barrier to developing molecular devices. It is critical to know the organization and arrangement of molecules on surfaces when modeling charge transport. Conceptually, by arranging and orienting porphyrins on well-defined surfaces, local surface measurements of charge transport can be enabled for different pathways through the molecules.

A key objective for our scanning probe studies is to apply high-throughput nanoscale lithography to construct arrays of designed test structures with defined orientation. By using a combined approach with AFM imaging, nanolithography and conductive probe measurements with designed molecular platforms of selected porphyrins, we plan to tackle persistent questions about the role of intramolecular organization in electron transfer. It has been predicted that quantum effects in electronic conduction will be observed as the size of electronic devices approach molecular scales. Our strategy will be to arrange and orient designed porphyrins on well-defined surfaces to enable local measurements of charge transport for different pathways through

the molecules, as well as to incorporate architectures of reference molecules of *n*-alkanethiol or organosilane SAMs to serve as an internal standard for calibration at the nanoscale.

CHAPTER 6: CONCLUSIONS AND FUTURE PROSPECTUS

6.1 Conclusions

The experimental results of this dissertation demonstrate the capabilities of scanning probe microscopy for characterizing samples and measuring properties at the nanoscale. The combination of high-resolution imaging with micro- and nanoscopic measurements is useful in the emerging field of molecular electronics. In this dissertation, atomic force microscopy (AFM) was used to characterize cobaltacarborane porphyrins as a model nanomaterial. Modes of AFM were used to characterize the properties of the porphyrins to evaluate the influence of designed molecular structures for measuring surface properties. Conductive-probe AFM was used to compare the conductive properties of cobaltacarborane porphyrins at the nanoscale. The arrangement of substituents and molecular symmetry were shown to affect surface self-assembly and conductive properties of cobaltacarborane nanocrystals.

The AFM can also be used to visualize the arrangement of molecules on surfaces, and experiments can be designed to evaluate surface changes with modifications of environmental parameters or chemical reactions. When operated in a liquid environment, adhesive meniscus forces that are present when operating in air are greatly reduced to enable capture of high resolution images. Steps of chemical reactions or electrochemistry can be monitored *in situ* for experiments in optically transparent liquids using time-lapse AFM. Nanofabrication can be accomplished using an AFM probe in liquid environments with protocols of nanografting and nanoshaving. Biological samples can be examined using liquid AFM in non-denaturing environments.

A key objective for this dissertation was to apply approaches with high-throughput nanoscale lithography to construct arrays of designed test structures for molecular measurements with AFM. Using a combined approach with AFM imaging, nanolithography and particle

lithography combined with vapor deposition, nanopatterns were prepared of alkanethiols on gold substrates, and nanostructures of organosilanes on Si(111). The nanopatterns were used as a surface template to direct the deposition of nanocrystals of cobaltacarborane porphyrins into well-defined surface sites. The hydrophobic characteristics of alkanethiols were used to prevent non-specific attachment at methyl-terminated areas of the SAM, porphyrin crystals were selectively depositied to fill the nanopore areas of the substrate. The porphyrin nanocrystals deposited within the nanopores were visualized using contact mode and tapping-mode AFM.

6.2 Future Prospectus

Using AFM imaging, nanolithography and conductive probe measurements with designed molecular platforms of selected porphyrins, we plan to address questions about the role of intramolecular organization for conductive properties. As the size of electronic devices approach molecular scales, it has been predicted that quantum effects will be observed in electronic conduction. By nanopatterning porphyrins of selected designs into well-defined arrangements on surfaces we plan to obtain measurements of charge transport for different pathways through the molecules, and will integrate reference molecules of *n*-alkanethiol or organosilane SAMs to serve as an internal standard for calibration at the nanoscale. Current-voltage profiles of regular arranged porphyrin nanocrystals can be acquired using CP-AFM, to provide experimental measurements to form the basis of predictive models. Designing the size and structures of porphyrin nanocrystals will provide insight of how molecular structure affects molecular conductance.

Over time, electronic devices increase in temperature, particularly in real-world devices that are exposed to heated environments or sunlight. Candidate organic thin films and nanomaterials being tested for applications in molecular electronics need to be stable for a range of temperatures. Experiments with CP-AFM can be evaluated for temperature stability using CP-AFM measurements with a heated sample stage. Porphyrin samples can be characterized at

successively higher temperatures and heating-cooling cycles using a heated AFM sample stage. The molecular changes of porphyrin nanocrystals that occur as the temperature changes can be characterized and visualized using AFM.

Porphyrins have previously been studied as organic films incorporated in the designs of for dye-sensitized solar cells.[260, 300-301] Imaging and measurements of photocurrents can be accomplished with AFM to evaluate the photoconductive properties of porphyrins. The operation of photocurrent AFM is similar to conductive probe AFM, however a sample bias is not applied for measuring photocurrents. Instead, an external light source generates charge flow in the molecule and the conductive AFM tip is used to map and records the generated photocurrents.

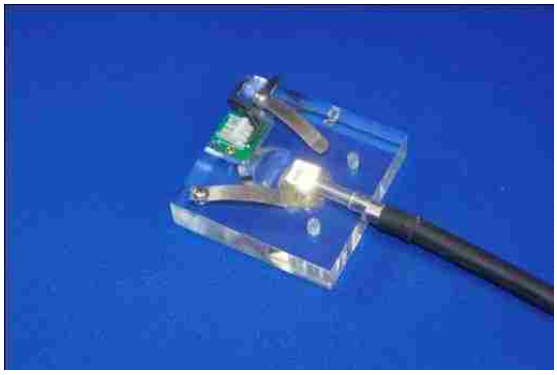

Figure 6.1 Prototype polycarbonate sample stage used for measuring photocurrents with AFM. Samples will require a transparent substrate.

We have begun to build and test a prototype sample stage for measurements of photocurrent (Figure 6.1). The stage can be constructed of glass, quartz or polycarbonate, and incorporates a fiber optic cable and focusing prism lens to focus light through the sample. Not only is the sample stage manufactured with transparent materials, the substrate also needs to be conductive and transparent. Indium-tin oxide (ITO) is a transparent conductive substrate that has been used previously for photocurrent measurements.[302-303] Organosilanes SAMs have been prepared on ITO surfaces.[304] In future planned experiments, particle lithography will be used to

pattern organosilane SAMs on surfaces of ITO for directing the arrangement of porphyrin nanocrystals for measurements with photocurrent AFM.

6.3 Summary

Advancement of molecule-based electronic systems will require the ability to achieve reliable and precise measurements of conductance and charge transport for nano-sized molecular test structures. A considerable challenge is posed for developing reliable and reproducible methods for nanoscale measurements with molecular systems, for scaling nanostructures to nanometer length scales, and for evaluating the effects of molecular structure on electrical properties. The function and efficiency of the molecules in devices is largely attributable to how the molecules are organized on surfaces. Understanding the self-organization and assembly of porphyrins is critical for optimizing the function of these molecules in device applications. Equally important are accurate and sensitive measurements of I-V spectroscopy for systems of individual or small ensembles of candidate molecules. Conceptually, by arranging and orienting molecules on well-defined surfaces, local measurements of charge transport and photocurrents can be enabled for different pathways through the molecules. Also, the resulting size-dependent properties can be evaluated with reliability and sensitivity. Accurate and precise electronic property measurements will give insight on the fundamental mechanisms that give rise to properties such as resistance and rectification with changes in chemical structure towards the development of predictive theoretical models.

REFERENCES

1. Muller, D. J.; Engel, A., The height of biomolecules measured with the atomic force microscope depends on electrostatic interactions. *Biophys. J.* **1997,** *73*, 1633-1644.

2. Lyubchenko, Y. L.; Shlyakhtenko, L. S., Visualization of supercoiled DNA with atomic force microscopy *in situ*. *Proc. Natl. Acad. Sci. USA* **1997,** *94*, 496-501.

3. Scheuring, S.; Müller, D.; Stahlberg, H.; Engel, H.-A.; Engel, A., Sampling the conformational space of membrane protein surfaces with the AFM. *Eur. Biophys. J* **2002,** *31*, 172-178.

4. Senden, T. J.; Drummond, C. J., Surface chemistry and tip-sample interactions in atomic force microscopy. *Colloids Surf., A* **1995,** *94*, 29-51.

5. Kenseth, J. R.; Harnisch, J. A.; Jones, V. W.; Porter, M. D., Investigation of Approaches for the Fabrication of Protein Patterns by Scanning Probe Lithography. *Langmuir* **2001,** *17*, 4105-4112.

6. Rynders, R. M.; Alkier, R. C., Use of In Situ Atomic Force Microscopy to Image Copper Electrodeposits on Platinum. *J. Eectrochem. Soc.* **1994,** *141*, 1166-1173.

7. Lee, Y.; Ding, Z.; Bard, A. J., Combined Scanning Electrochemical/Optical Microscopy with Shear Force and Current Feedback. *Anal. Chem.* **2002,** *74*, 3634-3643.

8. Manne, S.; Hansma, P. K.; Massie, J.; Elings, V. B.; Gewirth, A. A., Atomic-Resolution Electrochemistry with the Atomic Foce Microscope: Copper Deposition on Gold. *Science* **1991,** *251*, 183-186.

9. Xu, S.; Laibinis, P. E.; Liu, G.-y., Accelerating the Kinetics of Thiol Self-Assembly on Gold A Spatial Confinement Effect. *J. Am. Chem. Soc.* **1998,** *120*, 9356-9361.

10. Liu, J.-F.; Cruchon-Dupeyrat, S.; Garno, J. C.; Frommer, J.; Liu, G.-Y., Three-Dimensional Nanostructure Construction via Nanografting: Positive and Negative Pattern Transfer. *Nano Lett.* **2002,** *2*, 937-940.

11. Land, T. A.; DeYoreo, J. J.; Lee, J. D., An in-situ AFM investigation of canavalin crystallization kinetics. *Surf. Sci.* **1997,** *384*, 136-155.

12. Xu, S.; Liu, G. Y., Nanometer-scale fabrication by simultaneous nanoshaving and molecular self-assembly. *Langmuir* **1997,** *13*, 127-129.

13. Hansma, P. K.; Cleveland, J. P.; Radmacher, M.; Walters, D. A.; Hillner, P. E.; Bezanilla, M.; Fritz, M.; Vie, D.; Hansma, H. G.; Prater, C. B.; Massie, J.; Fukunaga, L.; Gurley, J.; Elings, V., Tapping Mode Atomic-Force Microscopy In Liquids. *Appl. Phys. Lett.* **1994,** *64*, 1738-1740.

14. Binnig, G.; Rohrer, H., Scanning Tunneling Microscopy. *Helv. Phys. Acta* **1982,** *55*, 726-735.

15. Binnig, G.; Quate, C. F.; Gerber, C., Atomic Force Microscope. *Phys. Rev. Lett.* **1986,** *56*, 930.

16. Marti, O.; Drake, B.; Hansma, P. K., Atomic Force Microscopy Of Liquid-Covered Surfaces - Atomic Resolution Images. *Appl. Phys. Lett.* **1987,** *51*, 484-486.

17. Drake, B.; Prater, C. B.; Weisenhorn, A. L.; Gould, S. A. C.; Albrecht, T. R.; Quate, C. F.; Cannell, D. S.; Hansma, H. G.; Hansma, P. K., Imaging crystals, polymers, and processes in water with the atomic force microscope. *Science* **1989,** *243*, 1586-1588.

18. Bippes, C. A.; Muller, D. J., High-resolution atomic force microscopy of native membrane proteins. *Rep. Prog. Phys.* **2011,** *74*, 086601.

19. Lyubchenko, Y. L.; Shlyakhtenko, L. S.; Ando, T., Imaging of nucleic acids with atomic force microscopy. *Methods* **2011,** *54*, 274-283.

20. Erlandsson, R.; McClelland, G. M.; Mate, C. M.; Chiang, S., Atomic force microscopy using optical interferometry. *J Vac. Sci. Technol. A* **1988,** *6*, 266-270.

21. Abraham, D. W.; Williams, C.; Slinkman, J.; Wickramasinghe, H. K., Lateral dopant rofiling in semiconductors by force microscopy using capacitive detection. *J. Vac. Sci. Technol. B* **1991,** *9*, 703-706.

22. Edwards, H.; Taylor, L.; Duncan, W.; Melmed, A. J., Fast, high-resolution atomic force microscopy using a quartz tuning fork as actuator and sensor. *J. Appl. Phys.* **1997,** *82*, 980-984.

23. Giessibl, F. J., High-speed force sensor for force microscopy and profilometry utilizing a quartz tuning fork. *Appl. Phys. Lett.* **1998,** *73*, 3956-3958.

24. Tortonese, M.; Barrett, R. C.; Quate, C. F., Atomic resolution with an atomic force microscope using piezoresistive detection. *Appl. Phys. Lett.* **1993,** *62*, 834-836.

25. Xu, S.; Laibinis, P. E.; Liu, G. Y., Accelerating the kinetics of thiol self-assembly on gold - A spatial confinement effect. *J. Am. Chem. Soc.* **1998,** *120*, 9356-9361.

26. Browning-Kelley, M. E.; Wadu-Mesthrige, K.; Hari, V.; Liu, G. Y., Atomic Force Microscopic Study of Specific Antigen/Antibody Binding. *Langmuir* **1997,** *13*, 343-350.

27. Schoenwald, K.; Peng, Z. C.; Noga, D.; Qiu, S. R.; Sulchek, T., Integration of atomic force microscopy and a microfluidic liquid cell for aqueous imaging and force spectroscopy. *Rev. Sci. Instrum.* **2010,** *81*, 053704.

28. Kiridena, W.; Jain, V.; Kuo, P. K.; Liu, G.-Y., Nanometer-scale Elasticity Measurements on Organic Monolayers Using Scanning Force Microscopy. *Surf. Interface Anal.* **1997,** *25*, 383-389.

29. Jourdan, J. S.; Cruchon-Dupeyrat, S. J.; Huan, Y.; Kuo, P. K.; Liu, G. Y., Imaging Nanoscopic Elasticity of Thin Film Materials by Atomic Force Microscopy: Effects of Force Modulation Frequency and Amplitude. *Langmuir* **1999,** *15*, 6495-6504.

30. Li, J.-R.; Garno, J. C., Elucidating the role of surface hydrolysis in preparing organosilane nanostructures via particle lithography. *Nano Lett.* **2008,** *8*, 1916-1922.

31. Pina, C. M.; Pimentel, C.; Garcia-Merino, M., High resolution imaging of the dolomite (104) cleavage surface by atomic force microscopy. *Surf. Sci. 604*, 1877-1881.

32. Xu, S.; Miller, S.; Laibinis, P. E.; Liu, G. Y., Fabrication of nanometer scale patterns within self-assembled monolayers by nanografting. *Langmuir* **1999,** *15*, 7244-7251.

33. Yu, J.-J.; Tan, Y. H.; Li, X.; Kuo, P.-K.; Liu, G.-Y., A nanoengineering aproach to regulate the lateral heterogeneity of self-assembled monolayers. *J. Am. Chem. Soc.* **2006,** *128*, 11574-11581.

34. Putman, C. A. J.; VanderWerf, K.; De Grooth, B. G.; VanHulst, N. F.; Greve, J., Tapping Mode Atomic Force Microscopy in Liquid. *Appl. Phys. Lett.* **1994,** *64*, 2454-2456.

35. Han, W.; Lindsay, S. M.; Jing, T., A magnetically driven oscillating probe microscope for operation in liquids. *Appl. Phys. Lett.* **1996,** *69*, 4111-4113.

36. Noy, A.; Sanders, C. H.; Vezenov, D. V.; Wong, S. S.; Lieber, C. M., Chemically-Sensitive Imaging in Tapping Mode by Chemical Force Microscopy: Relationship between Phase Lag and Adhesion. *Langmuir* **1998,** *14*, 1508-1511.

37. Price, W. J.; Leigh, S. A.; Hsu, S. M.; Patten, T. E.; Liu, G.-y., Measuring the Size Dependence of Young's Modulus Using Force Modulation Atomic Force Microscopy. *J. Phys. Chem. A* **2006,** *110*, 1382-1388.

38. Fukuma, T.; Kobayashi, K.; Matsushige, K.; Yamada, H., True molecular resolution in liquid by frequency-modulation atomic force microscopy. *Appl. Phys. Lett.* **2005,** *86*, 193108.

39. Fukuma, T.; Kobayashi, K.; Matsushige, K.; Yamada, H., True atomic resolution in liquid by frequency-modulation atomic force microscopy. *Appl. Phys. Lett.* **2005,** *87*.

40. Rode, S.; Oyabu, N.; Kobayashi, K.; Yamada, H.; Kuhnle, A., True Atomic-Resolution Imaging of (1014) Calcite in Aqueous Solution by Frequency Modulation Atomic Force Microscopy. *Langmuir* **2009,** *25*, 2850-2853.

41. Asakawa, H.; Fukuma, T., The molecular-scale arrangement and mechanical strength of phospholipid cholesteral mixed bilayers investigated by frequency modulation atomic force microscopy in liquid. *Nanotech.* **2009,** *20*, 264008.

42. Fukuma, T., Subnanometer-Resolution Frequency Modulation Atomic Force Microscopy in Liquid for Biological Applications. *Jap. J. Appl. Phys.* **2009,** *48*, 08JA01.

43. Weisenhorn, A. L.; Hansma, P. K.; Albrecht, T. R.; Quate, C. F., Forces In Atomic Force Microscopy In Air And Water. *Appl. Phys. Lett.* **1989,** *54*, 2651-2653.

44. Weisenhorn, A. L.; Maivald, P.; Butt, H.-J.; Hansma, P. K., Measuring adhesion, attraction and repulsion between surfaces in liquids with an atomic-force microscope. *Phys. Rev. B* **1992,** *45*, 11226-11231.

45. Butt, H.-J.; Cappella, B.; Kappl, M., Force measurements with the atomic fore microscope: Technique, interpretation and applications. *Surf. Sci. Reports* **2005,** *59*, 1-152.

46. Zlatanova, J.; Lindsay, S. M.; Leuba, S. H., Single molecule force spectroscopy in biology using the atomic force microscope. *Biphys. Molec. Biol.* **2000,** *74*, 37-61.

47. Goldsbury, C.; Kistler, J.; Aebi, U.; Arvinte, T.; Cooper, G. J. S., Watching Amyloid Fibrils Grow by Time-lapse Atomic Force Microscopy. *J. Mol. Biol.* **1999,** *285*, 33-39.

48. Cisneros, D. A.; Hung, C.; Franz, C. M.; Muller, D. J., Observing growth steps of collagen self-assembly by time-lapse high-resolution atomic force microscopy. *J. Struct. Biol.* **2006,** *154*, 232-245.

49. Jiao, Y.; Cherny, D. I.; Heim, G.; Jovin, T. M.; Schaffer, T. E., Dynamic Interactions of p53 with DNA in Solution by Time-Lapse Atomic Force Microscopy. *J. Mol. Biol.* **2001,** *314*, 233-243.

50. Stolz, M.; Stoffler, D.; Aebi, U.; Goldsbury, C., Monitoring biomolecular interactions by time-lapse atomic force microscopy. *J. Struct. Biol.* **2000,** *131*, 171-180.

51. Wadu-Mesthrge, K.; Amro, N. A.; Garno, J. C.; Xu, S.; Liu, G.-Y., Fabrication of nanometer-sized protein patterns using AFM and selective immobilization. *Biophys. J.* **2001** *80*, 1891-1899.

52. Ngunjiri, J. N.; Garno, J. C., AFM-Based Lithography for Nanoscale Protein Assays. *Anal. Chem.* **2008,** *80*, 1361-1369.

53. Bard, A. J.; Fan, F.-R. F.; Pierce, D. T.; Unwin, P. R.; Wipf, D. O.; Zhou, F., Chemical Imaging of Surfaces with the Scanning Electrochemical Microscope. *Science* **1991,** *254*, 68-74.

54. Bu, D. L.; Mullen, T. J.; Liu, G. Y., Regulation of Local Structure and Composition of Binary Disulfide and Thiol Self-Assembled Monolayers Using Nanografting. *ACS Nano 4*, 6863-6873.

55. Bard, A. J.; Fan, F.-R. F.; Kwak, J.; Lev, O., Scanning Electrochemical Microscopy. Introduction and Principles. *Anal. Chem.* **1989,** *61*, 132-138.

56. Sun, P.; Laforge, F. O.; Mirkin, M. V., Scanning electrochemical microscopy in the 21st century. *Phys. Chem. Chem. Phys.* **2007,** *9*, 802-823.

57. Macpherson, J. V.; Unwin, P. R., Combined Scanning Electrochemical-Atomic Force Microscope. *Anal. Chem.* **2000,** *72*, 276-285.

58. Manne, S.; Hansma, P. K.; Massie, J.; Elings, V. B.; Gewirth, A. A., Atomic-Resolution Electrochemistry with the Atomic Force Microscope: Copper Deposition on Gold. *Science* **1991,** *251*, 183-186.

59. Frederix, P. L. T. M.; Bosshart, P. D.; Akiyama, T.; Chami, M.; Gullo, M. R.; Blackstock, J. J.; Dooleweerdt, K.; deRooij, N. F.; Staufer, U.; Engel, A., Conductive supports for combined AFM-SECM on biological membranes. *Nanotech.* **2008,** *19*, 384004.

60. Pierce, D. T.; Unwin, P. R.; Bard, A. J., Scanning Electrochemicl Microscopy. 17. Studies of Enzyme-Mediator Kinetics for Membrane- and Surface- Immobilized Glucose Oxidase. *Anal. Chem.* **1992,** *64*, 1795-1804.

61. Zhang, H.; Ma, Y.; Lu, Z.; Gu, Z.-Z., Self-assembly films of tetrakis(hydroxyphenyl) porphyrins. *Colloids Surf., A* **2005,** *257-258*, 291-294.

62. Shen, Y.; Trauble, M.; Wittstock, G., Electrodeposited noble metal particle in polyelectrolyte multilayer matrix as electrocatalyst for oxygen reduction studied using SECM. *Phys. Chem. Chem. Phys.* **2008,** *10*, 3635-3644.

63. Davoodi, A.; Pan, J.; Leygraf, C.; Norgren, S., In Situ Investigation of Localized Corrosion of Aluminum Alloys in Chloride Solution Using Integrated EC-AFM/SECM Techniques. *Electrochem. Solid State Lett.* **2005,** *8*, B21-B24.

64. Diakowski, P. M.; Ding, Z., Interrogation of living cells using alternating current scanning electrochemical microscopy (AC-SECM). *Phys. Chem. Chem. Phys.* **2007,** *9*, 5966-5974.

65. Lie, L. H.; Mirkin, M. V.; Hakkarainen, S.; Houlton, A.; Horrocks, B. R., Electrochemical detection of lateral charge transport in metal complex-DNA monolayers sythesized on Si(111) electrodes. *J. Electroanal. Chem.* **2007,** *603*, 67-80.

66. Shou, J.; Wipf, D. O., Deposition of Conducting Polyaniline Patterns with the Scanning Electrochemical Microscope. *J. Electrochem. Soc.* **1997,** *144*, 1202-1207.

67. Nijhuis, C. A.; Sinha, J. K.; Wittstock, G.; Huskens, J.; Ravoo, B. J.; Reinhoudt, D. N., Controlling the Supramolecular Assembly of Redox-Active Dendrimers at Molecular Printboards by Scanning Electrochemical Microscopy. *Langmuir* **2006,** *22*, 9770-9775.

68. Chen, C.-h.; Washburn, N.; Gewirth, A. A., In Situ Atomic Force Microscope Study of Pb Underpotential Deposition on Au(111): Structural Properties of the Catalytically Active Phase. *J. Phys. Chem.* **1993,** *97*, 9754-9760.

69. Meltzer, S.; Mandler, D., Microwriting of Gold Patterns with the Scanning Electrochemical Microscope. *J. Eectrochem. Soc.* **1995,** *142*, L82-L84.

70. Ku, S.-Y.; Wong, K.-T.; Bard, A. J., Surface Patterning with Fluorescent Molecules Using Click Chemistry Directed by Scanning Electrochemical Microscopy. *J. Am. Chem. Soc.* **2008,** *130*, 2392-2393.

71. Yu, J.-J.; Ngunjiri, J. N.; Kelley, A. T.; Garno, J. C., Nanografting versus Solution Self Assembly of α,ω-Alkanedithiols on Au(111) Investigated by AFM. *Langmuir* **2008,** *24*, 11661-11668.

72. Xu, S.; Liu, G.-Y., Nanometer-scale fabrication by simultaneous nanoshaving and molecular self-assembly. *Langmuir* **1997,** *13*, 127-129.

73. Ryu, S.; Schatz, G. C., Nanografting: Modeling and simulation. *J. Am. Chem. Soc.* **2006,** *128*, 11563-11573.

74. Ngunjiri, J. N.; Kelley, A. T.; Lejeune, Z. M.; Li, J. R.; Lewandowski, B. R.; Serem, W. K.; Daniels, S. L.; Lusker, K. L.; Garno, J. C., Achieving precision and reproducibility for writing patterns of n-alkanethiol self-assembled monolayers with automated nanografting. *Scanning* **2008,** *30*, 123-136.

75. Yang, G.; Garno, J. C.; Liu, G.-Y., *Scanning Probe-Based Lithography for Production of Biological and Organic Nanostructures on Surfaces (4.01)*. Elsevier B. V.: Amsterdam, 2011.

76. Tian, T.; LeJeune, Z. M.; Serem, W. K.; Yu, J.-J.; Garno, J. C., Nanografting: a method for bottom-up fabrication of designed nanostructures. . In *Tip-Based Nanofabrication*, Tseng, A. A., Ed. Springer-Verlag: New York, 2011.

77. Ngunjiri, J. N.; Li, J.-R.; Garno, J. C., Nanolithography: Towards fabrication of nanodevices for life sciences. In *Nanodevices for the Life Sciences*, Kumar, C. S. S. R., Ed. Wiley-VCH: 2006.

78. Liu, J. F.; Cruchon-Dupeyrat, S.; Garno, J. C.; Frommer, J.; Liu, G. Y., Three-dimensional nanostructure construction via nanografting: Positive and negative pattern transfer. *Nano Letters* **2002,** *2*, 937-940.

79. Zhou, D. J.; Wang, X. Z.; Birch, L.; Rayment, T.; Abell, C., AFM study on protein immobilization on charged surfaces at the nanoscale: Toward the fabrication of three-dimensional protein nanostructures. *Langmuir* **2003,** *19*, 10557-10562.

80. Price, W. J.; Kuo, P. K.; Lee, T. R.; Colorado, R.; Ying, Z. C.; Liu, G. Y., Probing the local structure and mechanical response of nanostructures using force modulation and nanofabrication. *Langmuir* **2005,** *21*, 8422-8428.

81. Price, W. J.; Leigh, S. A.; Hsu, S. M.; Patten, T. E.; Liu, G. Y., Measuring the size dependence of Young's modulus using force modulation atomic force microscopy. *J. Phys. Chem. A* **2006,** *110*, 1382-1388.

82. Liang, J.; Rosa, L. G.; Scoles, G., Nanostructuring, Imaging and molecular manipulation of dithiol monolayers on au(111) surfaces by atomic force Microscopy. *J. Phys Chem. C* **2007,** *111*, 17275-17284.

83. Ngunjiri, J.; Garno, J. C., AFM-based lithography for nanoscale protein assays. *Anal. Chem.* **2008,** *80*, 1361-1369.

84. Yu, J. H.; Ngunjiri, J. N.; Kelley, A. T.; Garno, J. C., Nanografting versus Solution Self-Assembly of alpha,omega-Alkanedithiols on Au(111) Investigated by AFM. *Langmuir* **2008,** *24*, 11661-11668.

85. Tan, Y. H.; Liu, M.; Nolting, B.; Go, J. G.; Gervay-Hague, J.; Liu, G. Y., A Nanoengineering Approach for Investigation and Regulation of Protein Immobilization. *ACS Nano* **2008,** *2*, 2374-2384.

86. Amro, N. A.; Kotra, L. P.; Wadu-Mesthrige, K.; Bulychev, A.; Mobashery, S.; Liu, G.-y., High-Resolution Atomic Force Microscopy Studies of the Escherichia coli Outer Membrane:â€‰ Structural Basis for Permeability. *Langmuir* **2000,** *16*, 2789-2796.

87. Schenk, A. D.; Werten, P. J. L.; Scheuring, S.; deGroot, B. L.; Muller, S. A.; Stahlberg, H.; Philippsen, A.; Engel, A., The 4.5 A Structure of Human AQP2. *J. Mol. Biol.* **2005,** *350*, 278-289.

88. Scheuring, S.; Ringler, P.; Borgnia, M.; Stahlberg, H.; Muller, D. J.; Agre, p.; Engel, A., High resolution AFM topographs of the Escherichia coli water channel aquaporin Z. *EMBO J.* **1999,** *18*, 4981-4987.

89. Muller, D. J.; Schabert, F. A.; Buldt, G.; Engel, A., Imaging Purple membranes in Aqueous Solutions at Sub-Nanometer Resolution by Atomic Force Microscopy. *Biophys. J.* **1995,** *68*, 1681-1686.

90. Frederix, P., L. T. M. ; Gullo, M. R.; Akiyama, T.; Tonin, A.; deRooij, N. F.; Staufer, U.; Engel, A., Assessment of insulated conductive cantilevers for biology and electrochemistry. *Nanotech.* **2005,** *16*, 997.

91. Boussaad, S.; Tao, N. J., Electron transfer and adsorption of myoglobin on self-assembled surfactant films: An electrochemical tapping-mode AFM study. *J. Am. Chem. Soc.* **1999,** *121*, 4510-4515.

92. Putman, C. A. J.; Van der Werf, K. O.; De Grooth, B. G.; Van Hulst, N. F.; Greve, J., Tapping mode atomic force microscopy in liquid. *Appl. Phys. Lett.* **1994,** *64*, 2454.

93. Sousa, S. R.; Bras, M. M.; Moradas-Ferreira, P.; Barbosa, M. A., Dynamics of fibronectin adsorption on TiO(2) surfaces. *Langmuir* **2007,** *23*, 7046-7054.

94. Kienberger, F.; Stroh, C.; Kada, G.; Moser, R.; Baumgartner, W.; Pastushenko, V.; Rankl, C.; Schmidt, U.; Muller, H.; Orlova, E.; LeGrimellec, C.; Drenckhahn, D.; Blaas, D.; Hinterdorfer, P., Dynamic force microscopy imaging of native membranes. *Ultramicroscopy* **2003,** *97*, 229-237.

95. Müller, D. J.; Engel, A.; Matthey, U.; Meier, T.; Dimroth, P.; Suda, K., Observing Membrane Protein Diffusion at Subnanometer Resolution. *J. Mol. Biol.* **2003,** *327*, 925-930.

96. Deng, Z.; Lulevich, V.; Liu, F. T.; Liu, G. Y., Applications of Atomic Force Microscopy in Biophysical Chemistry of Cells. *J. Phys. Chem. B 114*, 5971-5982.

97. Zink, T.; Deng, Z.; Chen, H.; Yu, L.; Liu, F. T.; Liu, G. Y., High-resolution three-dimensional imaging of the rich membrane structures of bone marrow-derived mast cells. *Ultramicroscopy* **2008,** *109*, 22-31.

98. Hansma, H. G.; Vesenka, J.; Siegerist, C.; Kelderman, G.; Morrett, H.; Sinsheimer, R. L.; Elings, V.; Bustamante, C.; Hansma, P. K., Reproducible Imaging and Dissection of Plasmid DNA Under Liquid with the Atomic Force Microscope. *Science* **1992,** *256* (5060), 1180-1184.

99. Humphris, A. D. L.; Round, A. N.; Miles, M. J., Enhanced imaging of DNA via active quality factor control. *Surf. Sci.* **2001,** *491*, 468-472.

100. Kasas, S.; Thomson, N. H.; Smith, B. L.; Hansma, H. G.; Zhu, X.; Guthold, M.; Bustamante, C.; Kool, E. T.; Kashlev, M.; Hansma, P. K., Escherichia coli RNA Polymerase Activity Observed Using Atomic Force Microscopyâ€ *Biochemistry* **1997,** *36*, 461-468.

101. Liang, Y.; Fotiadis, D.; Filipek, S.; Saperstein, D. A.; Palczewski, K.; Engel, A., Organization of the G protein-coupled receptors rhodopsin and opsin in native membranes. *J. Biol. Chem.* **2003,** *278*, 21655-21662.

102. Müller, D. J.; Dencher, N. A.; Meier, T.; Dimroth, P.; Suda, K.; Stahlberg, H.; Engel, A.; Seelert, H.; Matthey, U., ATP synthase: constrained stoichiometry of the transmembrane rotor. *FEBS Letters* **2001,** *504*, 219-222.

103. Guthold, M.; Bezanilla, M.; Erie, D. A.; Jenkins, B.; Hansma, H. G.; Butstamante, C., Following the assembly of RNA polymerase-DNA complexes in aqueous solutions with the scanning force microscope. *Proc. Natl. Acad. Sci. USA* **1994,** *91*, 12927-12931.

104. Schoenenberger, C.-A.; Hoh, J. H., Slow cellular dynamics in MDCK and R5 cells monitored by time-lapse atomic force microscopy. *Biophys. J.* **1994,** *67*, 929-936.

105. Lyubchenko, Y. L.; Shlyakhtenko, L. S., AFM for analysis of structure and dynamics of DNA and protein-DNA complexes. *Methods* **2009,** *47*, 206-213.

106. Liu, M.; Amro, N. A.; Liu, G.-Y., Nanografting for Surface Physical Chemistry *Annu. Rev. Phys. Chem.* **2008,** *59*, 367-386.

107. Case, M. A.; McLendon, G. L.; Hu, Y.; Vanderlick, T. K.; Scoles, G., Using Nanografting to Achieve Directed Assembly of de novo Designed Metalloproteins on Gold. *Nano Lett.* **2003,** *3*, 425-429.

108. Hu, Y.; Das, A.; Hecht, M. H.; Scoles, G., Nanografting de novo proteins onto gold surfaces. *Langmuir* **2005,** *21*, 9103-9109.

109. Amro, N. A.; Liu, G.-y., Positioning protein molecules on surfaces: A nanoengineering approach to supramolecular chemistry. *Proc. Natl. Acad. Sci. U.S.A.* **2002,** *99*, 5165-5170.

110. Tan, Y. H.; Liu, M.; Nolting, B.; Go, J. G.; Gervay-Hague, J.; Liu, G.-Y., A Nanoengineering Approach for Investigation and Regulation of Protein Immobilization. *Acs Nano* **2008,** *2*, 2374-2384.

111. Schwartz, P. V., Meniscus Force Nanografting: Nanoscopic Patterning of DNA. *Langmuir* **2001,** *17*, 5971-5977.

112. Mirmomtaz, E.; Castronovo, M.; Grunwald, C.; Bano, F.; Scaini, D.; Ensafi, A. A.; Scoles, G.; Casalis, L., Quantitative Study of the Effect of Coverage on the Hybridization Efficiency of Surface-Bound DNA Nanostructures. *Nano Lett.* **2008,** *ASAP*.

113. Liu, M.; Amro, N. A.; Chow, C. S.; Liu, G.-Y., Production of Nanostructures of DNA on Surfaces. *Nano Lett.* **2002,** *2*, 863-867.

114. Liu, M.; Liu, G.-Y., Hybridization with nanostructures of single-stranded DNA. *Langmuir* **2005,** *21*, 1972-1978.

115. Castronovo, M.; Radovic, S.; Grunwald, C.; Casalis, L.; Morgante, M.; Scoles, G., Control of steric hindrance on restriction enzyme reactions with surface-bound DNA nanostructures. *Nano Lett.* **2008,** *8*, 4140-4145.

116. Rosei, F., Nanostructured surfaces: challenges and frontiers in nanotechnology. *J. Phys.: Condens. Matter* **2004,** *16*, S1373-S1436.

117. Carroll, R. L.; Gorman, C. B., The Genesis of Molecular Electronics. *Angew. Chem. Int. Ed.* **2002,** *41*, 4378-4400.

118. Joachim, C.; Gimzewski, J. K.; Aviram, A., Electronics using hybrid-molecular and mono-molecular devices. *Nature* **2000,** *408*, 541-548.

119. Colton, R. J., Nanoscale measurements and manipulation. *J. Vac. Sci. Technol., B* **2004,** *22*, 1609-1635.

120. Frommer, J., Scanning tunneling microscopy and atomic force microscopy in organic chemistry. *Angew. Chem. Int. Ed.* **1992,** *31*, 1298-1328.

121. Hansma, H. G.; Hoh, J. H., Biomolecular imaging with the atomic force microscope. *Ann. Rev. Biophys. Biomol. Struct.* **1994,** *23*, 115-139.

122. James, D. K.; Tour, J. M., Electrical Measurements in Molecular Electronics. *Chem. Mater.* **2004,** *16*, 4423-4435.

123. Tomfohr, J.; Ramachandran, G. K.; Sankey, O. F.; Lindsay, S. M., Ch. 11, Making Contacts to Single Molecules: Are We There Yet? In *Introducing Molecular Electronics*, Cuniberti, G.; Fagas, G.; Richter, K., Eds. Springer-Verlag: The Netherlands, 2005.

124. Reed, M. A.; Zhou, C.; Muller, C. J.; Burgin, T. P.; Tour, J. M., Conductance of a Molecular Junction. *Science* **1997,** *278*, 252-254.

125. Kergueris, C.; Bourgoin, J.-P.; Palacin, S.; Esteve, D.; Urbina, C.; Magoga, M.; Joachim, C., Electron transport through a metal-molecule-metal junction. *Phys. Rev. B* **1999,** *59*, 12505-12513.

126. Muller, C. J.; Vleeming, B. J.; Reed, M. A.; Lamba, J. J. S.; Hara, R.; Jones, L.; Tour, J. M., Atomic probes: a search for conduction through a single molecule. *Nanotechnology* **1996,** *7*, 409-411.

127. Reed, M. A.; Zhou, C.; Muller, C. J.; Burgin, T. P.; Tour, J. M., Conductance of a molecular junction. *Science* **1997,** *278*, 252-254.

128. Gonsalves, K. E.; Merhari, L.; Wu, H.; Hu, Y., Organic-Inorganic Nanocomposites: Unique Resists for Nanolithography. *Adv. Mater.* **2001,** *13*, 703-714.

129. Cui, X. D.; Primak, A.; Zarate, X.; Tomfohr, J.; Sankey, O.; Moore, A. L.; Moore, T. A.; Gust, D.; Harris, G.; Lindsay, S., Reproducible Measurement of Single-Molecule Conductivity. *Science* **2001,** *294*, 571-574.

130. Ramachandran, G. K.; Tomfohr, J. K.; Li, J.; Sankey, O. F.; Zarate, X.; Primak, A.; Terazono, Y.; Moore, T. A.; Moore, A. L.; Gust, D.; Nagahara, L. A.; Lindsay, S. M., Electron transport properties of a carotene molecule in a metal-(single molecule)-metal junction. *J. Phys. Chem. B* **2003,** *107*, 6162-6169.

131. Dorogi, M.; Gomez, J.; Osifchin, R.; Andres, R. P., Room-temperature Coulomb blockade from a self-assembled molecular nanostructure. *Phys. Rev. B* **1995,** *52*, 9071-9077.

132. Kushmerick, J. G.; Holt, D. B.; Pollack, S. K.; Ratner, M. A.; Yang, J. C.; Schull, T. L.; Naciri, J.; Moore, M. H.; Shashidhar, R., Effect of Bond-Length Alternation in Molecular Wires. *J. Am. Chem. Soc.* **2002,** *124*, 10654-10655.

133. Kushmerick, J. G.; Holt, D. B.; Yang, J. C.; Naciri, J.; Moore, M. H.; Shashidhar, R., Metal-molecule contacts and charge transport across monomolecular layers: Measurement and theory. *Phys. Rev. Lett.* **2002,** *89*, 868021-868024.

134. Kushmerick, J. G.; Blum, A. S.; Long, D. P., Metrology for molecular electronics. *Anal. Chim. Acta* **2006,** *568*, 20-27.

135. Austin, M. D.; Chou, S. Y., Fabrication of a molecular self-assembled monolayer diode using nanoimprint lithography. *Nano Lett.* **2003,** *3*, 1687-1690.

136. Wang, W.; Lee, T.; Reed, M. A., Mechanism of electron conduction in self-assembled alkanethiol monolayer devices. *Phys. Rev. B* **2003,** *68*, 354161-354167.

137. Tour, J. M.; Rawlett, A. M.; Kozaki, M.; Yao, Y.; Jagessar, R. C.; Dirk, S. M.; Price, D. W.; Reed, M. A.; Zhou, C.-W.; Chen, J.; Wang, W.; Campbell, I., Synthesis and Preliminary Testing of Molecular Wires and Devices. *Chem. Eur. J.* **2001,** *7*, 5118-5134.

138. Chen, J.; Reed, M. A.; Rawlett, A. M.; Tour, J. M., Large On-Off Ratios and Negative Differential Resistance in a Molecular Electronic Device. *Science* **1999,** *286*, 1550-1551.

139. Sachs, S. B.; Dudek, S. P.; Hsung, R. P.; Sita, L. R.; Smalley, J. F.; Newton, M. D.; Feldberg, S. W.; Chidsey, C. E. D., Rates of Interfacial Electron Transfer through pi-Conjugated Spacers. *J. Am. Chem. Soc.* **1997,** *119*, 10563-10564.

140. Carter, M. T.; Rowe, G. K.; Richardson, J. N.; Tender, L. M.; Terrill, R. H.; Murray, R. W., Distance Dependence of the Low-Temperature Electron Transfer Kinetics of

(Ferrocenylcarboxy)-Terminated Alkanethiol Monolayers. *J. Am. Chem. Soc.* **1995,** *117*, 2896-2899.

141. Miller, C.; Cuendet, P.; Gratzel, M., Adsorbed w-Hydroxy Thiol Monolayers on Gold Eelctrodes: Evidence for Electron Tunneling to Redox Species in Solution. *J. Phys. Chem.* **1991,** *95*, 877-886.

142. Chabinyc, M. L.; Chen, X.; Holmlin, R. E.; Jacobs, H.; Skulason, H.; Frisbie, C. D.; Mujica, V.; Ratner, M. A.; Rampi, M. A.; Whitesides, G. M., Molecular Rectification in a Metal-Insulator-Metal Junction Based on Self-Assembled Monolayers. *J. Am. Chem. Soc.* **2002,** *124*, 11730-11736.

143. Holmlin, R. E.; Haag, R.; Chabinyc, M. L.; Ismagilov, R. F.; Cohen, A. E.; Terfort, A.; Rampi, M. A.; Whitesides, G. M., Electron transport through thin organic films in metal-insulator-metal junctions based on self-assembled monolayers. *J. Am. Chem. Soc.* **2001,** *123*, 5075-5085.

144. Wold, D. J.; Frisbie, C. D., Formation of metal-molecule-metal tunnel junctions: Microcontacts to alkanethiol monolayers with a conducting AFM tip. *J. Am. Chem. Soc* **2000,** *122*, 2970-2971.

145. Leatherman, G.; Durantini, E. N.; Gust, D.; Moore, T. A.; Moore, A. L.; Stone, S.; Zhou, Z.; Rez, P.; Liu, Y. Z.; Lindsay, S. M., Carotene as a molecular wire: Conducting atomic force microscopy. *J. Phys. Chem. B* **1999,** *103*, 4006-4010.

146. Ishida, T.; Mizutani, W.; Aya, Y.; Ogiso, H.; Sasaki, S.; Tokumoto, H., Electrical Conduction of Conjugated Molecular SAMs Studied by Conductive Atomic Force Microscopy. *J. Phys. Chem. B* **2002,** *106*, 5886-5892.

147. Salmeron, M.; Neubauer, G.; Folch, A.; Tomitori, M.; Ogletree, D. F.; Sautet, P., Viscoelastic and Electrical Properties of Self-Assembled Monolayers on Au(111) Films. *Langmuir* **1993,** *9*, 3600-3611.

148. Fan, F.-R. F.; Yang, J.; Cai, L.; Price, D. W.; Dirk, S. M.; Kosynkin, D. V.; Yao, Y.; Rawlett, A. M.; Tour, J. M.; Bard, A. J., Charge Transport through Self-Assembled Monolayers of Compounds of Interest in Molecular Electronics. *J. Am. Chem. Soc.* **2002,** *124*, 5550-5560.

149. Bumm, L. A.; Arnold, J. J.; Dunbar, T. D.; Allara, D. L.; Weiss, P. S., Electron Transfer through Organic Molecules. *J. Phys. Chem. B* **1999,** *103*, 8122-8127.

150. Hong, S.; Reifenberger, R.; Tian, W.; Datta, S.; Henderson, J.; Kubiak, C. P., Molecular conductance spectroscopy of conjugated, phenyl-based molecules on Au(111): the effect of end groups on molecular conduction. *Superlattices Microstruct.* **2000,** *28*, 289-303.

151. Seminario, J. M.; Zacarias, A. G.; Tour, J. M., Molecular Current-Voltage Characteristics. *J. Phys. Chem. A* **1999,** *103*, 7883-7887.

152. Tian, W.; Datta, S.; Hong, S.; Reifenberger, R.; Henderson, J. I.; Kubiak, C. P., Conductance spectra of molecular wires. *J. Chem. Phys.* **1998,** *109*, 2874-2882.

153. Kang, B. K.; Aratani, N.; Lim, J. K.; Kim, D.; Osuka, A.; Yoo, K.-H., Electrical transport properties and their reproducibility for linear porphyrin arrays. *Mater. Sci. Eng.* **2006,** *26*, 1023-1027.

154. Kang, B. K.; Aratani, N.; Lim, J. K.; Kim, D.; Osuka, A.; Yoo, K.-H., Length and temperature dependence of electrical conduction through dithiolated porphyrin arrays. *Chem. Phys. Lett.* **2005,** *412*, 303-306.

155. Sedghi, G.; Sawada, K.; Esdaile, L. J.; Hoffmann, M.; Anderson, H. L.; Bethell, D.; Haiss, W.; Higgins, S. J.; Nichols, R. J., Single Molecule Conductance of Porphyrin Wires with Ultralow Attenuation. *J. Am. Chem. Soc.* **2008,** *web release*.

156. Yanov, I.; Kholod, Y.; Leszczynski, J.; Palacios, J. J., Electron transport properties of the porphyrin molecule located between gold electrodes. *Chem. Phys. Lett.* **2007,** *445*, 238-242.

157. Choi, J.; Chipara, M.; Xu, B.; Yang, C. S.; Doudin, B.; Dowben, P. A., Comparison of the pi-conjugated ring orientations in polyaniline and polypyrrole *Chem. Phys. Lett.* **2004,** *343*, 193.

158. Auwarter, W.; Weber-Bargioni, A.; Riemann, A.; Schiffrin, A.; Groning, O.; Fasel, R.; Barth, J. V., Self-assembly and conformation of tetrapyridyl-porphyrin molecules on Ag(111). *J. Chem. Phys.* **2006,** *124*, 194708.

159. Venkataraman, L.; Klare, J. E.; Nuckolls, C.; Hybertsen, M. S.; Steigerwald, M. L., Dependence of single-molecule junction conductance on molecular conformation. *Nature* **2006,** *442*, 904-907.

160. Kornilovitch, P. E.; Bratkovsky, A. M., Orientational dependence of current through molecular films. *Phys. Rev. B* **2001,** *64*, 195413.

161. Morita, S.; Ishizaka, T.; Sugawara, Y.; Okada, T.; Mishima, S.; Imai, S.; Mikoshiba, N., Surface Conductace of Metal-Surfaces in Air Studied With a Force Microscope. *Jpn. J. Appl. Phys., Part 2* **1989,** *28*, L1634-L1636.

162. Shafai, C.; Thomson, D. J.; Simard-Normandin, M. In *Two-dimensional delineation of semiconductor doping by scanning resistance microscopy*, Res. Triangle Park, North Carolina (USA), AVS: Res. Triangle Park, North Carolina (USA), 1994; pp 378-382.

163. Kelley, T. W.; Granstrom, E.; Frisbie, C. D., Conducting probe atomic force microscopy: a characterization tool for molecular electronics. *Adv. Mater.* **1999,** *11*, 261-264.

164. Park, J. Y.; Maier, S.; Hendriksen, B.; Salmeron, M., Sensing current and forces with SPM. *Mater. Today* **2010,** *13*, 38-45.

165. Beebe, J. M.; Engelkes, V. B.; Miller, L. L.; Frisbie, C. D., Contact Resistance in Metal−Molecule−Metal Junctions Based on Aliphatic SAMs: Effects of Surface Linker and Metal Work Function. *J. Am. Chem. Soc.* **2002,** *124*, 11268-11269.

166. Cui, X. D.; Primak, A.; Zarate, X.; Tomfohr, J.; Sankey, O. F.; Moore, A. L.; Moore, T. A.; Gust, D.; Harris, G.; Lindsay, S. M., Reproducible measurement of single-molecule conductivity. *Science* **2001,** *294*, 571-574.

167. Engelkes, V. B.; Beebe, J. M.; Frisbie, C. D., Length-Dependent Transport in Molecular Junctions Based on SAMs of Alkanethiols and Alkanedithiols: Effect of Metal Work Function and Applied Bias on Tunneling Efficiency and Contact Resistance. *J. Am. Chem. Soc.* **2004,** *126*, 14287-14296.

168. Leatherman, G.; Durantini, E. N.; Gust, D.; Moore, T. A.; Moore, A. L.; Stone, S.; Zhou, Z.; Rez, P.; Liu, Y. Z.; Lindsay, S. M., Carotene as a molecular wire: conducting atomic force microscopy. *J. Phys. Chem. B* **1998,** *103*, 4006-4010.

169. Li, X.; He, J.; Hihath, J.; Xu, B.; Lindsay, S. M.; Tao, N., Conductance of Single Alkanedithiols: Conduction Mechanism and Effect of Molecule−Electrode Contacts. *J. Am. Chem. Soc.* **2006,** *128*, 2135-2141.

170. Loiacono, M. J.; Granstrom, E. L.; Frisbie, C. D., Investigation of Charge Transport in Thin, Doped Sexithiophene Crystals by Conducting Probe Atomic Force Microscopy. *J. Phys. Chem. B* **1998,** *102*, 1679-1688.

171. Salomon, A.; Cahen, D.; Lindsay, S.; Tomfohr, J.; Engelkes, V. B.; Frisbie, C. D., Comparison of electronic transport measurements on organic molecules. *Adv. Mater.* **2003,** *15*, 1881-1890.

172. Kerimo, J.; Adams, D. M.; Barbara, P. F.; Kaschak, D. M.; Mallouk, T. E., NSOM Investigations of the Spectroscopy and Morphology of Self-Assembled Multilayered Thin Films *J. Phys. Chem. B* **1998,** *102*, 9451-9460.

173. O'Shea, S. J.; Atta, R. M.; Welland, M. E., Characterization of tips for conducting atomic force microscopy. *Rev. Sci. Instrum.* **1995,** *66*, 2508-2512.

174. Verveniotis, E.; Rezek, B.; Sípek, E.; Stuchlík, J.; Kocka, J., Role of current profiles and atomic force microscope tips on local electric crystallization of amorphous silicon. *Thin Solid Films* **2010,** *518*, 5965-5970.

175. Houze, F.; Meyer, R.; Schneegans, O.; Boyer, L., Imaging the local electrical properties of metal surfaces by atomic force microscopy with conducting probes. *Appl. Phys. Lett.* **1996,** *69*, 1975-1977.

176. Kelley, T. W.; Granstrom, E. L.; Frisbie, C. D., Conducting probe atomic force microscopy: A characterization tool for molecular electronics. *Adv. Mater.* **1999,** *11*, 261-264.

177. Wold, D. J.; Frisbie, C. D., Formation of Metal-Molecule-Metal Tunnel Junctions: Microcontacts to Alkanethiol Monolayers with a Conducting AFM Tip *J. Am. Chem. Soc.* **2000,** *122*, 2970-2971.

178. Leatherman, G.; Durantini, E. N.; Gust, D.; Moore, T. A.; Moore, A. L.; Stone, S.; Zhou, Z.; Rez, P.; Liu, Y. Z.; Lindsay, S. M., Carotene as a molecular wire: Conducting atomic force microscopy *J. Phys. Chem. B* **1999,** *103*, 4006-4010.

179. Wang, W.; Lee, T.; Reed, M. A., Ch. 10, Intrinsic Electronic Conduction Mechanisms in Self-Assembled Monolayers. In *Introducing Molecular Electronics*, Cuniberti, G.; Fagas, G.; Richter, K., Eds. Springer-Verlag Berlin Heidelberg: Netherlands, 2005.

180. Tour, J. M.; Rawlett, A. M.; Kozaki, M.; Yao, Y.; Jagessar, R. C.; Dirk, S. M.; Price, D. W.; Reed, M. A.; Zhou, C.-W.; Chen, J.; Wang, W.; Campbell, I., Synthesis and preliminary testing of molecular wires and devices *Chem. Eur. J.* **2001,** *7*, 5118-5134.

181. Tour, J. M., Molecular Electronics. Synthesis and Testing of Components *Acc. Chem. Res.* **2000,** *33*, 791-804.

182. Murrell, M. P.; Welland, M. E.; O'Shea, S. J.; Wong, T. M. H.; Barnes, J. R.; McKinnon, A. W.; Heyns, M.; Verhaverbeke, S., Spatially resolved electrical measurements of SiO[sub 2] gate oxides using atomic force microscopy. *Appl. Phys. Lett.* **1993,** *62*, 786-788.

183. O'Shea, S. J.; Atta, R. M.; Murrell, M. P.; Welland, M. E., Conducting atomic force microscopy study of silicon dioxide breakdown. *J. Vac. Sci. Technol. B* **1995,** *13*, 1945-1952.

184. Nxumalo, J. N.; Shimizu, D. T.; Thomson, D. J. In *Cross-sectional imaging of semiconductor device structures by scanning resistance microscopy*, Research Triangle Park, NC (USA), AVS: Research Triangle Park, NC (USA), 1996; pp 386-389.

185. Planès, J.; Houzé, F.; Chrétien, P.; Schneegans, O., *Conducting probe atomic force microscopy applied to organic conducting blends*. AIP: 2001; Vol. 79, p 2993-2995.

186. Wold, D. J.; Frisbie, C. D., Fabrication and characterization of metal-molecule-metal junctions by conducting probe atomic force microscopy. *J. Am. Chem. Soc.* **2001,** *123*, 5549-5556.

187. Ishida, T.; Mizutani, W.; Liang, T.-T.; Azehara, H.; Miyake, K.; Sasaki, S.; Tokumoto, H., Conductive probe AFM measurements of conjugated molecular wires. Blackwell Publishing Ltd: 2003; Vol. 1006, pp 164-186.

188. Jianwei, Z.; Jason, J. D., Force dependent metalloprotein conductance by conducting atomic force microscopy. *Nanotechnology* **2003,** *14*, 1023.

189. Tivanski, A. V.; Bemis, J. E.; Akhremitchev, B. B.; Liu, H.; Walker, G. C., Adhesion forces in conducting probe atomic force microscopy. *Langmuir* **2003,** *19*, 1929-1934.

190. Lee, H. J.; Park, S. M., Electrochemistry of conductive polymers. 30. Nanoscale measurements of doping distributions and current-voltage characteristics of electrochemically deposited polypyrrole films. *J. Phys. Chem. B* **2004,** *108*, 1590-1595.

191. Lee, H. J.; Park, S. M., Electrochemistry of conductive polymers 37. Nanoscale monitoring of electrical properties during electrochemical growth of polypyrrole and its aging. *J. Phys. Chem. B* **2005,** *109*, 13247-13254.

192. Pingree, L. S. C.; Hersam, M. C.; Kern, M. M.; Scott, B. J.; Marks, T. J., Spatially-resolved electroluminescence of operating organic light-emitting diodes using conductive atomic force microscopy. *Appl. Phys. Lett.* **2004,** *85*, 344-346.

193. Polspoel, W.; Vandervorst, W., Evaluation of trap creation and charging in thin SiO2 using both SCM and C-AFM. *Microelectron. Eng.* **2007,** *84*, 495-500.

194. Mativetsky, J. M.; Pace, G.; Elbing, M.; Rampi, M. A.; Mayor, M.; Samorì, P., Azobenzenes as Light-Controlled Molecular Electronic Switches in Nanoscale Metal−Molecule−Metal Junctions. *J. Am. Chem. Soc.* **2008,** *130*, 9192-9193.

195. Pawlowski, J.; Juhaniewicz, J.; Tymecka, D.; Sek, S., Electron Transfer Across α-Helical Peptide Monolayers: Importance of Interchain Coupling. *Langmuir* **2012,** *28*, 17287-17294.

196. Binnig, G.; Rohrer, H.; Gerber, C.; Weibel, E., Tunneling Through a Controllable Vacuum Gap. *Appl. Phys. Lett.* **1982,** *40*, 178-180.

197. Friedbacher, G.; Fuchs, H., Classification of scanning probe microscopies - (Technical report). *Pure Appl. Chem.* **1999,** *71*, 1337-1357.

198. Holmlin, R. E.; Haag, R.; Chabinyc, M. L.; Ismagilov, R. F.; Cohen, A. E.; Terfort, A.; Rampi, M. A.; Whitesides, G. M., Electron Transport through Thin Organic Films in Metal−Insulator−Metal Junctions Based on Self-Assembled Monolayers. *J. Am. Chem. Soc.* **2001,** *123*, 5075-5085.

199. Loiacono, M. J.; Granstrom, E. L.; Frisbie, C. D., Investigation of Charge Transport in Thin, Doped Sexithiophene Crystals by Conducting Probe Atomic Force Microscopy. *J. Phys. Chem. B* **1998,** *102*, 1679-1688.

200. Wildoer, J. W. G.; Venema, L. C.; Rinzler, A. G.; Smalley, R. E.; Dekker, C., Electronic structure of atomically resolved carbon nanotubes. *Nature* **1998,** *391*, 59-62.

201. Kaba, M. S.; Song, I. K.; Barteau, M. A., Ordered Array Formation and Negative Differential Resistance Behavior of Cation-Exchanged Heteropoly Acids Probed by Scanning Tunneling Microscopy. *J. Phys. Chem.* **1996,** *100*, 19577-19581.

202. Carroll, R. L.; Gorman, C. B., The Genesis of Molecular Electronics. *Angew. Chem. Int. Ed.* **2002,** *41*, 4378-4400.

203. Ratner, M. A.; Jortner, J. In *Molecular electronics: some directions*, Blackwell: 1997; pp 5-72.

204. Adams, D. M.; Brus, L.; Chidsey, C. E. D.; Creager, S.; Creutz, C.; Kagan, C. R.; Kamat, P. V.; Lieberman, M.; Lindsay, S.; Marcus, R. A.; Metzger, R. M.; Michel-Beyerle, M. E.; Miller, J. R.; Newton, M. D.; Rolison, D. R.; Sankey, O.; Schanze, K. S.; Yardley, J.; Zhu, X., Charge transfer on the nanoscale: current status. *J. Phys. Chem. B* **2003,** *107*, 6668-6697.

205. Dorogi, M.; Gomez, J.; Osifchin, R.; Andres, R. P.; Reifenberger, R., Room-temperature Coulomb blockade from a self-assembled molecular nanostructure. *Phys. Rev. B* **1995,** *52*, 9071-9077.

206. Haram, S. K.; Quinn, B. M.; Bard, A. J., Electrochemistry of CdS Nanoparticles: A Correlation between Optical and Electrochemical Band Gaps. *J. Am. Chem. Soc* **2001,** *123*, 8860-8861.

207. Templeton, A. C.; Wuelfing, W. P.; Murray, R. W., Monolayer-Protected Cluster Molecules. *Acc. Chem. Res.* **1999,** *33*, 27-36.

208. Bezryadin, A.; Dekker, C., Nanofabrication of electrodes with sub-5 nm spacing for transport experiments on single molecules and metal clusters. *J. Vac. Sci. Technol. B* **1997,** *15*, 793-799.

209. He, J.; Sankey, O.; Lee, M.; Tao, N.; Li, X.; Lindsay, S., Measuring single molecule conductance with break junctions. *Faraday Discuss.* **2006,** *131*, 145-154.

210. Yano, K.; Kyogaku, M.; Kuroda, R.; Shimada, Y.; Shido, S.; Matsuda, H.; Takimoto, K.; Albrecht, O.; Eguchi, K.; Nakagiri, T., Nanometer scale conductance change in a Langmuir-Blodgett film with the atomic force microscope. *Appl. Phys. Lett.* **1996,** *68*, 188-190.

211. Haag, R.; Rampi, M. A.; Holmlin, R. E.; Whitesides, G. M., Electrical Breakdown of Aliphatic and Aromatic Self-Assembled Monolayers Used as Nanometer-Thick Organic Dielectrics. *J. Am. Chem. Soc.* **1999,** *121*, 7895-7906.

212. Rampi, M. A.; Schueller, O. J. A.; Whitesides, G. M., Alkanethiol self-assembled monolayers as the dielectric of capacitors with nanoscale thickness. *Appl. Phys. Lett.* **1998,** *72*, 1781-1783.

213. Slowinski, K.; Fong, H. K. Y.; Majda, M., Mercury−Mercury Tunneling Junctions. 1. Electron Tunneling Across Symmetric and Asymmetric Alkanethiolate Bilayers. *J. Am. Chem. Soc.* **1999,** *121*, 7257-7261.

214. Adams, D. M.; Kerimo, J.; Liu, C. Y.; Bard, A. J.; Barbara, P. F., Electric field modulated near-field photo-luminescence of organic thin films. *J. Phys. Chem. B* **2000,** *104*, 6728-6736.

215. Burrows, H. D.; Gonsalves, A. M. R.; Leitao, M. L. P.; Miguel, M. D.; Pereira, M. M., Phase transitions and self-assembly in meso-tetrakis(undecyl)porphyrin. *Supramol. Sci.* **1997,** *4*, 241-246.

216. Fox, M. A., Fundamentals in the design of molecular electronic devices: Long-range charge carrier transport and electronic coupling. *Acc. Chem. Res.* **1999,** *32*, 201-207.

217. Kimura, M.; Saito, Y.; Ohta, K.; Hanabusa, K.; Shirai, H.; Kobayashi, N., Self-organization of supramolecular complex composed of rigid dendritic porphyrin and fullerene. *J. Am. Chem. Soc.* **2002,** *124*, 5274-5275.

218. Liu, C. Y.; Pan, H. I.; Fox, M. A.; Bard, A. J., High-density nanosecond charge trapping in thin-films of the photoconductance ZNODEP. *Science* **1993,** *261*, 897-899.

219. Tsuda, A.; Osuka, A., Fully Conjugated Porphyrin Tapes with Electronic Absorption Bands That Reach into Infrared. *Science* **2001,** *293*, 79-82.

220. Reimers, J. R.; Hall, L. E.; Crossley, M. J.; Hush, N. S., Rigid fused oligoporphyrins as potential versatile molecular wires. 2. B3LYP and SCF calculated geometric and electronic properties of 98 oligoporphyrin and related molecules. *J. Phys. Chem. A* **1999,** *103*, 4385-4397.

221. Jiao, J.; Anariba, F.; Tiznado, H.; Schmidt, I.; Lindsey, J. S.; Zaera, F.; Bocian, D. F., Stepwise formation and characterization of covalently linked multiporphyrin-imide architectures on Si(100). *J. Am. Chem. Soc.* **2006,** *128*, 6965-6974.

222. Liu, C. Y.; Pan, H. L.; Fox, M. A.; Bard, A. J., Reversible charge trapping/detrapping in a photoconductive insulator of liquid crystal zinc porphyrin. *Chem. Mater.* **1997,** *9*, 1422-1429.

223. Roth, K. M.; Dontha, N.; Dabke, R. B.; Gryko, D. T.; Clausen, C.; Lindsey, J. S.; Bocian, D. F.; Kuhr, W. G., Molecular approach toward information storage based on the redox properties of porphyrins in self-assembled monolayers. *J. Vac. Sci. Technol. B* **2000,** *18*, 2359-2364.

224. Roth, K. M.; Liu, Z. M.; Gryko, D. T.; Clausen, C.; Lindsey, J. S.; Bocian, D. F.; Kuhr, W. G., Charge-retention characteristics of self-assembled monolayers of molecular-wire-linked porphyrins on gold. In *Molecules as Components of Electronic Devices*, Lieberman, M., Ed. 2003; Vol. 844, pp 51-61.

225. Filippini, D.; Alimelli, A.; Di Natale, C.; Paolesse, R.; D'Amico, A.; Lundstrom, I., Chemical sensing with familiar devices. *Angew. Chem. Int. Ed.* **2006,** *45*, 3800-3803.

226. Malinski, T.; Taha, Z., Nitric-oxide release from a single cell measured insitu by a porphyrinic-based microsensor. *Nature* **1992,** *358*, 676-678.

227. Maree, C. H. M.; Roosendaal, S. J.; Savenije, T. J.; Schropp, R. E. I.; Schaafsma, T. J.; Habraken, F., Photovoltaic effects in porphyrin polymer films and heterojunctions. *J. Appl. Phys.* **1996,** *80*, 3381-3389.

228. Murata, K.; Ito, S.; Takahashi, K.; Hoffman, B. M., Photocurrent from photocorrosion of aluminum electrode in porphyrin/Al Schottky-barrier cells. *Appl. Phys. Lett.* **1997,** *71*, 674-676.

229. Baldo, M. A.; O'Brien, D. F.; You, Y.; Shoustikov, A.; Sibley, S.; Thompson, M. E.; Forrest, S. R., Highly efficient phosphorescent emission from organic electroluminescent devices. *Nature* **1998,** *395*, 151-154.

230. Chowdhury, A.; Chowdhury, J.; Pal, P.; Pal, A. J., Light-emitting diodes from molecularly thin porphyrin derivative: Effect of molecular packing. *Solid State Commun.* **1998,** *107*, 725-729.

231. Harima, Y.; Okazaki, H.; Kunugi, Y.; Yamashita, K.; Ishii, H.; Seki, K., Formation of Schottky barriers at interfaces between metals and molecular semiconductors of p- and n-type conductances. *Appl. Phys. Lett.* **1996,** *69*, 1059-1061.

232. Kwong, R. C.; Sibley, S.; Dubovoy, T.; Baldo, M.; Forrest, S. R.; Thompson, M. E., Efficient, saturated red organic light emitting devices based on phosphorescent platinum(II) porphyrins. *Chem. Mater.* **1999,** *11*, 3709-3713.

233. Reimers, J. R.; Lu, T. X.; Crossley, M. J.; Hush, N. S., Molecular electronic properties of fused rigid porphyrin-oligomer molecular wires. *Chem. Phys. Lett.* **1996,** *256*, 353-359.

234. Robertson, N.; McGowan, C. A., A comparison of potential molecular wires as components for molecular electronics. *Chem. Soc. Rev.* **2003,** *32*, 96-103.

235. Sendt, K.; Johnston, L. A.; Hough, W. A.; Crossley, M. J.; Hush, N. S.; Reimers, J. R., Switchable electronic coupling in model oligoporphyrin molecular wires examined through the measurement and assignment of electronic absorption spectra. *J. Am. Chem. Soc.* **2002,** *124*, 9299-9309.

236. Hao, E.; Jensen, T. J.; Courtney, B. H.; Vicente, M. G. H., Synthesis and cellular studies of porphyrin−cobaltacarborane conjugates. *Bioconjugate Chem.* **2005,** *16*, 1495-1502.

237. Hao, E.; Sibrian-Vazquez, M.; Serem, W.; Garno, J. C.; Fronczek, F. R.; Vicente, M. G. H., Synthesis, aggregation and cellular investigations of porphyrin–cobaltacarborane conjugates. *Chem. Eur. J.* **2007,** *13*, 9035-9042.

238. Hao, E.; Zhang, M.; E, W.; Kadish, K. M.; Fronczek, F. R.; Courtney, B. H.; Vicente, M. G. a. H., Synthesis and spectroelectrochemistry of N-cobaltacarborane porphyrin conjugates. *Bioconjugate Chem.* **2008,** *19*, 2171-2181.

239. Hao, E.; Vicente, M. G. H., Expeditious synthesis of porphyrin-cobaltacarborane conjugates. *Chem. Commun.* **2005,** 10, 1306-1308.

240. Sibrian-Vazquez, M.; Hao, E.; Jensen, T. J.; Vicente, M. G. H., Enhanced cellular uptake with a cobaltacarborane−porphyrin−HIV-1 Tat 48−60 conjugate. *Bioconjugate Chem.* **2006,** *17*, 928-934.

241. Masalles, C.; Teixidor, F.; Borrós, S.; Viñas, C., Cobaltabisdicarbollide anion [Co(C2B9H11)2]− as doping agent on intelligent membranes for ion capture. *J. Organomet. Chem.* **2002,** *657*, 239-246.

242. Ogunrinde, A.; Hipps, K. W.; Scudiero, L., A scanning tunneling microscopy study of self-assembled nickel(II) octaethylporphyrin deposited from solutions on HOPG. *Langmuir* **2006,** *22*, 5697-5701.

243. Palermo, V.; Palma, M.; Samori, P., Electronic characterization of organic thin films by Kelvin probe force microscopy. *Adv. Mater.* **2006,** *18*, 145-164.

244. Kronik, L.; Shapira, Y., Surface photovoltage phenomena: theory, experiment, and applications. *Surf. Sci. Rep.* **1999,** *37*, 1-206.

245. Matey, J. R.; Blanc, J., Scanning capacitance microscopy. *J. Appl. Phys* **1985,** *57*, 1437-1444.

246. Xu, S.; Arnsdorf, M. F., Electrostatic force microscope for probing surface charges in aqueous solutions. *PNAS* **1995,** *92*, 10384-10388.

247. Afsharimani, N.; Nysten, B., Scanning probe microscopy study of electronic properties in alkyl-substituted oligothiophene-based field-effect transitors. *Vacuum* **2013,** *90*, 17-24.

248. Jean, M. S.; Hudlet, S.; Guthmann, C.; Berger, J., Van der Waals and capacitive forces in atomic force microscopies. *J. Appl. Phys.* **1999,** *86*, 5245-5248.

249. Kodera, M.; Yoshimizu, Y.; Uchida, K., Potential Characterization of Interconnect Corrosion by Kelvin Probe and Electrostatic Force Microscopies. *Jpn. J. Appl. Phys.* **2012,** *51* (4).

250. Necas, D.; Klapetek, P., Gwyddion: an open-source software for SPM data analysis. *Cent. Eur. J. Phys.* **2012,** *10*, 181-188.

251. Matsumoto, K.; Ishii, M.; Segawa, K.; Oka, Y.; Vartanian, B. J.; Harris, J. S., Room temperature operation of a single electron transistor made by the scanning tunneling microscope nanooxidation process for the TiO[sub x]/Ti system. *Appl. Phys. Lett.* **1996,** *68*, 34-36.

252. Kim, T. W.; Choo, D. C.; Shim, J. H.; Jung, M.; Kang, S. O.; Lee, H. S.; Lee, J. Y., Nanocrystals acting as Coulomb islands operating at room temperature created using a focused ion-beam process. *Appl. Phys. Lett.* **2001,** *79*, 120-122.

253. Wakayama, Y.; Kubota, T.; Suzuki, H.; Kamikado, T.; Mashiko, S., Molecular Coulomb islands for single-electron tunneling in SiO[sub 2]/molecular layer/SiO[sub 2] multilayers on Si(100). *J. Appl. Phys.* **2003,** *94*, 4711-4713.

254. Milic, T.; Garno, J. C.; Batteas, J. D.; Smeureanu, G.; Drain, C. M., Self-Organization of Self-Assembled Tetrameric Porphyrin Arrays on Surfaces. *Langmuir* **2004,** *20*, 3974-3983.

255. Pasternack, R. F.; Bustamante, C.; Collings, P. J.; Giannetto, A.; Gibbs, E. J., Porphyrin assemblies on DNA as studied by a resonance light-scattering technique. *J. Am. Chem. Soc.* **1993,** *115*, 5393-5399.

256. Yokoyama, T.; Yokoyama, S.; Kamikado, T.; Okuno, Y.; Mashiko, S., Selective assembly on a surface of supramolecular aggregates with controlled size and shape. *Nature* **2001,** *413*, 619-621.

257. Burrell, A. K.; Officer, D. L.; Plieger, P. G.; Reid, D. C. W., Synthetic routes to multiporphyrin arrays. *Chem. Rev.* **2001,** *101*, 2751-2796.

258. Drain, C. M.; Varotto, A.; Radivojevic, I., Self-organized porphyrinic materials. *Chem. Rev.* **2009,** *109*, 1630-1658.

259. Hao, E. Syntheses and evaluation of porphyrin derivatives for applications in medicine and in material science. Louisiana State University, Baton Rouge, 2007.

260. Imahori, H.; Umeyama, T.; Ito, S., Large π-Aromatic Molecules as Potential Sensitizers for Highly Efficient Dye-Sensitized Solar Cells. *Acc. Chem. Res.* **2009,** *42*, 1809-1818.

261. Jurow, M.; Schuckman, A. E.; Batteas, J. D.; Drain, C. M., Porphyrins as molecular electronic components of functional devices. *Coord. Chem. Rev.* **2010,** *254*, 2297-2310.

262. Snitka, V.; Rackaitis, M.; Rodaite, R., Assemblies of TPPS4 porphyrin investigated by TEM, SPM and UV–vis spectroscopy. *Sens Actuators, B* **2005,** *109*, 159-166.

263. George, H.; Palmer, R. E.; Guo, Q.; Bampos, N.; Sanders, J. K. M., Needles and clusters of zinc porphyrin molecules on mica. *Surf. Sci.* **2006,** *600*, 3274-3279.

264. Meunier, B., Metalloporphyrins as versatile catalysts for oxidation reactions and oxidative DNA cleavage. *Chem. Rev* **1992,** *92*, 1411-1456.

265. Petty, M. C., *Molecular electronics : from principles to practice / Michael C. Petty*. Chichester, England ; Hoboken, NJ : John Wiley & Sons, c2007.: 2007.

266. Yang, S.-M.; Jang, S. G.; Choi, D.-G.; Kim, S.; Yu, H. K., Nanomachining by Colloidal Lithography. *Small* **2006,** *2*, 458-475.

267. Malinsky, M. D.; Kelly, K. L.; Schatz, G. C.; Van Duyne, R. P., Chain Length Dependence and Sensing Capabilities of the Localized Surface Plasmon Resonance of Silver Nanoparticles Chemically Modified with Alkanethiol Self-Assembled Monolayers. *J. Am. Chem. Soc* **2001,** *123*, 1471-1482.

268. Li, J. R.; Garno, J. C., Nanostructures of Octadecyltrisiloxane Self-Assembled Monolayers Produced on Au(111) Using Particle Lithography. *ACS Appl. Mater. Interfaces* **2009,** *1*, 969-976.

269. Li, J. R.; Lusker, K. L.; Yu, J. J.; Garno, J. C., Engineering the Spatial Selectivity of Surfaces at the Nanoscale Using Particle Lithography Combined with Vapor Deposition of Organosilanes. *ACS Nano* **2009,** *3*, 2023-2035.

270. Deckman, H. W.; Dunsmuir, J. H., Natural lithography. *Appl. Phys. Lett.* **1982,** *41*, 377-379.

271. Xia, Y.; Whitesides, G. M., Soft lithography. *Ann. Rev. Mater. Sci* **1998,** *28*, 153.

272. Cai, Y.; Ocko, B. M., Large-scale fabrication of protein nanoarrays based on nanosphere lithography. *Langmuir* **2005,** *21*, 9274-9279.

273. Ganesan, R.; Kratz, K.; Lendlein, A., Multicomponent protein patterning of material surfaces. *J. Mater Chem. 20*, 7322-7331.

274. Gao, P.; Cai, Y. G., A method for fabricating protein patterns on the octadecyltrichlorosialne(OTS) surface through paper swabbing. *Ultramicroscopy* **2009,** *109*, 1023-1028.

275. Garno, J. C.; Amro, N. A.; Wadu-Mesthrige, K.; Liu, G.-Y., Production of Periodic Arrays of Protein Nanostructures Using Particle Lithography. *Langmuir* **2002,** *18*, 8186-8192.

276. Hulteen, J. C.; Vanduyne, R. P., Nanosphere lithography - a materials general fabrication process for periodic particle array surfaces. *J. Vac. Sci. Technol. A* **1995,** *13*, 1553-1558.

277. Haynes, C. L.; Van Duyne, R. P., Nanosphere Lithography: A Versatile Nanofabrication Tool for Studies of Size-Dependent Nanoparticle Optics. *J. Phys. Chem. B* **2001,** *105*, 5599-5611.

278. Tian, T.; LeJeune, Z. M.; Garno, J. C., Directed Surface Assembly of 4-(Chloromethyl)phenyltrichlorosilane: Self-Polymerization within Spatially Confined Sites of Si(111) Viewed by Atomic Force Microscopy. *Langmuir* **2013,** *29*, 6529-6536.

279. Briseno, A. L.; Han, S.; Rauda, I. E.; Zhou, F.; Toh, C.-S.; Nemanick, E. J.; Lewis, N. S., Electrochemical Polymerization of Aniline Monomers Infiltrated into Well-Ordered Truncated Eggshell Structures of Polyelectrolyte Multilayers. *Langmuir* **2003,** *20*, 219-226.

280. Lusker, K. L.; Li, J.-R.; Garno, J. C., Nanostructures of Functionalized Gold Nanoparticles Prepared by Particle Lithography with Organosilanes. *Langmuir* **2011,** *27*, 13269-13275.

281. Chen, J.; Liao, W.-S.; Chen, X.; Yang, T.; Wark, S. E.; Son, D. H.; Batteas, J. D.; Cremer, P. S., Evaporation-Induced Assembly of Quantum Dots into Nanorings. *ACS Nano* **2008,** *3*, 173-180.

282. Lusker, K. L.; Yu, J.-J.; Garno, J. C., Particle lithography with vapor deposition of organosilanes: A molecular toolkit for studying confined surface reactions in nanoscale liquid volumes. *Thin Solid Films* **2011,** *519*, 5223-5229.

283. Englade-Franklin, L. E.; Saner, C. K.; Garno, J. C., Spatially selective surface platforms for binding fibrinogen prepared by particle lithography with organosilanes. *Interface Focus* **2013,** *3*.

284. Li, J. R.; Lewandowski, B. R.; Xu, S.; Garno, J. C., Detecting the Magnetic Response of Iron Oxide Capped Organosilane Nanostructures Using Magnetic Sample Modulation and Atomic Force Microscopy. *Anal. Chem.* **2009,** *81*, 4792-4802.

285. Wang, W.; Yuan, X.; Liu, X.; Gao, Q.; Qi, H.; Zhang, C., Selective DNA detection at Zeptomole level based on coulometric measurement of gold nanoparticle-mediated electron transfer across a self-assembled monolayer. *Sci. China Chem.* **2013,** *56*, 1009-1016.

286. Love, J. C.; Estroff, L. A.; Kriebel, J. K.; Nuzzo, R. G.; Whitesides, G. M., Self-Assembled Monolayers of Thiolates on Metals as a Form of Nanotechnology. *Chem. Rev.* **2005,** *105*, 1103-1170.

287. Geissler, M.; McLellan, J. M.; Chen, J. Y.; Xia, Y. N., Side-by-side patterning of multiple alkanethiolate monolayers on gold by edge-spreading lithography. *Angew. Chem. Int. Ed.* **2005,** *44*, 3596-3600.

288. Canepa, M.; Maidecchi, G.; Toccafondi, C.; Cavalleri, O.; Prato, M.; Chaudhari, V.; Esaulov, V. A., Spectroscopic ellipsometry of self assembled monolayers: interface effects. The case of phenyl selenide SAMs on gold. *Phys. Chem. Chem. Phys.* **2013,** *15*, 11559-11565.

289. Saner, C. K.; Lusker, K. L.; LeJeune, Z. M.; Serem, W. K.; Garno, J. C., Self-assembly of octadecyltrichlorosilane: Surface structures formed using different protocols of particle lithography. *Beil. J. Nanotechno.* **2012,** *3*, 114-122.

290. Kumar, A.; Biebuyck, H. A.; Whitesides, G. M., Patterning Self-Assembled Monolayers: Applications in Materials Science. *Langmuir* **1994,** *10*, 1498-1511.

291. Bong June, Z.; Jiyeon, P.; Kwang, J. K.; Hyungkee, Y., Biologically inspired tunable hydrophilic/hydrophobic surfaces: a copper oxide self-assembly multitier approach. *Bioinspir. Biomimet.* **2012,** *7*, 036011.

292. Tarnawski, R.; Ulbricht, M., Amphiphilic gold nanoparticles: Synthesis, characterization and adsorption to PEGylated polymer surfaces. *Colloids Surf. A* **2011,** *374*, 13-21.

293. Ye, W.; Yan, J.; Ye, Q.; Zhou, F., Template-Free and Direct Electrochemical Deposition of Hierarchical Dendritic Gold Microstructures: Growth and Their Multiple Applications. *J. Phys. Chem. C* **2010,** *114*, 15617-15624.

294. Xiaorong, X.; Hanein, Y.; Jiandong, F.; Yanbing, W.; Weihua, W.; Schwartz, D. T.; Bo; x; hringer, K. F., Controlled multibatch self-assembly of microdevices. *Microelectromech. Sys., J.* **2003,** *12*, 117-127.

295. Hegner, M.; Wagner, P.; Semenza, G., Ultralarge atomically flat template-stripped Au surfaces for scanning probe microscopy. *Surf, Sci.* **1993,** *291*, 39-46.

296. Muller, D. J.; Engel, A., The height of biomolecules measured with the atomic force microscope depends on electrostatic interactions. *Biophys. J.* **1997,** *73*, 1633-1644.

297. Tocha, E.; Song, J.; SchÃ¶nherr, H.; Vancso, G. J., Calibration of Friction Force Signals in Atomic Force Microscopy in Liquid Media. *Langmuir* **2007,** *23*, 7078-7082.

298. Weisenhorn, A. L.; Maivald, P.; Butt, H. J.; Hansma, P. K., Measuring adhesion, attraction, and repulsion between surfaces in liquids with an atomic-force microscope. *Phys. Rev. B* **1992,** *45*, 11226.

299. Florin, E.-L.; Radmacher, M.; Fleck, B.; Gaub, H. E., Atomic force microscope with magnetic force modulation. *Rev. Sci. Inst.* **1994,** *65*, 639-643.

300. Gust, D.; Moore, T. A.; Moore, A. L., Mimicking photosynthetic solar energy transduction. *Acc. Chem. Res* **2001,** *34*, 40-48.

301. Wasielewski, M. R., Energy, charge, and spin transport in molecules and self-assembled nanostructures inspired by photosynthesis. *J. Org. Chem.* **2006,** *71*, 5051-5066.

302. Lipson, A. L.; Hersam, M. C., Conductive Scanning Probe Characterization and Nanopatterning of Electronic and Energy Materials. *J. Phys. Chem. C* **2013,** *117*, 7953-7963.

303. Coffey, D. C.; Reid, O. G.; Rodovsky, D. B.; Bartholomew, G. P.; Ginger, D. S., Mapping Local Photocurrents in Polymer/Fullerene Solar Cells with Photoconductive Atomic Force Microscopy. *Nano Lett.* **2007,** *7*, 738-744.

304. Hatton, R. A.; Day, S. R.; Chesters, M. A.; Willis, M. R., Organic electroluminescent devices: enhanced carrier injection using an organosilane self assembled monolayer (SAM) derivatized ITO electrode. *Thin Solid Films* **2001,** *394*, 291-296.

APPENDIX A

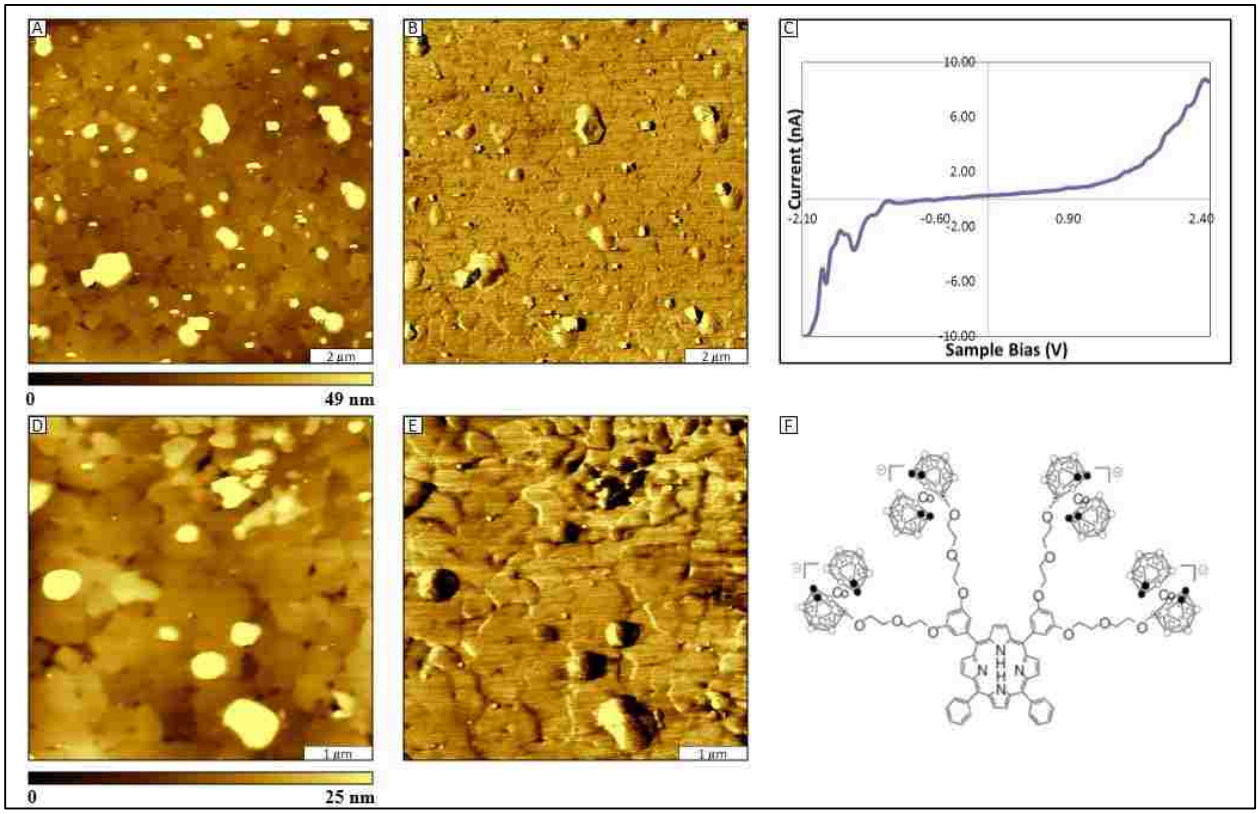

Figure A1 Cobaltacarborane porphyrin compound 4 samples prepared on gold substrates imaged with contact-mode AFM. (A) Topography and (B) corresponding lateral force image obtained in air with a MikroMasch tip with a tip radius of less than 35 nm (C) Representative current-voltage profile for porphyrin nanocrystal obtained with conductive probe AFM using point contact current sweep; (D) zoom-in topograph and (E) corresponding lateral force image; (F) molecular structure for cobaltacarborane porphyrin compound 4.

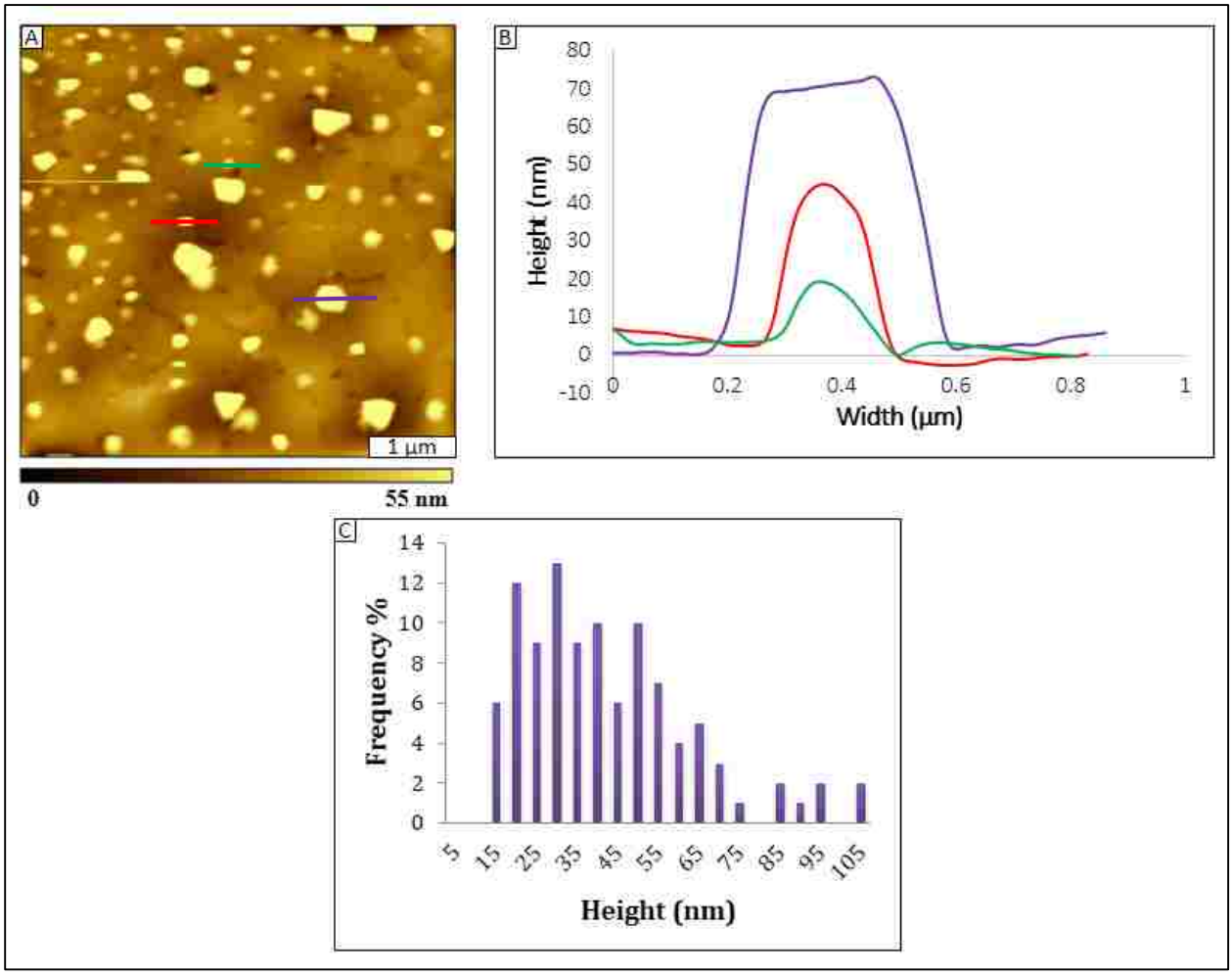

Figure A2 Height distribution data acquired from topography images for cobaltacarborane porphyrin compound 4. (A) Topograph of porphyrin nanocrystals on gold acquired with contact mode AFM in air; (B) cursor profiles for corresponding lines in ***A.*** (C) Height distribution frequency of Co-Por 4 measured with cursor profiles (n = 100).

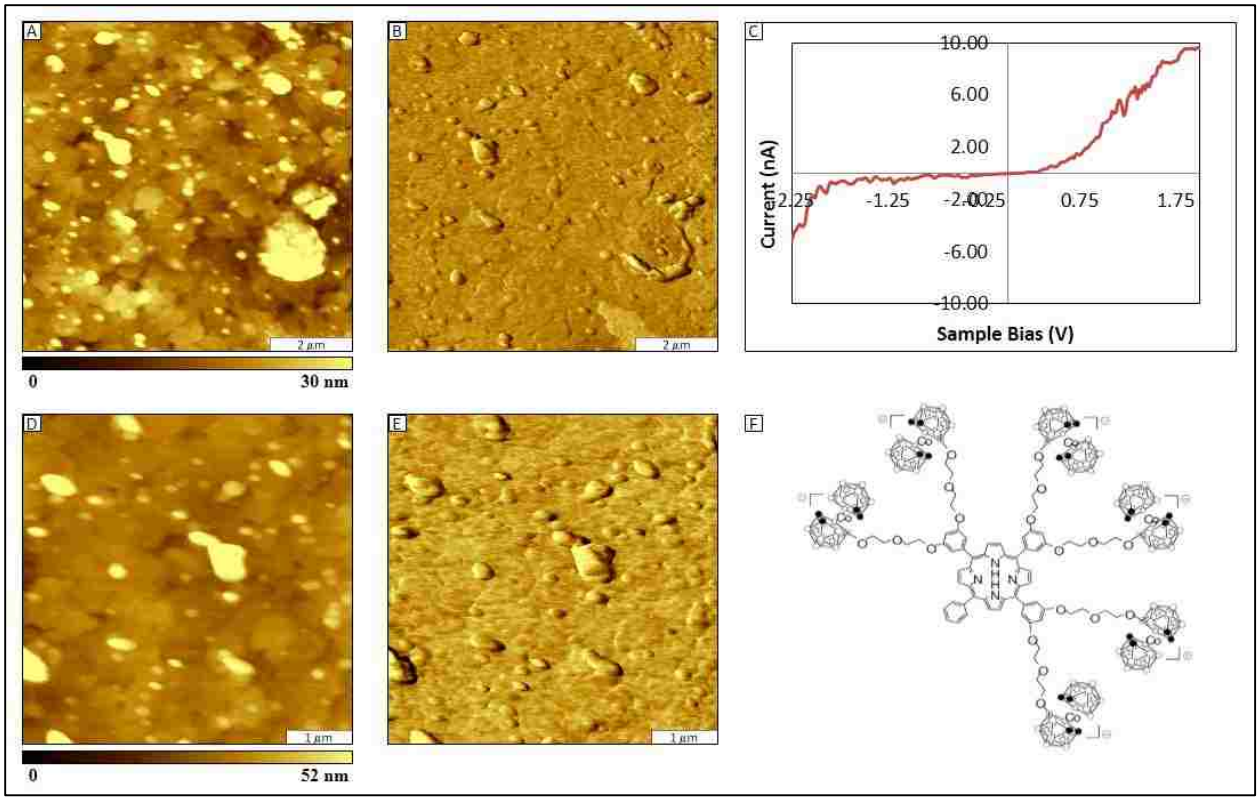

Figure A3 Cobaltacarborane porphyrin compound 5 sample drop-deposited on gold, dried in ambient conditions overnight, and imaged with conductive probe AFM in air. (A) Topography image and (B) corresponding lateral force image acquired with a MikroMasch tip (C) Representative current-voltage profile for porphyrin nanocrystal (D) zoom-in topograph and (E) corresponding lateral force image. (F) Molecular structure for cobaltacarborane porphyrin compound 5.

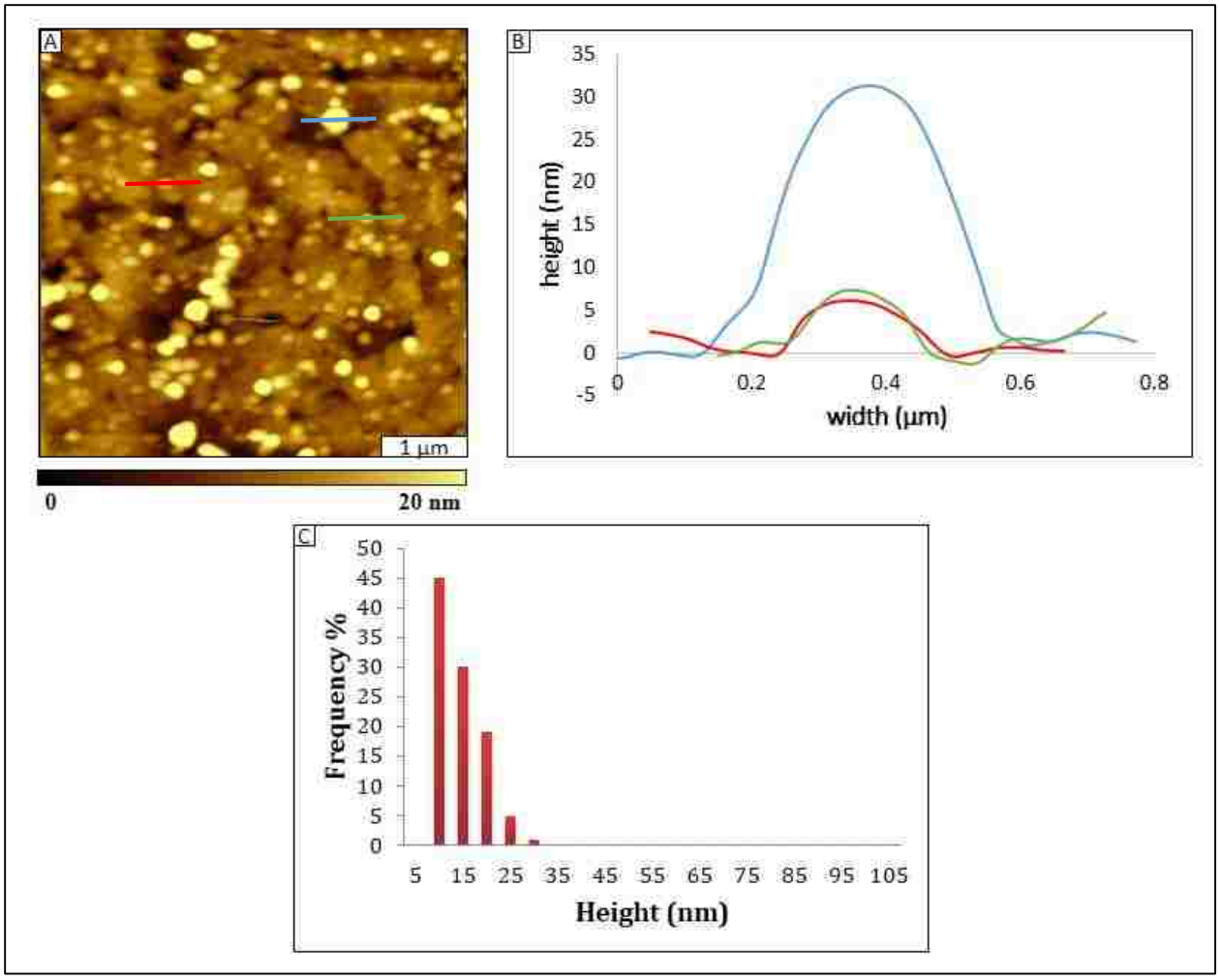

Figure A4 Height distribution data acquired from topography images for cobaltacarborane porphyrin conjugate 5. (A) Contact-mode AFM Topograph of porphyrin aggregates on gold; (B) cursor profiles for corresponding lines in (A); (C) Height frequency distribution of Co-Por 5 measured with cursor profiles (n = 100).

APPENDIX B

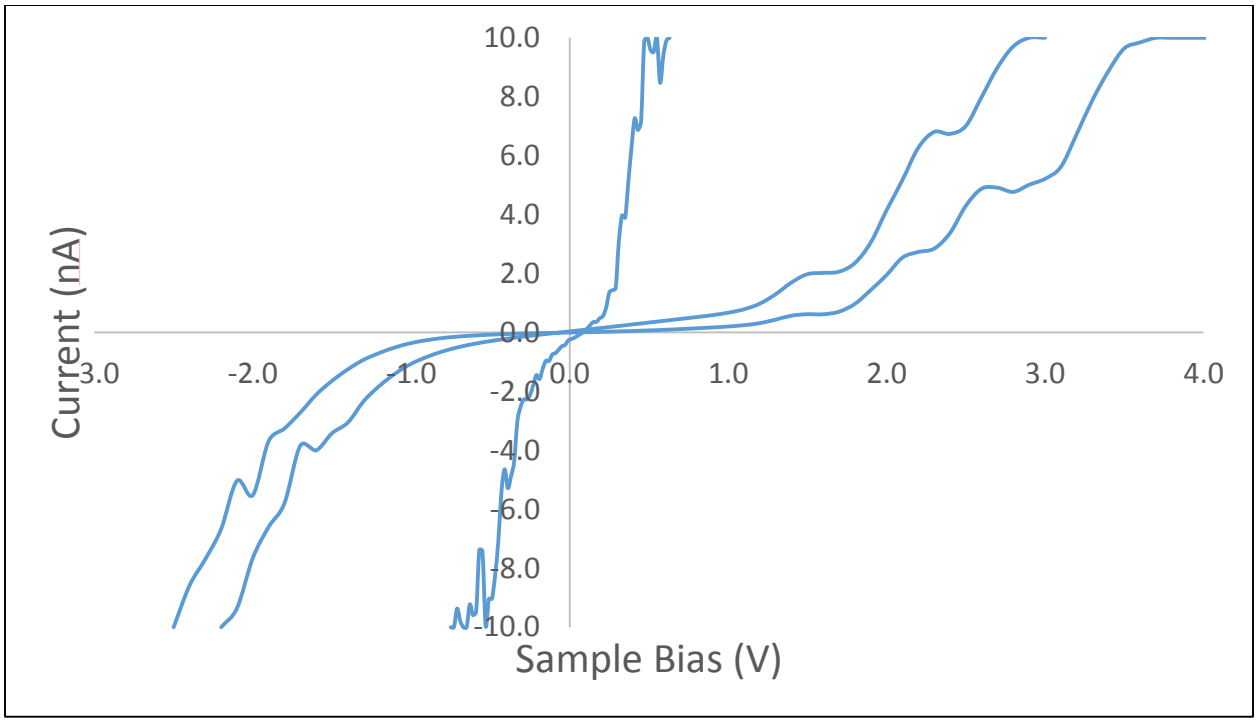

Figure B1 Current-voltage profiles of different size cobaltacarborane porphyrin compound 1 aggregates obtained with conductive-probe AFM in air using a conductively coated MikroMasch tip.

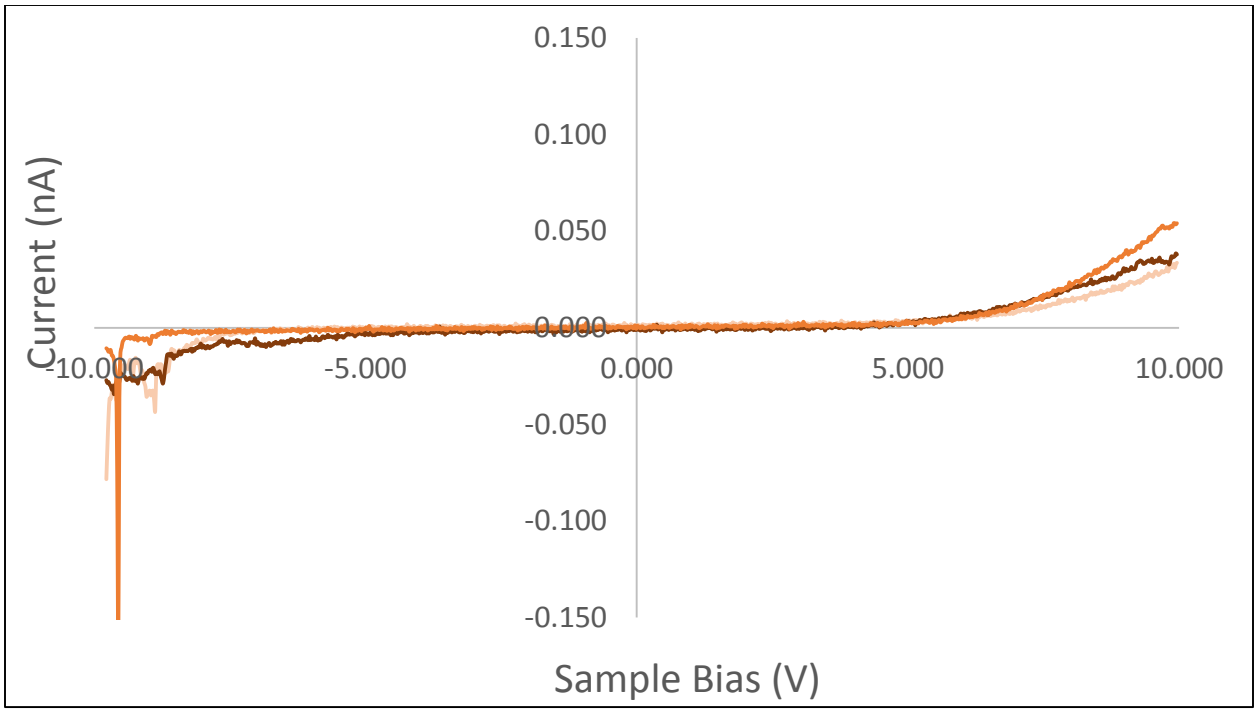

Figure B2 Current-voltage profiles of cobaltacarborane porphyrin compound 2 acquired with conductive probe AFM.

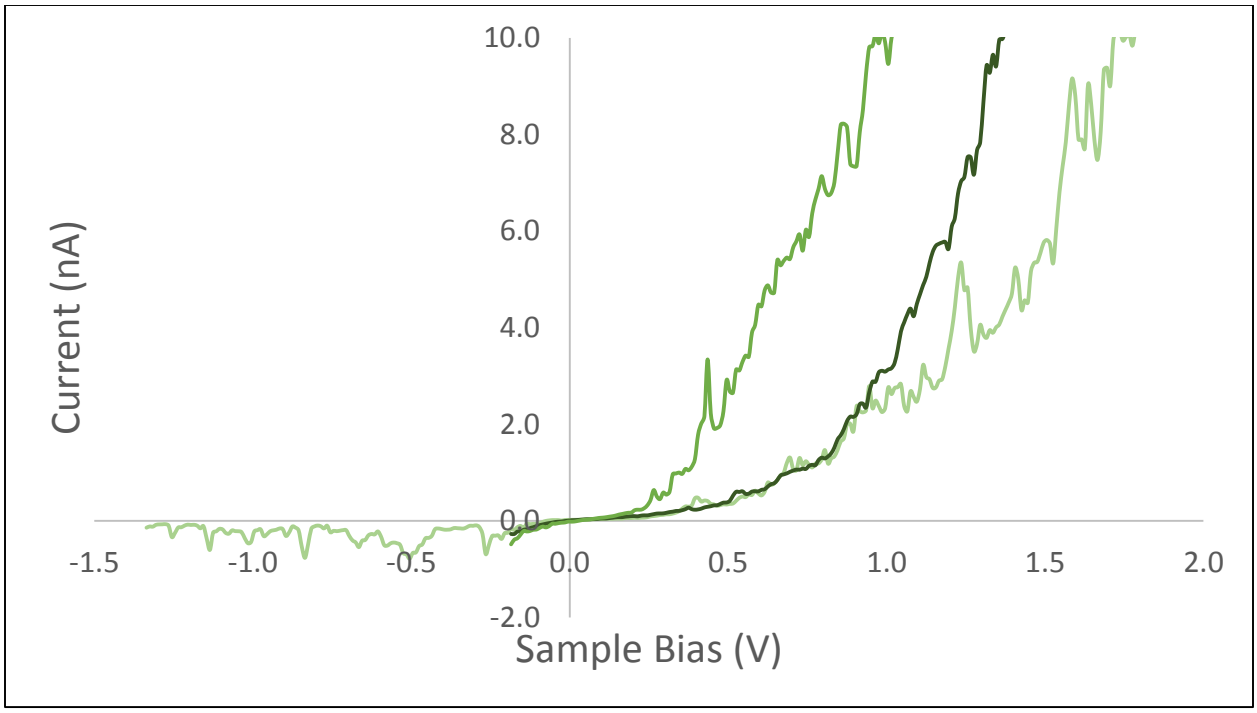

Figure B3 Current-voltage profiles of Co-Por 3 obtained using conductive probe AFM.

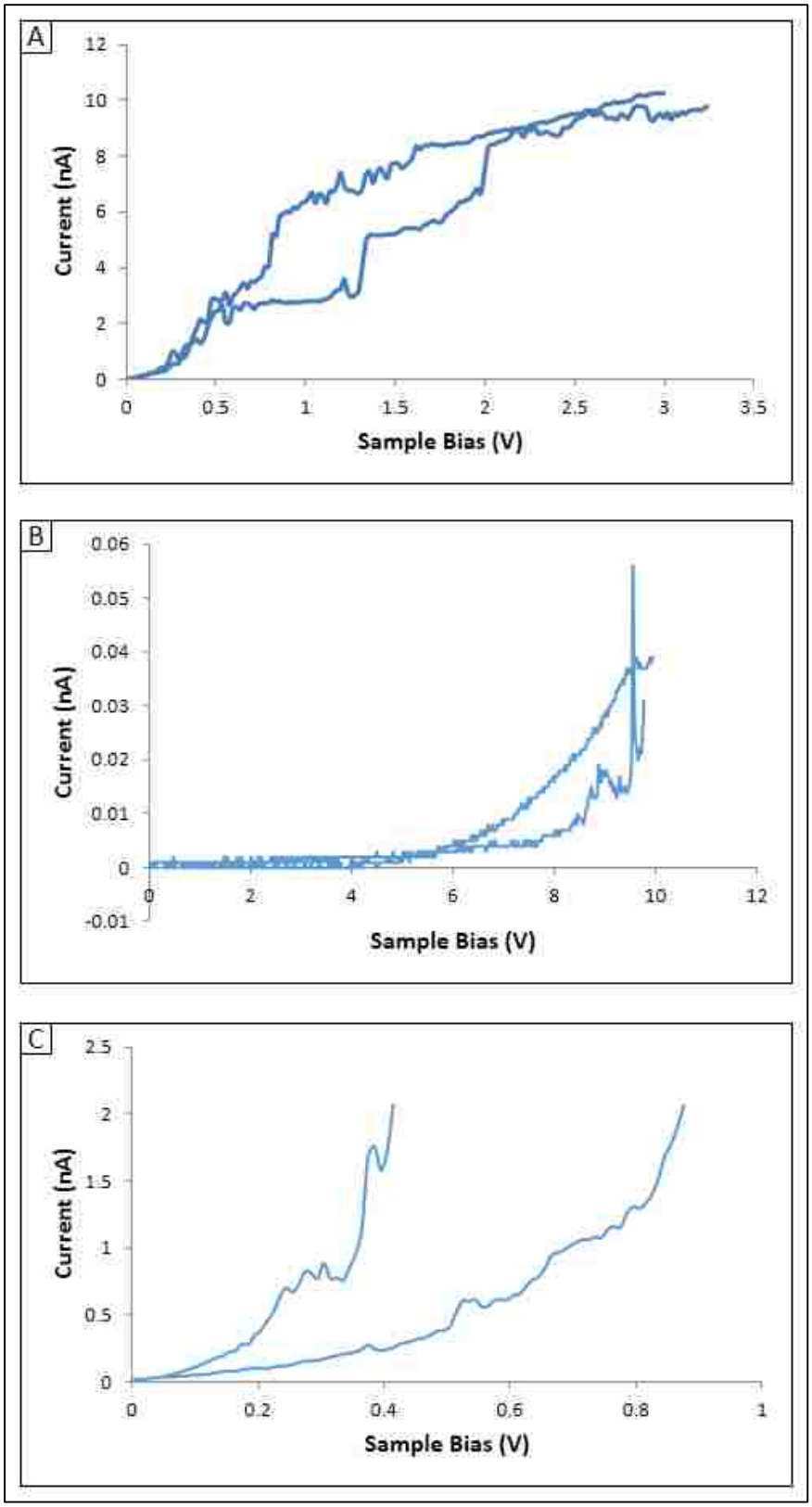

Figure B4 Overlay of current-voltage profile for (A) Co-Por 1 (B) Co-Por 2 and (C) Co-Por 3.

APPENDIX C

Copyright Clearance Center RightsLink®

Home | Account Info | Help

Springer
the language of science

Title: Surface Characterization Using Atomic Force Microscopy (AFM) in Liquid Environments
Author: Venetia D. Lyles
Publication: Springer eBook
Publisher: Springer
Date: Jan 1, 2013
Copyright © 2013, Springer-Verlag Berlin Heidelberg

Logged in as:
Venetia Lyles
Account #:
3000453046
LOGOUT

Order Completed

Thank you very much for your order.

This is a License Agreement between Venetia D Lyles ("You") and Springer ("Springer"). The license consists of your order details, the terms and conditions provided by Springer, and the payment terms and conditions.

Get the printable license.

License Number	3258871181260
License date	Oct 30, 2013
Licensed content publisher	Springer
Licensed content publication	Springer eBook
Licensed content title	Surface Characterization Using Atomic Force Microscopy (AFM) in Liquid Environments
Licensed content author	Venetia D. Lyles
Licensed content date	Jan 1, 2013
Type of Use	Thesis/Dissertation
Portion	Full text
Number of copies	1
Author of this Springer article	Yes and you are the sole author of the new work
Title of your thesis / dissertation	Surface Studies of Organic Thin Films Using Scanning Probe Microscopy and Nanofabrication
Expected completion date	Dec 2013
Estimated size(pages)	110
Total	0.00 USD

VITA

Venetia Lyles is a native of South Carolina. She attended South Carolina State University in Orangeburg, SC for her undergraduate degree. While at SCSU, Venetia was an active participant in the band program, performing in the marching and symphonic bands for four years and joined Tau Beta Sigma, National Honorary Band Sorority Inc. in 2007. She was also initiated into Alpha Kappa Alpha Sorority Inc. during her undergraduate tenure. After graduating with a Bachelors of Science degree in chemistry from SCSU in 2009, she joined the chemistry graduate program at Louisiana State University. While at LSU, Venetia continued to be a tutor to school children in the local community. When not studying, Venetia enjoys running and playing with her dog, Bourbon. After completion of her graduate degree, Venetia plans on teaching chemistry at an undergraduate institution.